Kristoffer Westby Stien

# Assessment of the relationship between Measurement While Drilling parameters and resulting data from pre-excavation grouting

A case study on the Fv. 659 Nordøyvegen project

Master's thesis in Geology - Environmental and Geotechnology
Supervisor: Eivind Grøv
May 2020

Norwegian University of Science and Technology
Faculty of Engineering
Department of Geoscience and Petroleum

NTNU
Norwegian University of
Science and Technology

**NTNU**
**Norges teknisk-naturvitenskapelige universitet**

**Fakultet for ingeniørvitenskap**
**Institutt for geovitenskap og petroleum**

# Ingeniørgeologi
# Masteroppgave 60p

**Studentens navn:** Kristoffer Westby Stien

**Studieretning:** Miljø- og geoteknologi, ingeniørgeologi

**Tittel:** Assessment on the relationship between Measurement While Drilling parameters and resulting data from pre-excavation grouting.

A case study on the Fv. 659 Nordøyvegen project

**Faglærer:** Prof. II Eivind Grøv

**Samarbeidspartner, bedrift el.l:** Bever Control AS, Skanska Norge AS og Statens vegvesen.

**Utfyllende tekst for oppgaven:**

Det er et utrykt ønske fra tunnelbransjen om å ta mer aktivt i bruk MWD-data under tunneldriving. Det fulle potensialet ved bruk av disse data er enda ikke fullt utnyttet i alle ledd av drivefasen samtidig som Bever Control utvikler nye og supplerende tjenester. Dette gjelder særlig for oppfølgingen av selve injeksjonsutførelsen.

Denne oppgaven ønsker å ta for seg muligheten til å bruke MWD-data mer aktivt i injeksjonsforløpet. Mer spesifikt er målsettingen å undersøke om det finnes signifikant korrelasjon mellom de ulike tolkede MWD data som innhentes fra borriggen, og injeksjonsparametere som finnes for injeksjonsarbeidet som utføres i de sammen hullene. Disse resultatene vil først brukes til å forstå injeksjonsarbeidene bedre og dernest bidra til å kunne bestemme hvilke parametere som bør inngå i et mer automatisert injeksjonssystem basert på MWD.

For denne oppgaven skal det benyttes data fra prosjektet Nordøyvegen som består av flere seriekoblede undersjøiske vegtunneler og som bygges av Skanska AS med SVV som byggherre. Oppgaven gjennomføres i nært samarbeide med Bever Control som utvikler oppfølgingsverktøyet. Det skal også benyttes PF-indeksen som ble utviklet av PhD Helene Strømsvik gjennom hennes PhD-arbeid i forskningsprosjektet TIGHT.

**Innleveringsfrist:** 15. mai 2020

Grøv Eivind
Digitally signed by Grøv Eivind
DN: cn=Grøv Eivind
Date: 2020.05.12 17:55:06 +02'00'

**Faglærer**

# Abstract

Uncontrolled drainage of groundwater into the tunnel space represents one of the most serious threats to any tunnel project. Water-ingress into tunnel spaces is associated with multiple negative consequences, such as: settlement damage on surrounding structure, disturbance of surrounding ecosystems, stability issues during and after construction, including unfavorable working conditions inside the tunnel. A common mitigation method to control the water-ingress is called *pre-excavation grouting*, where cement is grouted ahead of the advancing tunnel face, forming a protective curtain surrounding the advancing tunnel. *Measurement while drilling* (MWD), is a drilling technology that allows for continuously monitoring and logging of drilling parameters from the drilling jumbos. The tunneling industry has expressed a desire to use this MWD data more actively during the construction phase, and that includes using MWD data more actively during the grouting process.

The main objective of this master thesis is to gain a deeper understanding of the presumed relationship between these interpreted MWD parameters (MWD DPI), and the different grouting parameters. This is done through various statistical methods. For this purpose, data from a large ongoing infrastructure project (2020) located in western Norway, Fv.659 Nordøyvegen, is used. MWD DPI- and grouting data are gathered from 13 different chainages across 2 different tunnels, comprising over 350 boreholes. The grouting data is also analyzed for hydraulic jacking events (HJ), relying on the newly developed PF index.

The main conclusions from this research, indicate that *no* apparent relationship exists between the MWD DPI- and grouting variables. Suggesting that alternative approaches to the research question are needed, to further verify or dismiss this relationship. Furthermore, it is advised that further developments in today's MWD technology are likely needed before it can be relied on as an effective tool in the grouting process. It is found that MWD DPI's are successful in detecting larger scale weakness zones ahead of the tunnel face. The ability to use the PF index as a visual tool in detecting potential hydraulic jacking events (HJ) has been tested. It is found that 23% of all grouted holes were possibly exposed to HJ events. Indications for higher grouted volumes and time consumption for HJ holes were also found. This thesis highlights some possibilities and limitations of today's industry-standard MWD technology, including the relationship between the MWD- and grouting-data, which is not yet fully understood.

# Sammendrag

Ukontrollert drenering av grunnvann inn i en tunnel, representerer en av de vanskeligste utfordringene for et hvert tunnelprosjekt. Vannlekkasjer inn i tunnelen er assosiert med flere negative konsekvenser, som f.eks. setningsskader på omkringliggende bygninger og infrastruktur, forstyrrelser av økosystemer, stabilitetsproblemer i tunnel både under og etter bygging, og ugunstige forhold for arbeid på tunnelstuff. Den vanligste metoden for å motvirke innlekkasje er gjennom *forinjeksjon*, hvor sement injiseres med høyt trykk foran tunnelstuffen. Slik at det formes en beskyttende skjerm rundt tunnelkonturen. *Measurement while drilling* (MWD), er en boreteknologi som muliggjør fortløpende logging og monitorering av bergmassen fra boreriggen. Det er uttrykt et klart ønske fra tunnelindustrien om å bruke denne MWD dataen mer aktivt i selve injeksjonsprosessen, i et forsøk på å forbedre og effektivisere metoden.

Hovedformålet med denne masteroppgaven, er å etablere en dypere forståelse for sammenhengen mellom disse MWD- og infeksjonsparameterne. Dette er gjort gjennom forskjellige statistiske metoder. For dette formålet er data innhentet fra et stort pågående infrastrukturprosjekt (2020) lokalisert i Vest-Norge, Fv.659 Nordøyvegen. Både MWD- og injeksjonsdata er hentet inn fra 13 forskjellige stuffer og 2 tunneler, med et totalt datagrunnlag på over 350 borehull. Injeksjonsdataen er også analysert for tilfeller av hydraulisk jekking (HJ), ved hjelp av den nylig utviklede PF indeksen.

Denne masteroppgaven konkluderer med at *ingen* signifikante korrelasjoner ble funnet mellom MWD DPI- og injeksjonsparameterne. Hvilket innebærer at det trengs alternative tilnærminger til denne problemstillingen, for å videre kunne verifisere eller avkaste påstanden om sammenheng mellom disse to datagruppene. Videre er det foreslått et behov for nyutviklinger i dagens MWD teknologi, for å forbedre kvaliteten til MWD og muliggjøre bruken av denne dataen i en injeksjons-sammenheng. Muligheten til å bruke PF indeksen visuelt for å bestemme tilfeller av HJ i injeksjondata er blitt testet. Potensielle tilfeller av HJ, ble funnet i 23% av alle injiserte borehull. Det ble også funnet en viss sammenheng mellom økt tidsforbruk og volum for hull med HJ. Denne avhandlingen belyser noen muligheter og begrensninger til dagen MWD-teknologi, samt sammenhengen mellom MWD- og injeksjon, som enda ikke er helt forstått.

# Acknowledgments

This master's thesis is done as the conclusive work of the 2-year Master's program in geology, Environmental and Geotechnology, at NTNU.

First and foremost, I would like to express my sincere gratitude towards my supervisor, Eivind Grøv. For his valuable help not only during but also prior to the master's work. Establishing valuable contacts which made this research possible, and for allowing me great freedom and help in developing my own research problem. I would also like to thank Helene Strømsvik, who offered valuable help on the usage of the PF index, including important discussions regarding the research approach.

I would like to thank Thorvald Wetlesen Jr. and Sr., Emil Festing, and Christian Haugen Svendsen from *Bever Control AS*. For their important collaboration and sharing of knowledge on MWD data, and giving full access to MWD data from the Fv. 659 project.

I would also like to thank the people at *Skanska Norge AS*, for their enthusiasm and collaboration with this research. Henrik Kvikne, project engineer at Fv. 659, for his constant availability and help in retrieving grouting data directly from the different tunnels as they were made available, and project manager Anne Brit Moen, for enabling the collaboration with this research.

Furthermore, I would like to thank my fellow students, for making my time at NTNU memorable (at least before the Covid-19 outbreak). At last, I would like to extend my gratitude towards my family and my better half, Geena, for their endless positivity and support.

Trondheim, 14 May 2020

*Kristoffer Westby Stien*

# Table of Contents

# List of Figures

# List of Tables

# List of Abbreviations

| | |
|---|---|
| **AUC** | Area under curve. |
| **BTO** | Bever Team Online. |
| **D&B** | Drill and blast. |
| **$d_{95}$** | Measure on cement particle size. |
| **DPI** | Drill Parameter Interpretation. |
| **FI** | Fracturing Index. |
| **FMI** | Fullbore Formation Microimager. |
| **GIN** | Grout Intensity Number. |
| **HI** | Hardness Index. |
| **HJ** | Hydraulic jacking. |
| **IDE** | Integrated Development Environment. |
| **KMO** | Kaiser-Meyer-Olkin test for sampling adequacy. |
| **LRIR** | Limit of Residual Inflow Rate. |
| **MFC** | Microfine cement. |
| **ML** | Machine learning. |
| **MWD** | Measurement While Drilling. |
| **NPRA** | Norwegian Public Road Administration (Statens vegvesen). |
| **OPC** | Ordinary Portland Cement (industry standard cement). |
| **OTV** | Optical Televiewer. |
| **PC** | Principal Component. |
| **PCA** | Principal Component Analysis. |
| **PF index** | Pressure Flow index. |
| **PR** | Penetration Rate. |
| **ROC** | Receiver Operating Characteristic curve. |
| **RTGC** | Real Time Grouting Control method. |

| | |
|---|---|
| **SP** | Superplasticizer, dispersive additive for cements. |
| **SVM** | Support Vector Machine. |
| **UCS** | Uniaxial Compressive Strength. |
| **UFC** | Ultrafine cement. |
| **W/C** | Water to Cement ratio. |
| **WI** | Water Index. |

Chapter 1

# Introduction

## 1.1 Background

The exposure of pressurized water represents one of the most challenging conditions faced during underground excavations. The ability to efficiently reduce and control the water-inflow when utilizing underground space, is of great importance for the performance as well as the time/cost aspect of an underground excavation project.

It has been estimated that 20-30% of construction-costs associated with modern tunneling, is directly contributed by rock mass grouting (Holmøy et al., 2015). Holmøy and Nilsen (2014), defines five challenges caused by groundwater inflow:

- Risk of groundwater lowering - potentially causing settlements and damages to surface buildings.
- Drainage of surface areas and lakes - potentially damaging vegetation and recreational areas, interrupting natural discharge system and local eco-systems.
- Difficulties with cost estimates of tunneling projects due to the high degree of uncertainty connected to location and quantity of groundwater inflow.
- Problems related to rock mass stability during and after excavation.
- Expensive and time-consuming grouting (pre- and post-excavation).

A better understanding of the method, as well as optimization and best-practice studies, is of great concern to the tunneling industry as a whole. The standard Norwegian practice for rock

mass grouting in tunneling projects, is pre-excavation grouting, using high pressures and grouting recipes largely based on experience gained from previous projects, as well as the experience of the grouting technicians. *Measurement while drilling*, or simply MWD, allows for continuous monitoring and logging of drilling parameters, this allows for real-time rock mass characterization during excavation. It is believed that this technology could be used more actively for grouting purposes in future applications. However, more research is still needed on the classification accuracy of MWD, including its relation to the different grouting variables.

## 1.2 Thesis purpose and structure

The main purpose of this thesis is to gain better insight into how the different MWD parameters relate to the grouting parameters, this is mainly done through statistical analyses. The data used is gathered from a large infrastructure project located in western Norway, Fv.659 Nordøyvegen, comprising of multiple subsea tunnel, land reclamation, and new roads.

A large amount of time was used for the initial literature study, to gain a fundamental understanding of all relevant aspects of both grouting theory and MWD data. Investigation on potential projects for data gathering was done early, including then establishing contacts within the relevant contractors and companies to get access to as-built project data on both grouting and MWD. A great deal of time was used in establishing strategies for data gathering, including evaluating different methods on how to conduct the data analyses.

The overall disposition of the thesis is as follows:

- A brief literature review on the presence and influence of water in the rock mass is presented chapter 2.
- Literature review on existing theories and methods for rock mass grouting including the phenomenon of hydraulic jacking, with a focus on Norwegian conditions, is presented in chapter 3
- Literature review on the current state of art and possibilities of MWD technology is presented in chapter 4.
- A review of some multivariate statistical methods is presented in chapter 5.
- Project description and methods for data gathering is presented in chapter 6.

- Results from the data analysis are presented in chapter 7.
- Discussions and critical review of the research results, including a review on important limitations and suggestions for further work, are presented in chapter 8.
- Concluding remarks are presented in chapter 9.

## 1.3 Extent and limitations

All data used are gathered from two different tunnels from the same project area. Considering the grouting data, differences in grouting recipes such as w/c ratio, cement type, and additives are *not* taken into account in the data analysis. As the emphasis is put on analyzing the physical variables of the grouting procedure, e.g. pressure, volume, flow, and time.

The grouting procedure used for this project in conjunction with Norwegian grouting practice. That means high pressure, systematic pre-excavation grouting. Data used in this research is therefore not necessarily comparable to that of other grouting practices in other countries. Information and measurements of rock mass stresses are not a part of the gathered data, and its influence on the grouting procedure will not be considered in the data analysis.

The time-consuming nature of retrieving and accessing the data, as well as matching the MWD- and grouting data sets, was a limiting factor for the amount of data available for analysis. Problems concerning data gathering are discussed in greater detail in section 6.4 and 8.7. It was also desired to investigate more that one weakness zone and their related MWD DPI responses, as presented in section 7.1. However, due to limited advance on the tunnels at the time of this research, only one of the interpreted weakness zones had been intersected by the tunneling advance.

Chapter 2

# Hydrogeology

## 2.1 Groundwater in fractured rock

The groundwater's ability to flow through a rock medium is mainly governed by its fractures and fracture systems (Gunnar Gustafson, 2012). The flow of water through a fractured medium can be simplified and explained through mathematical treatment. Central to the theoretical treatment of water flow in fractured and porous media is *Darcy's Law*:

$$q = \frac{Q}{A} = -\frac{dh}{dl} \cdot K \tag{2.1}$$

The law states that the flow, $q$, is proportional to the gradient $\frac{dh}{dl}$, with proportionality constant $K$, which is referred to as the *hydraulic conductivity* $[m^3/s(m^2)]$. This describes ideal flow in a pipe-section of length $l$ with a difference in groundwater level $\Delta h$.

As a simplification, fractures can be described as 2D-structures, with a finite extent, $l$, and a slot aperture $b$ (see figure 2.1). We now need a proportionality constant in the expression (2.1), that can take into account how the flow of water passes through a unit width ($l$) of the water-bearing fracture. We refer to this constant as the fracture *transmissivity*, $T_f$, defined as:

$$T_f = \frac{\rho_w g}{\mu} \cdot \frac{b^3}{12} = K_f \cdot b \tag{2.2}$$

Where $\rho_w$, $g$, and $\mu$ represents the density, acceleration due to gravity, and viscosity of the water, respectively. Equation 2.2, also states that the transitivity is proportional to the cube of the slot aperture, often referred to as the *cubic law*. This implies that a small change in slot aperture will

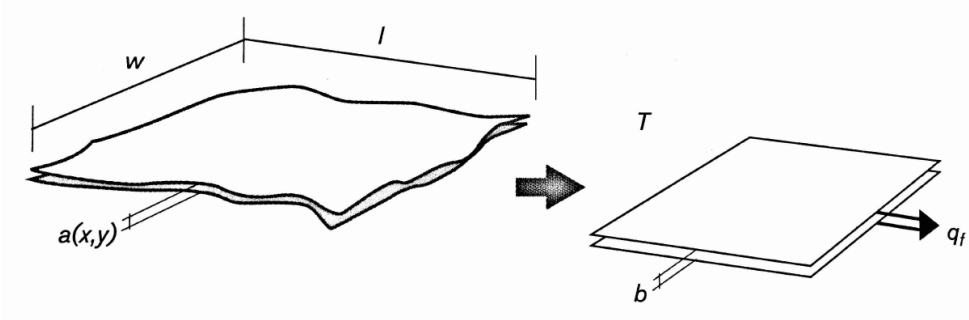


**Figure 2.1:** Conceptual figure, showing how an uneven fracture plane on the left, can be regarded as an equivalent disc structure (on the right), with aperture ($b$) and flow ($q_f$). Figure taken from Gunnar Gustafson (2012).

result in a large increase in transmissivity. This illustrates the importance of fracture aperture width, in the general conductivity of the rock mass. Taking the fracture transmissivity into account, we can then write the Darcy-relationship (eq. 2.1), as:

$$q_f = \frac{Q}{w} = -\frac{dh}{dl} \cdot T_f \tag{2.3}$$

Where $w$ is the fracture width and $l$ the fracture length. The groundwater can then be thought of as flowing through a 2D "fracture disc", with transmissivity ($T$) (see figure 2.1).

## 2.2 Influence of rock type

Even though the most significant contribution to the rock mass in terms of increasing the hydraulic conductivity, comes from the degree of fracturing and fracture properties, there is evidence that certain rock types are generally more permeable than others (Gunnar Gustafson, 2012). This is can be explained by the mechanical properties dependency on the mineralogical composition of the rock types. It is generally found that dark, mafic rock types (rocks with very low silica content, typically basalt and gabbro), are less permeable than their lighter felsic counterpart (rocks with higher silica content, typically granite). The more mafic rock types tend to have a higher tensile strength but lower modulus of elasticity, than the felsic rock types. This means a generally increased stress concentration in the felsic rock types because of the high elasticity modulus, and in turn, this will cause more brittle fracturing. The dark rock types tend to decompose more easily, resulting in more abundant filling of fractures and a further reduction in permeability (Gunnar Gustafson, 2012).

## 2.3 Influence of fracture anisotropy and depth

The hydraulic properties of a water-conducting fracture system are *anisotropic*, this is because the fracture system is anisotropic. I.e. it is expected that the measured transmissivities of a fracture system, will fluctuate depending on the direction of measuring. Another factor that influences the permeability of the rock mass is the *depth* to the fracture system. Naturally, the increase of stress with depth will also decrease the width of the fracture apertures, reducing the overall conductivity of the fractures. The depth trend can be described as reducing the conductivity by *one* order of magnitude each 380 m (Gunnar Gustafson, 2012). The depth trend will often not have profound implications on the overall hydro-geological conditions for a typical underground construction, but should be considered especially when dealing with very deep-lying projects.

## 2.4 Fracture and crush zones

Hydrogeological properties can change dramatically when the rock mass is affected by fracture zones. A fracture zone is a localized concentration of fractures caused by brittle deformation, often with an obvious structural orientation that can be expressed with strike and dip, usually associated with an active or inactive deformation zone (i.e. fault zone) (Gunnar Gustafson, 2012). These zones (often referred to as *weakness zones*), in many cases, represent the most challenging conditions for underground excavations. Not only in terms of high water inflow due to the high permeability of these zones but also because these zones represent structurally unstable parts to the tunnel excavation, permitting uncontrolled collapse during or even a long time after the completion of the project (Bjørn Nilsen and Arild Palmström, 2000). Fracture zones represent anomalous weak structures in the surrounding, stronger rock mass. The large number of fractures that occur throughout a fracture zone means there is often a high probability of representing a high permeable zone (Gunnar Gustafson, 2012). However, the permeability of such zones will vary greatly depending on the structural formation mechanism, mineralogical composition, and dimensions of the fracture/crush zones. The actual permeability of a fracture zone can be classified based on its *permeability structures*.

Caine et al. (1996), discuss and classifies these systems in great detail, and describes how the permeability structures of fracture zones (fault zones) can be influenced by highly localized

conduits and/or distributed conduits, but also as barriers or combined conduit-barrier systems for fluid flow. The central zones of a fault which has undergone considerable displacement, know as the *fault core*, is often associated with lower permeability due to the presence of clay-materials and other slip materials (Bjørn Nilsen and Arild Palmström, 2000). Meaning, it is often the area surrounding the fault core, know as the *damage zone* (which comprises the are just outside the fault core and the *transition zone*), that is often consistent with high permeability structures (see figure 2.2).

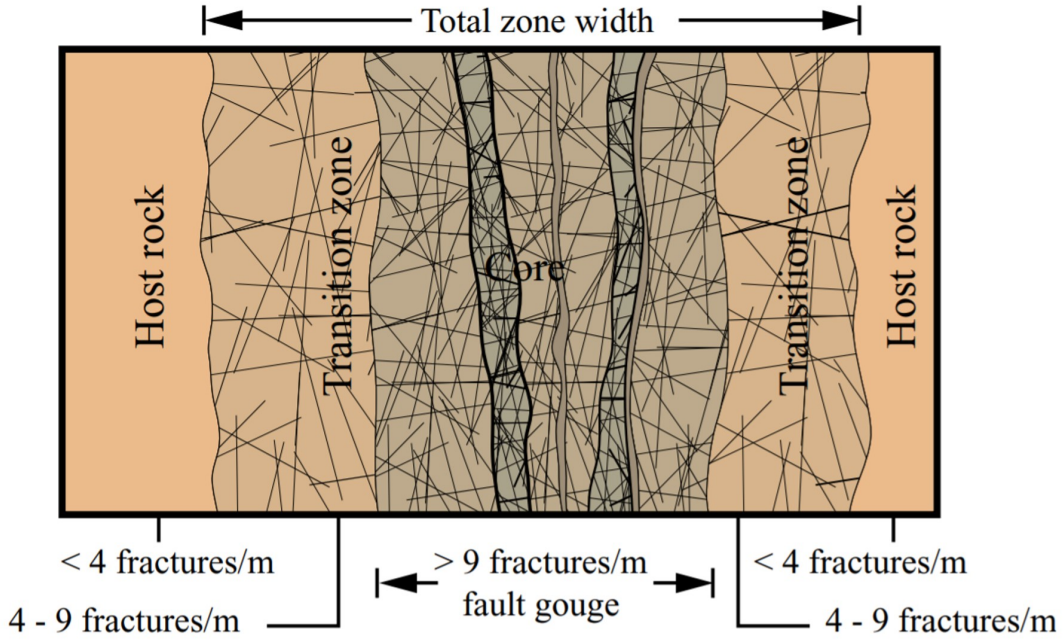


**Figure 2.2:** Conceptual model of a typical fracture zone. Figure taken from Munier et al. (2003).

Chapter 3

# Rock mass grouting

The most common method for achieving sufficient sealing against undesired water ingress in underground excavations is *rock mass grouting*. What is defined as "sufficient sealing" of the tunnel is determined by the predetermined requirements for *allowable inflow*. The maximum allowable water inflow is commonly quantified as liter per minute per 100m tunnel-section, often referred to as *Limit of Residual Inflow Rate* or simply LRIR [l/min/100m] (Arnulf Hansen and Grøv, 2017). The practiced LRIR will vary from project to project, often governed by practical, project-specific limitations. The Norwegian Public Road Administration (NPRA), suggests the following LRIR-requirements for Norwegian tunneling.

| **Extremely strict** | **Strict** | **Intermediate** | **Moderate** |
|---|---|---|---|
| < 1–3 LRIR | 3–7 LRIR | 7–15 LRIR | > 15 LRIR |
| Urban tunnels, high sensitivity to settlements. | Urban tunnels, sensitivity to disruption of fauna. | Rural transport tunnels and rock caverns. | Rural tunnels. |

**Table 3.1:** Maximum allowable inflow (LRIR) classification and examples of typical excavation types, as suggested by Klüver and Kveen (2004) and Arnulf Hansen and Grøv (2017).

## 3.1 Properties of grouts

The use of cement-based grout mixtures is by far the most preferred throughout the industry as it is both cost-efficient and poses little direct threat to environmental concerns (Stille, 2015). Alternately, chemical-based grout mixtures can be used, which comprises as all grout masses which have no particles in suspension i.e. they are chemical solutions (Arnstein Aarset and Frogner, 2010). These chemical solutions have very strict usage terms due to the environmental

| **Cement type** | **Blaine**[$m^2$/kg] | **Specific surface**[$m^2$/kg] | $\mathbf{d_{95}}$[$\mu$m] |
|---|---|---|---|
| **OPC** | | | |
| Industri (Norcem) | 550 | - | 40 |
| Injisering (Cementa) 30 | - | 1300 | 30 |
| **MFC** | | | |
| Microfine (Norcem) 20 | 750 | 2550 | 20 |
| Microfin (Mapei) 20 | - | - | 20 |
| MasterRoc MP 650 (BASF) 20 | 650 | - | 20 |
| Ultrafin 16 (Norcem) | - | 1600 | 16 |
| MasterRoc MP 800 (BASF) | 800 | - | 15 |
| Ultrafin 12 (Norcem) | - | 2200 | 12 |

**Table 3.2:** Typical grout cements available on the Norwegian market 2019 (table modified from Strømsvik (2019); Arnstein Aarset and Frogner (2010).

risk they represent, they are also much more costly than their cement-based counterpart (Kjell I. Davik and Heimli, 2002). Chemical grout mixes are usually only used during post-grouting in Norwegian practice (Arnstein Aarset and Frogner, 2010). Since chemical-based grout's are used predominantly in post-grouting, and not pre-grouting, chemical grouting substances will not be discussed further.

Mainly two different cement grout types are used in conventional grouting, industrial cement (OPS) and microfine-cement (MFC), with multiple subcategories mainly based on the particle size of the cement. Arnstein Aarset and Frogner (2010), provides a list of the main grouting cements used in Norwegian tunneling (see table 3.2). Important properties of the grout include:

- *W/C - ratio*, which is the grout cements water to cement ratio. High values will often yield low viscosity liquid with flow characteristic similar to water, while low values tend to be associated with more viscose flow.
- *Blaine fineness*, is a measure on the fineness of a OPS cement, which is measured in specific area (square meter per kg cement).
- $d_{95}$, measure on the overall particle size of the cement, 95% of particle sizes in cement < given value.
- *Bleeding*, refers to the phenomenon in which water and cement disperse in a grout mix, where free water flows to the top of the mixture, this is generally unwanted.

The rheological properties will be governed mainly be the w/c, specific surface and grain size (Blaine) of the grout mix (Scwarz and Krizek, 2000; Stille, 2015). Another important prerequisite for ensuring good performance of the cement-based grout mixes, is the use of fresh cements which is stored properly (Arnstein Aarset and Frogner, 2010; Stille, 2015).

## 3.2 Grouting methods and principles

There are two different methodology's in rock mass grouting in tunnels; *pre-excavation grouting* or *post-excavation grouting*. In pre-excavation grouting or simply *pre-grouting*, the grout is injected in front of the tunnel face in what is called a *grouting curtain*. Each grouting curtain is made up off 20-70, 18-24m long boreholes (see figure 3.1). The pre-grouting is normally executed after each third or fourth blast round in in conventional drill and blast (D&B) tunneling, with each blast round usually set at 5m. Achieving a 6-8m overlap between the grouting curtains is important in order to achieve good interaction between the different curtains, as well as preventing grouting mass from entering into the tunnel space (Arnstein Aarset and Frogner, 2010). The grouting is usually done starting with the bottom holes (invert) and continuing upwards towards the roof (crown) (Arnstein Aarset and Frogner, 2010). Probe drilling is done continuously at the tunnel face to evaluate the water ingress ahead of the face (Arnulf Hansen and Grøv, 2017).

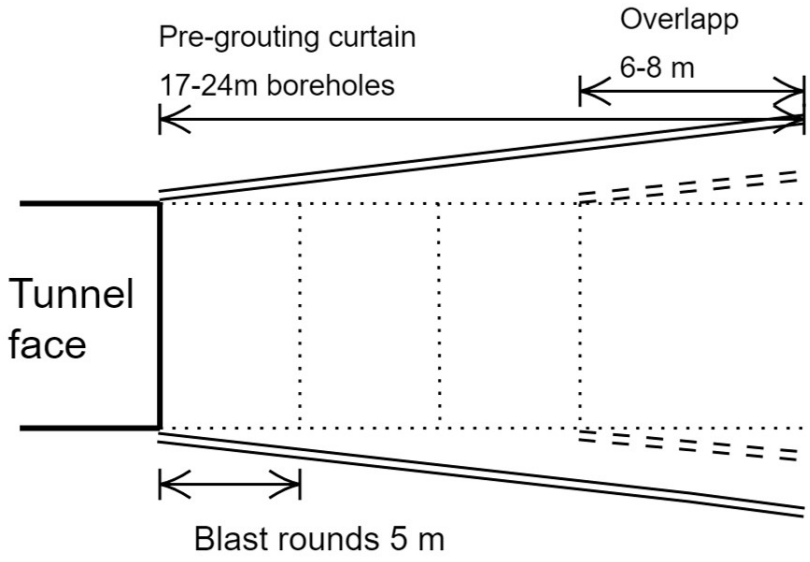


**Figure 3.1:** Schematic view of the basic concept behind pre-grouting.

The alternative method, is referred to as post-excavation grouting or simply *post-grouting*. Post-grouting is done *behind* (rather than in front of) the advancing tunnel face. This method is rarely done systematically due to the difficulty and time- and cost inefficient nature of the method. However, it can be used as a supplementary grouting campaign to the systematic pre-grouting, when the pre-grouting water inflow allowance is not met (Arnulf Hansen and Grøv, 2017; Arnstein Aarset and Frogner, 2010; Grøv et al., 2014).

### Stop criteria for rock mass grouting

The stop criteria is a condition defined prior to grouting, and serves as a threshold criterion for which the grouting is stopped for each hole. In Norwegian practice, this is usually defined based on either maximum grout take (liter grout for each hole) or end-pressure (Arnstein Aarset and Frogner, 2010). The grout end-pressure is achieved through varying the grout flow, pressure, and w/c ratio during grouting. If a end-pressure cannot be achieved, the stop criteria is usually set at a predefined maximum grout take (liters). Another aid in achieving the stop criteria is the ability to control the curing time of the grout, by introducing additives such as *accelerators* into the grout mix.

## 3.2.1 GIN method

This theoretical grouting method was originally developed for grouting curtains used in dam foundations, as described by Lombardi and Deere (1993). The method relies on the *Grout Intensity Number* (GIN), which is the product of grout take (in liters per borehole meter) and pressure ($v \cdot p$). The idea is to have control over the energy in which is expended into each borehole. This is done practically by monitoring the pressure, flow rate, penetrability, and volume with time until the threshold value for volume, pressure or GIN-number is reached. The limiting GIN threshold value is indicated by the hyperbolic curve on a $p - v$ diagram. From figure 3.2, different grouting paths, all representing different *fracture apertures* can be seen in relation to the GIN threshold. The tightest fracture (path 4) is associated with higher grouting pressure, whilst the open fractures (path 1) will result in higher grout takes at lower pressures to reach the designated GIN threshold value.

As previously stated, this method is developed for use in foundation grouting related to dam constructions. An analysis of the applicability of the theoretical basis for this method for tun-

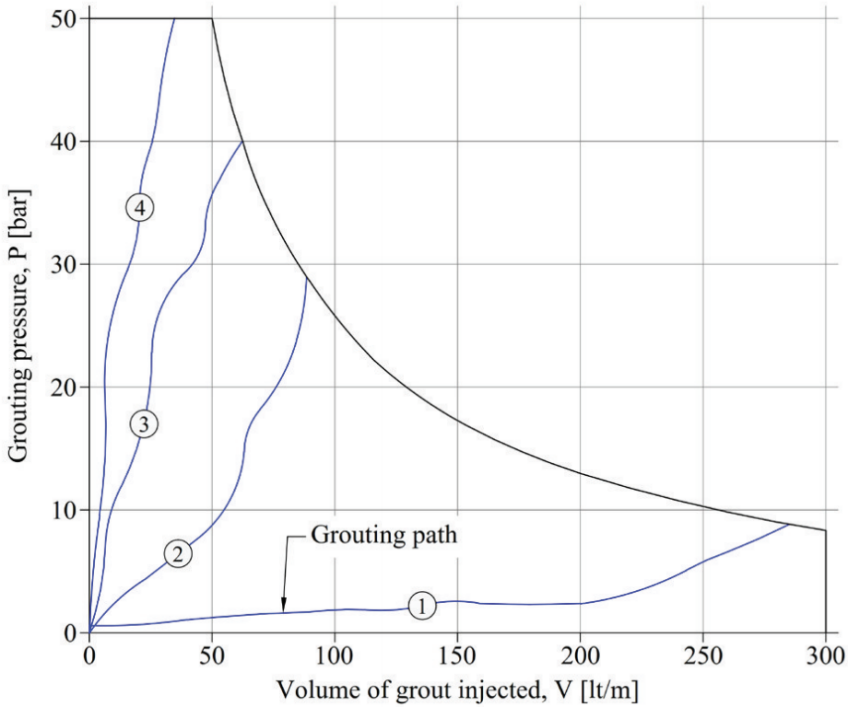


**Figure 3.2:** Figure shows different grouting paths (path 1-4) for different fissure apertures (narrowing from 1-4) in a pressure vs. grout take diagram. The hyperbole represents the limiting value defined by the GIN. Figure taken from Kettle and Katterbach (2015).

neling use was conducted by Brantberger et al. (2000). The theoretical basis for the method was applied for a tunneling project, with a focus on establishing a theoretical basis for the grout spread and prediction of hydraulic jacking (HJ) of the rock mass in a tunneling context. It was found that the theoretical relation developed by the original GIN-method for preventing hydraulic jacking, was not satisfactory in predicting the risk of hydraulic jacking in a tunneling application.

### 3.2.2 RTGC method

The *Real Time Grouting Control* (RTGC), is a concept for controlling the grouting in "real-time". The method is based on the theoretical treatment of grout mass rheology, fracture aperture and penetration length. The stop criteria for this method, is defined as when the penetration depth of the finest fractures ($b_{min}$) has reached a predefined "target value", or when the penetration depth of the largest fractures ($b_{crit}$) reaches a predefined "limiting value", in which both values is based on preliminary calculations (Kobayashi et al., 2008). Perquisites for this method, is that the rheological properties (viscosity [Pa-s], yield strength [Pas], density [kg/m$^3$] and bleed [%]), and the penetrability of the grout (min and max penetration length) have been established prior to grout execution (Rolf Christiansson and Carlsson, 2014; Kobayashi et al.,

2008).

The algorithmic structure of the RTGC method, is illustrated in figure 3.3. The method can be conceptualized to the following steps:

- Rheological properties of the grout, yield stress ($\tau_0$) and viscosity ($\mu$), are measured in laboratory methods and assumed constant with time. Penetrability properties of the grout mix, and slot apertures; $b_{min}$ and $b_{crit}$ are established.
- Penetration length of the grout ($I_D$) is calculated real time based on relative grouting time ($t_D$) required to obtain sufficient grout penetration.
- The grouting pressure ($p_n$), is chosen based on desired penetration length in addition to preventing jacking due to high pressure (see section 3.3).
- Real time comparison of recorded- and estimated flow, is used to verify assumptions on grout- and fracture dimensionality.
- This is repeated through time steps - n, until the penetration depth ($I$) coincides with a predefined stop criteria ("target value" or "limiting value").

Kobayashi et al. (2008), claims that the method is applicable for predicting water leakage into the tunnel and establishing the risk of uplift (hydraulic jacking). The method has been developed over many years of research, predominantly in Sweden, and has been performance-tested and verified in underground excavation projects with satisfactory results (Rolf Christiansson and Carlsson, 2014; M. Holmberg and Stille, 2012). The algorithmic structure also illustrates the possibilities for real-time monitoring and analytical applications using RTGC.

### 3.2.3 Grout penetrability

An important property of the grout is its ability to penetrate into very fine fractures in a rock mass, is dependent on the fineness of particles which are suspended in a cement-based grout mixture. Grout is a mixture in which various cement particles are held in suspension with a variable w/c-ratio. Cement particles in a suspension, especially grouts of the finer constituents (MFC and UFC), tend to fluctuate and form so called *filter cakes* during the hydration process (Stille, 2015). These filter cakes will prohibit the grouts ability to penetrate finer fractures, and is therefore unwanted. To counteract such behavior of the cement particles in suspension, dis-

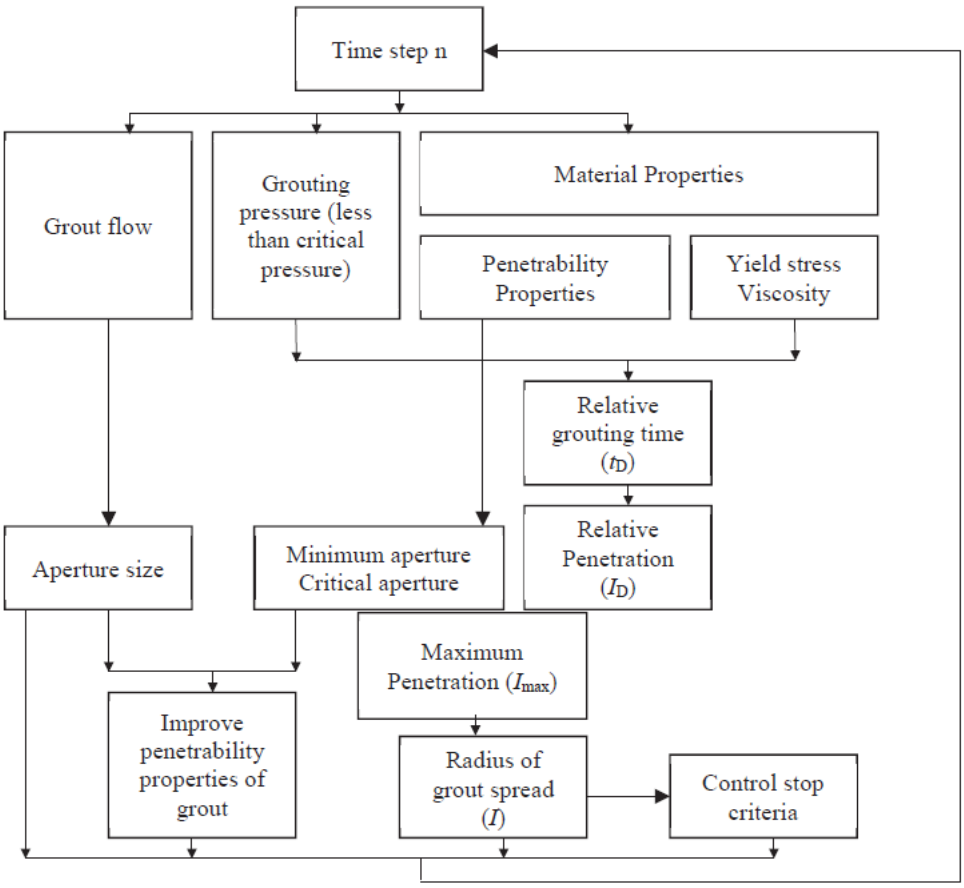


**Figure 3.3:** Algorithmic structure of RTGC (Jalaleddin Rafi and Johansson, 2017).

persive additives such as *superplasticizers (SP)* are usually added (Arnstein Aarset and Frogner, 2010).

A method for evaluating the grouts ability to penetrate a rock fracture of aperture $b$, including describing this filtration process, has been conducted by Eriksson and Stille (2003). The study found that the grout's ability to penetrate was largely dependent on the aperture size of the fractures. If the aperture sizes of the fractures is larger than an upper limit ($b_{crit}$), the grout is allowed to flow freely without filtration and filter-cake formation. Contrarily, if the aperture sizes are too small ($b_{min}$), no grout will be passed through the fracture. Considering aperture sizes between this upper and lower limit, filtration over time may cause gradual pressure build-up and turbulence or even complete blockage of the slot (Stille, 2015).

These limiting values ($b_{min}$ and $b_{crit}$) can be established by using the *Penetrability Meter* (see Eriksson and Stille (2003)). The general perception regarding cement grain size and penetra-

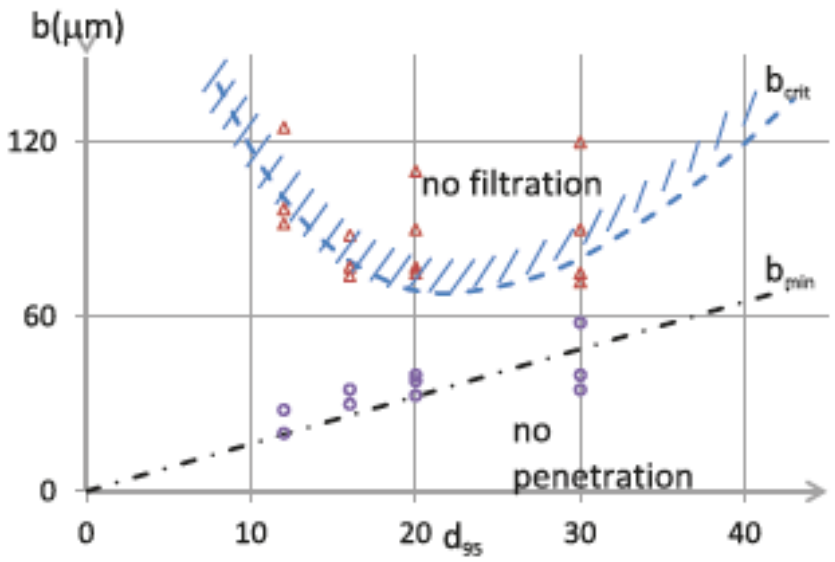


**Figure 3.4:** $b_{crit}/b_{min}$ as a function of grain size ($d_{95}$), derived from laboratory testing conducted by Eklund and Stille (2008) (figure taken from Stille (2012)

.

bility, has been that an decrease in grain size ($d_{95}$) will allow for penetration into finer fracture apertures ($b_{crit}$). Laboratory research conducted by Eklund and Stille (2008), indicates that the penetrability in regards of $b_{crit}$, does not decrease for finer $d_{95}$, it actually increases, as can be seen in figure 3.4. This is because of the high surface activity and high specific surface of fine cements, which are more prone to cluster formation. According to Stille (2015), the chosen grout mix should be based on its ability to penetrate of the smallest fractures.

There are, however, differences of opinion regarding the relationship between $d_{95}$ and grout penetrability. Barton and Quadros (2019), argues that the Swedish approach of testing the penetrability by using of the *filter pump*, which is developed by the Swedish State Power Board (Stille, 2015); is inadequate in describing flow through at fixed aperture. This because of a supposedly unnatural blockage phenomenon that occurs in the filter when testing the desirable UFC and MFC with low w/c-ratios through this filter pump, which is similar to what occurs when grout flows through a porous media such as sand or a similar porous rock medium due to extensional velocity effects (increase in viscosity during penetration causing a "stiffening" grout front (Khan et al., 2004)), and not necessarily representative of grout flow in typical hard rock conditions with sporadic aperture slots.

## 3.3 Hydraulic jacking

A grouting pressure above the surrounding ground-water pressure is the basic prerequisite for grout to intrude into the fracture systems around the boreholes. In Norwegian grouting practice, the use of high pressure has become the norm, the use of high pressure has become the norm, sometimes utilizing pressures up 100 bar above actual water head (Grøv et al., 2014). It is important to distinguish the phenomenons *hydraulic jacking* (also termed hydraulic uplift in some literature) from *hydraulic splitting* (also termed hydraulic fracturing or hydro-fracturing in some literature), which is the formation of new fractures in previous competent rock due to pressure exceeding the tensile strength of the intact rock (Lombardi, 2003; Arnstein Aarset and Frogner, 2010). Hydraulic fracturing have many different appliances in rock- and petroleum engineering; it is used for conducting rock stress measurements in-situ, and is also an important concept in the petroleum industry to increase reservoir capacities.

When the pressure of the grout in the fractures ($p_g$), exceeds the the normal pressure acting on the fracture (the in-situ effective stresses $\sigma_n{}'$), this could lead to hydraulic jacking (HJ) of the grouted fracture, resulting in an increase of the fracture aperture. Based on this, the following basic criteria describes when HJ can be expected to occur in a grouted bore hole:

$$p_g > \sigma_n - p_w \tag{3.1}$$

Where $p_g$ is the grouting pressure inside the borehole, $p_w$ the water-pressure, and $\sigma_n$ the in-situ total normal stress. Another analytical method for establishing the risk of HJ, was developed by Brantberger et al. (2000), which is based on the GIN-method (see section 3.2.1). It is based on the relation between normalized pressure exerted by the grout ($p_n$), and normalized grout spread ($I_n$), which is a function of fracture density, grout spread and fracture aperture:

$$p_n < 1 + \frac{1}{I_n} + \frac{1}{3 \cdot I_n^2} \tag{3.2}$$

Equation 3.2, defines the condition for which $p_n$-values represent *no risk* for hydraulic jacking. $p_n$ is described by the following:

$$p_n = \frac{p' \cdot k_2}{3 \cdot \rho \cdot g \cdot h} \tag{3.3}$$

Where:

$p'$ = effective grouting pressure ($p_g - p_w$).
$k_2$ = factor describing the grout spreading angle.
$\rho$ = density of rock.
$g$ = acceleration due to gravity.
$h$ = height to fracture from ground level.

Equation 3.3, suggests the pressure required to cause hydraulic jacking, is equal to 3 times the overburden weight pressure. Assuming a horizontal fracture, which is deemed to be the most critical fracture orientation (Brantberger et al., 2000).

Stille (2015) suggest three stages of grouting-related hydraulic jacking:

1. Initially the stresses in the borehole have not yet reached the normal stresses acting on the fractures ($p_g < \sigma_n$). This will result in reduction of the contact forces acting between asperities in the fracture. Aperture widening due to the stress change is only marginal, in the scale of $10\,\mu\mathrm{m}$.

2. When grouting pressure is exceeding the normal stresses ($p_g > \sigma_n$), elastic deformation of the fracture will occur. Depending on the grouting pressure and elastic modulus of the rock mass. This stage is associated with the positive effects of HJ, such as increased grout spread and penetrability rate. Even though the deformation of the rock mass is elastic, it will not be reversible due to the hardened grout present in the fracture. This could also lead to jacking of fractures outside the grouted zone, with an increase of permeability outside the grouted zone.

3. The last stage is referred to as *ultimate jacking*. It relates to when the ultimate bearing capacity of the rock mass has been reached ($p_g >> \sigma_n$), this is the same condition as illustrated by equation 3.2. The deformations will potentially be uncontrollable and permanent.

### 3.3.1 Consequences of HJ

It has been conducted a number of researches on the presumed consequences of HJ.
Stille (2015), states that HJ events in a grouting context, poses the risk of:

- Uncontrollable grout *spread and penetration*.
- Considerable *permanent deformation* to the surrounding rock mass, in the case of ultimate

jacking.

- Potentially causing uplift and disturbance of sensitive structures at ground level (above the excavation).
- Decreased *rock mass stability* at the tunnel face, including limited *sealing effect.*
- Strømsvik (2019), concludes in *increased grout and time consumption* for holes where HJ was detected.

## 3.4 Detection of jacking events

Methods for discovering events of HJ from grouting data has been investigated in multiple studies, including: Strømsvik (2019), Lombardi and Deere (1993) and Stille (2015). These include analyzing the time series plot of pressure and flow versus time, and deriving qualitative and/or quantitative approaches for discovering the presence and onset of potential HJ events.

Pioneering work for discovering HJ events was made by Lombardi and Deere (1993). In this study, it was suggested to use relationship between grouting pressure $p$ and grout flow $q$, which is defined as the grout *penetrability* - $p/v$, plotted against time. Possible HJ events can then be defined by qualitative assessment of the plot (see figure 3.5). The pressure build up is described by the increase in total cohesive forces between the grout and rock fissures as the grout spreads and fills voids in the rock mass. The onset of HJ can be observed by sharp spikes or peaks in the penetrability (see figure 3.5).

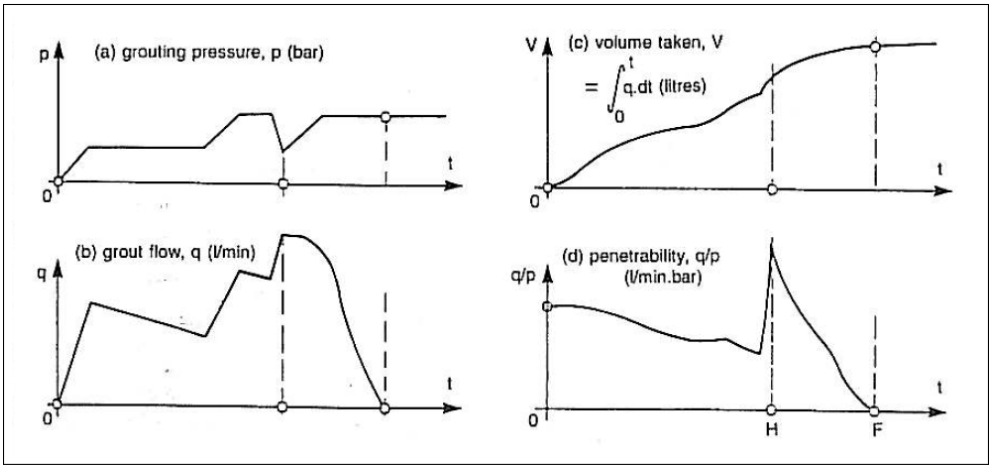


**Figure 3.5:** Time series plots from the grouting process, (a) - pressure ($p$), (b) - grout flow ($q$) and (d) - penetrability ($q/p$). Plot (d) at lower right, shows interpreted onset of HJ event at point H. Figure from Lombardi and Deere (1993).

Stille (2015, 2012), bases the detection of HJ events on the RTGC method (see section 3.2.2). Where the jacking events are indicated by a deviation of the recorded flow path from the predicted flow path. A basic assumption using the RTGC method, is that the predicted grout flow path will start to drop once constant pressure is achieved. And if the recorded flow remains approximately constant, this is an indication that jacking has occurred (as seen in figure 3.6). Another indication of hydraulic jacking according to RTGC, include constant pressure at increasing flow. These scenarios are both considered to be effects of either hydraulic jacking or due to wrong assumptions on the calculated theoretical apertures or dimensionality (1D or 2D) of the fractures.

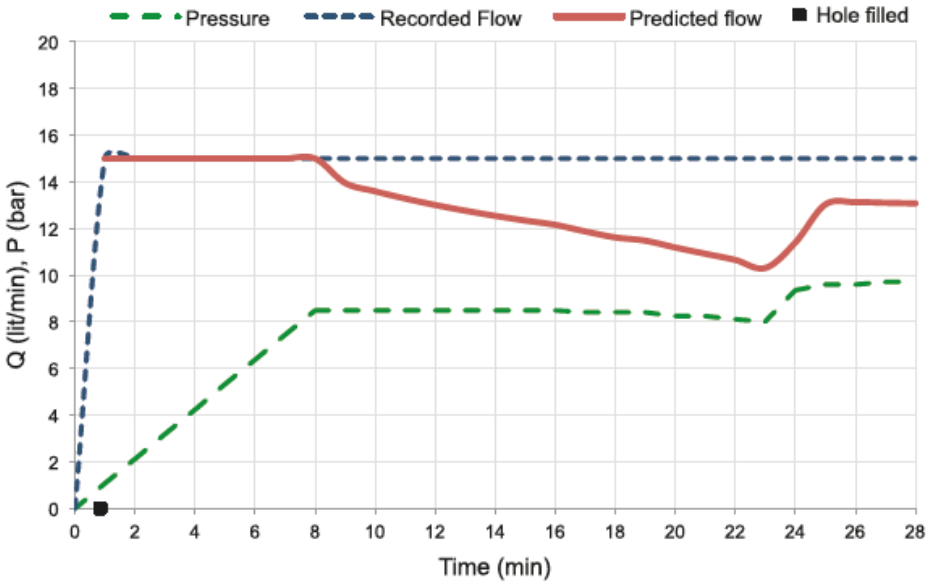


**Figure 3.6:** Figure depicts an interpreted jacking event, using the RTGC method for predicted flow path. Note the deviation between the predicted and recorded flow paths, (Stille, 2015).

### 3.4.1 PF index

The approach presented by Lombardi and Deere (1993), was found unrepresentative for Norwegian conditions by Strømsvik (2019), due to the use of significant higher pressures in Norwegian grouting practices. The use of high pressure grouting implies relatively high pressure rates compared to the flow rate, which often causes too small or negligible responses in $q/p$ ratio. To compensate for this effect and providing an applicable method for high pressure grouting in detecting possible HJ events, Strømsvik et al. (2018) introduces the *PF index*. The PF index is

a dimensionless index value which, among other purposes, can be used to detect the onset of possible HJ events. The PF index is defined as:

$$PF\,index = 0.9\,min/l * Q_v - \frac{0.9 * P}{1\,bar} + 81 \tag{3.4}$$

$Q_v$ is the mom. flow in l/min while $P$ is the pressure measure at the grouting rig. Before applying the PF index method, the input pressure ($p$) and the calculated PF index must be filtered. The pressure filtration involves applying a simple moving median (SMM) with a window of 3 samples, this data smoothing technique removes some unwanted disturbances in the pressure series, such as momentous pressure drops and increases unrelated to HJ events. Filtration of the PF index involves applying a double moving average (DMA) with a window of 5 samples, this smoothing filtration removes unwanted noise caused by pump oscillation (Strømsvik et al., 2018).

The actual onset of a possible HJ event is found by implementing the PF index together with the logged pressure and flow with time in an algorithmic approach. The full algorithm defined by Strømsvik et al. (2018), defines various conditional arguments to be achieved for each sampling interval, in which the boundary condition for possible HJ events are based on literature study, hydraulic fracturing test, numerical modeling and study of grouting logs. Figure 3.7, shows the PF index logged together width the pressure and flow, on two different grouting logs. Looking at figure 3.7 - example (a), the PF index algorithm detects an possible HJ event after approx. 7 minutes, this is because it detects a pressure drop together with a constant flow. In example (b), a possible HJ event is detected just after 35 minutes, starting from at this point there is both decreasing pressure and increasing flow.

The PF index can also be used as a visual tool in de tecting possible HJ events. This is done by analyzing graphs of the PF index together with the logged pressure and flow. Strømsvik and Grøv (2017) defines some characteristic features which can be used as tools in visual interpretation of pressure/flow graphs to evaluate the presence of HJ events:

- Momentary decrease in pressure while the flow remains constant.
- Momentary increase in flow while the pressure remains constant.

- Increase in flow and decrease in pressure.
- Stable flow and pressure, after a period of pressure increase.

While these are all indications of jacking events in a borehole, the same behavior will be seen due to other indicators *not* related to HJ events, such as: when fracture infill are cleared out by the penetrating grout, movement of still grout in the fracture system, grout pressure fluctuations due to operator control and grouting rig pump, and low-pressure grouting in a rock mass with an open fracture system. This makes it difficult to determine if the observed indications are actual jacking events or due to other, "false" effects (Strømsvik and Grøv, 2017; Strømsvik et al., 2018). Another limitation to consider when applying the PF index, is that the grouting rig i required to provide a sampling frequency of approximately one sample every 10th second. This implies that PF index as a method for detecting HJ events, can *not* be applied when considering data with a lower sampling frequency.

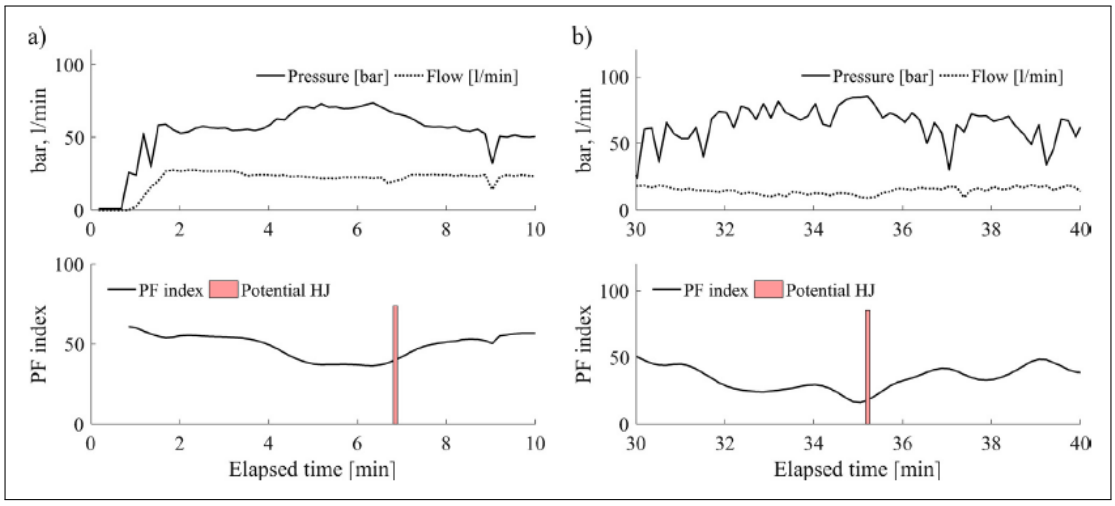


**Figure 3.7:** Figure shows time series of pressure and flow on top for grouting instances a and b with corresponding PF index beneath. Potential HJ events are indicated in both instances. Figure taken from Strømsvik et al. (2018).

Chapter 4

# Measurement While Drilling data

Measurement while drilling (MWD), is a drilling technology that allows for continuously logging and monitoring of numerical drilling data collected from instrumented drilling jumbos. The technology has been used in the petroleum industry since the early 1900s, after pioneering work on downhole electrical logging was done by Schlumberger in 1911. But it wasn't until the introduction of the computer that the real applicability of MWD technology was fully realized (Segui and Higgins, 2002). MWD technology has in recent years been developed into an important tool for tunneling and underground excavation, although its application today is mostly limited to ahead geological monitoring through probe drilling, and as an evaluation tool for rock support based on weakness zones and water inflow (Arnulf Hansen and Grøv, 2017). Use of MWD data directly for evaluating grouting methods is not common practice today, and a very limited number of studies have been done on this area (Høien and Nilsen, 2014).

## 4.1 MWD parameters

There are predominantly 8 different physical *drill parameters* measured (depending on instrumentation specifications of the drilling jumbo), representing the *raw* MWD data from the drill rig:

- Penetration rate (PR) [m/min]
- Percussion/Hammer Pressure (HP) [bar]
- Feeding Pressure (FP) [bar]
- Rotation Speed (RS) [rpm]

- Rotation Pressure (RP) [bar]
- Dampening Pressure (DP) [bar]
- Water Flow [l/min]
- Water Pressure [bar]

During drilling, all these parameters together with the hole depth, time and hammer ID are logged and saved in corresponding files for each borehole. According to van Eldert et al. (2017), these drilling parameters can be categorized into either *dependent* or *independent* parameters, depending on their drill-bit to rock dependency. The independent parameters include hammer pressure, feeding pressure, and rotation speed. These are dependent on the operator, settings and control system of the drilling rig, and not the interaction between the drill bit and rock. On the contrary, the dependent parameters are dependent on the interaction between the rock mass and drill bit. These parameters include penetration rate, torque pressure, rotation pressure and dampening pressure as well as water flow and pressure. Navarro et al. (2018), studied the inter-correlation between the MWD-parameters and suggested that the feeding pressure parameter influenced greatly on the response of other parameters, implying that changes in the feed pressure are indicative of changes in other parameters in the drilling system and can, therefore, be used for rock mass characterization.

## 4.2 Drill parameter interpretation

In order for the MWD data, which has been readily logged and stored, to be useful in any practical sense, it must be processed, interpreted and presented for the user. This is done by the *drill parameter interpretation* (DPI). These interpreted parameters are usually divided into hardness, fracturing, and water index (water disturbance factor). The actual interpretation are provided by various different software's, such as: GPM+ (Rockma AB, 2011), Bever Team Online/BT3 (Bever Control AS, 2019), Underground Manager (Atlas Copco/Epirock, 2019) and Sandvik iSure (Sandvik AB, 2019).

Generally, these software vendors will be able to provide at least three interpreted parameters: *hardness*, *fracturing* or *water disturbance*; but often various other interpreted models are also available, such as geological classes (lithology), rock quality indexes, etc. Some vendors will provide insight into the algorithms which are used for the different interpretation models, while

others are more secretive about their data processing approach (Jakobsen and van Oosterhout, 2018).

### 4.2.1 Pre-processing of MWD data

A fundamental challenge with measured data is the presence of erroneous and faulty data in the logged data set. These values are not representative of actual conditions, this could be due to human error, uncalibrated equipment, incorrect measuring or irregular measuring conditions (e.g. vibrations, temperature or humidity). These erroneous influences should be removed before further usage, unless dealt with, these data points will obscure the DPI results. An initial step to raw data pre-processing is described by Ghosh (2017). Unrealistic raw data, e.g. negative and/or unreasonably high penetration rates are removed from the data-set by defined filtration intervals, this important step in the data processing is called *filtering*.

Differences in drilling equipment and operators used will result in differences in the measured data. These effects which in many cases can be removed by data normalization. According to van Eldert et al. (2017), there are several unwanted external influences which should be removed by data normalization and filtration:

- The penetration rate parameter decreases with increasing drill hole diameters and hole length due to larger energy dissipation from friction and between the couplings of the extension rods. These are examples of effects that must be normalized, to correlate data collected from different drill sources (e.g. grouting holes and blast holes).

- During extension rod changes, the feed pressure will decrease considerably with a gradual increase towards the average value. Data collected during rod extensions are not representative of actual rock mass characteristics (Vezhapparambu et al., 2018).

- The very beginning of the drilling process for each hole, a reduced drilling pressure and speed are applied. This data is unrepresentative for the true drilling conditions and should, therefore, be removed from the datasets.

Effective DPI algorithms will effectively seek to filter and remove these adverse effects from the data.

### 4.2.2 Hardness index

The *hardness index* (HI), is often descriptive of the drillability of the rock mass (Van Eldert, 2018). The parameter can be derived from a large variety of MWD parameters, depending on the software. In Bever Control algorithms, the interpreted hardness is based on normalized penetration rate with respect to variations in both feeder- and hammer pressure (Bever Control AS, 2019). In Underground Manager 2019, it is based on normalized penetration rate, hole depth and percussive pressure (Van Eldert, 2018). HI, unless properly calibrated, will only indicate a relative ranking in terms of hardness. In the case of calibration, this can be done by using: Schmidt hammer, UCS, point load test or Brazil test (tensile strength), which allows for absolute hardness to be estimated (van Eldert et al., 2017).

### 4.2.3 Fracture index

An important DPI parameter derived from the MWD data is the estimated degree of fracturing; namely, the *Fracture index or Fracture factor* (FI). This interpretation is can be derived from the variance of both the normalized penetration rate parameters (PR) and normalized rotation pressure from MWD, according to Bever Control (Bever Control AS, 2019). As these three dependent parameters are found to be most sensitive to variance in fracturing across a borehole and can, therefore, be used for fracture detection (van Eldert et al., 2019, 2017; Khorzoughi et al., 2018). Barr (1985) conducted laboratory drilling trails of an imitated rock mass block (made of a concrete compound) with inbuilt fractures, these tests were able to successfully detect fractures as well as determining whether the fractures had infilling or not. The idea is that when the drill bit crosses an open fracture, an immediate but short-lived increase in PR can be noticed, while an instantaneous drop in torque just as the drill bit enters the fracture void. Upon reconnection with the rock mass, after the drill bit has crossed the fracture void, the thrust, rotation pressure and torque will increase and normalize around values characteristic of the rock mass (Barr, 1985; Khorzoughi et al., 2018).

It should be stated that although these parameters have all been found to respond well to fracturing in a rock mass, variations in other physical properties of the rock mass such as hardness, porosity, and soft rock layers will also produce responses in the same parameters (Khorzoughi et al., 2018). Difficulties in detecting fractures of particularly steep inclination to the borehole (>60°), has been reported by both Barr (1985) and Khorzoughi et al. (2018).

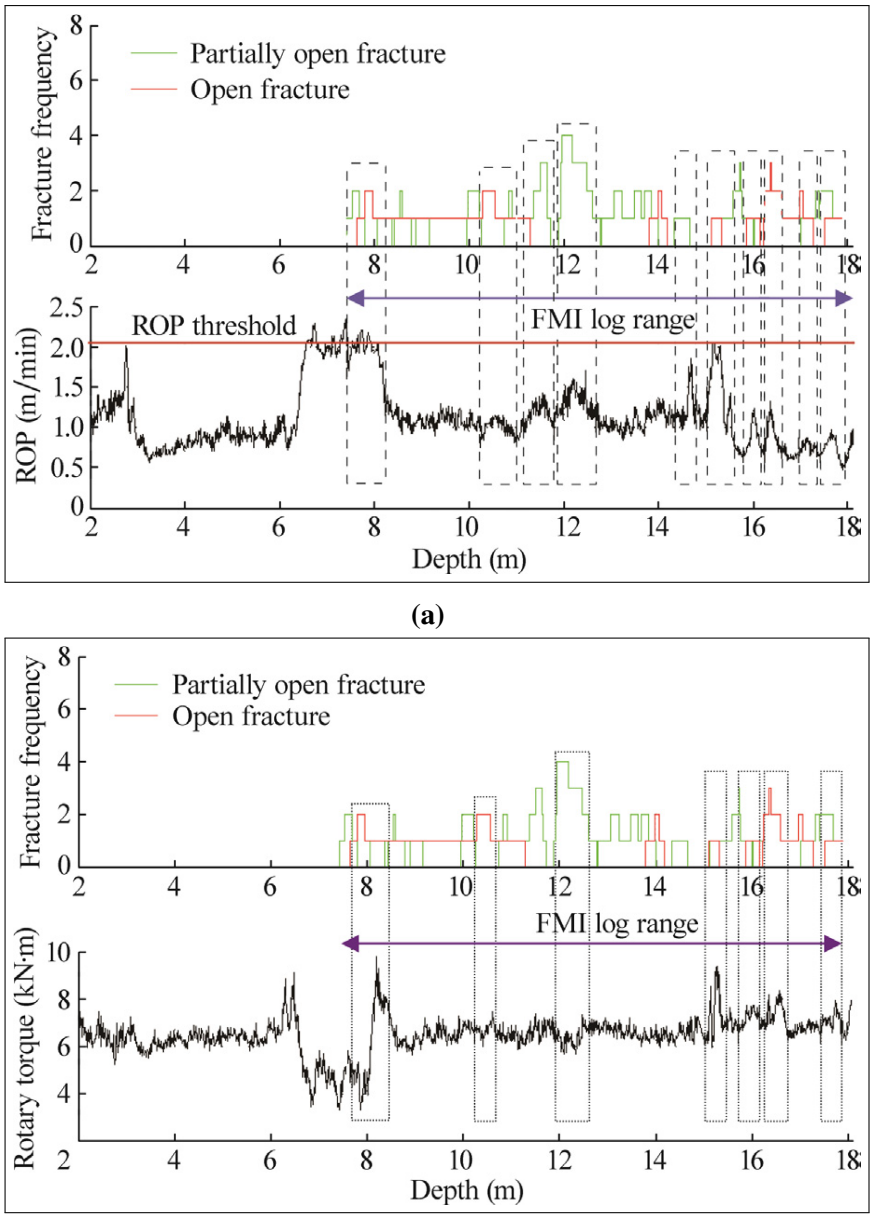


**Figure 4.1:** Responses in both PR (a) and torque (b) when the drill bit crosses both partially open and open fractures in a borehole, figures from Khorzoughi et al. (2018).

Figure 4.1, shows the response in the drilling parameters: rate of penetration and torque when fractures of known location and dimensions are crossed by the drilling bit. The fracture densities of the borehole are established by processed FMI logs (Fullbore Formation Microimager; an optical logging method) (Khorzoughi et al., 2018). The FMI can provide data on fracture density, aperture, and orientation. Considering the PR (in 4.1a), the instant but short-lived increase just as the drill bit crosses an open fracture can be seen multiple times at different fracture density peaks as illustrated by the dashed rectangles. A drop in torque as the high fracture

density zones are crossed can also be seen (in 4.1b). The sudden increase and decrease of PR and torque, respectively, at the 6- 8m interval, are due to control system interference; When a certain threshold is reached for these values, the feeding pressure of the drilling system is automatically reduced to compensate for this effect. The feeding pressure will under optimal conditions remain constant through the drilling procedure (Khorzoughi et al., 2018).

### 4.2.4 Water index

Interpreted water or Water Index (WI) is normally based on normalized water flow and changes in water pressure during drilling, and will give indications of where water is present and flowing from the rock (Bever Control AS, 2019). Høien and Nilsen (2014), compared fold-out tunnel profiles of both DPI water factor from MWD and manually mapped water leakages. Based on the comparison, it was found a fairly good relationship between the water factor and mapped water leakages. However, the manual leakage mapping was conducted after the grouting was completed, which entails that the initial water conditions were obscured and quite possibly not representative of the water conditions indicated by the interpreted Water factor.

Because water is also commonly used as a flushing medium in rotary percussive drilling (top hammer - drilling method used for most modern drill jumbos in the tunneling industry), the Water Index could be obscured by the introduction of pressurized flushing water from the drilling rig into the borehole. Therefore, potentially limiting the reliability of the WI interpretation.

### 4.2.5 Presentation of MWD data

In terms of data presentation, there are many possibilities. For simple graphical presentation of MWD and DPI, both 2D and 3D options are used. Drill rigs are often equipped with monitoring solutions that can be used for real-time assessment of the drill parameters. Figure 4.2, is a screenshot taken from the GPM+ software (Rockma AB, 2011), it shows how graphical logging of each borehole can be done. Bever Team Online module allows for specifying chainage intervals for extraction of any raw MWD or DPI parameters. An example of 3D visualization of MWD DPI's by *Bever Control*, can be seen in figure 4.3.

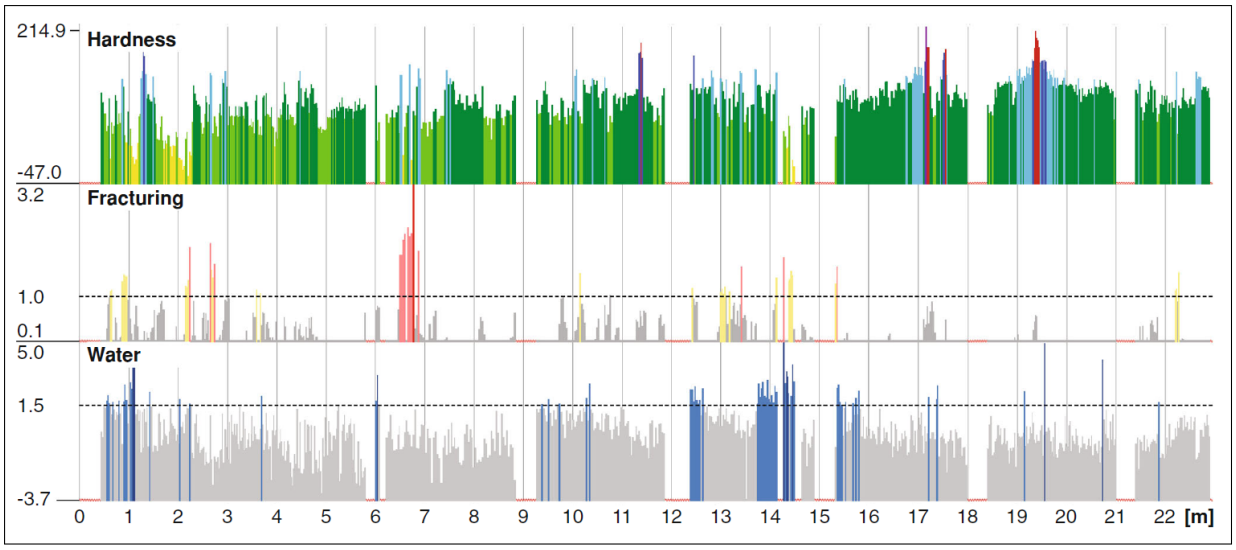


**Figure 4.2:** Graphs of different interpreted indices of the same borehole as done in the GPM+ software (taken from Høien and Nilsen (2014))

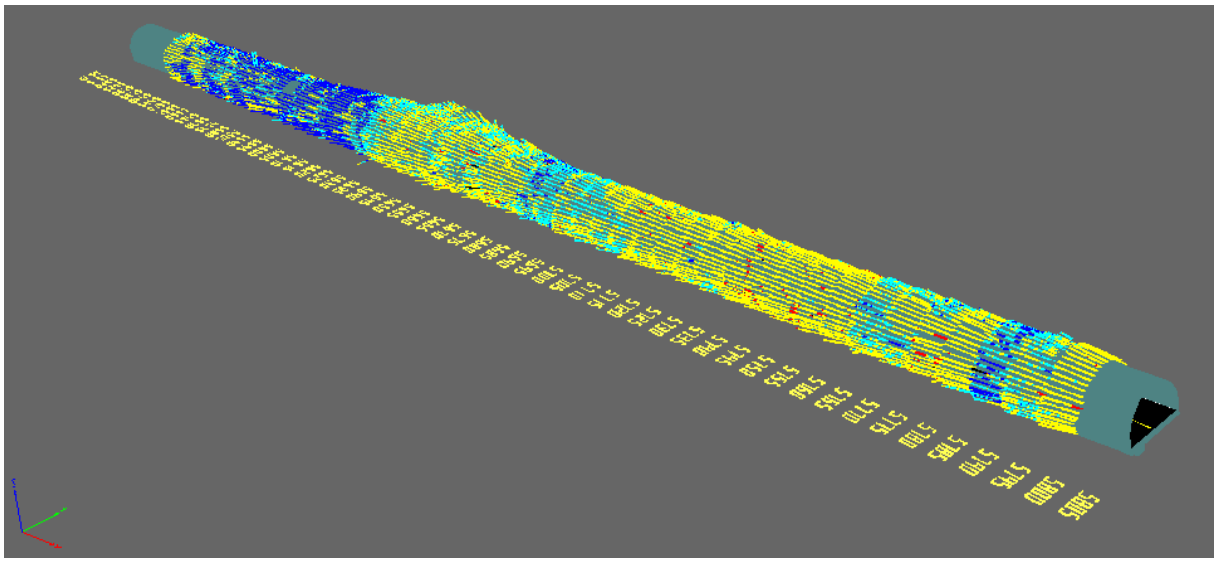

**Figure 4.3:** 3D visualisation of MWD DPI gathered at each blast round for approx. 250 m of tunnel. Color gradient indicate interpreted hardness, yellow indicate lower int. hardness (rel. weaker rock mass) while blue colors indicate higher int. hardness. (rel. stronger rock mass). Figure taken from Bever Team Online module, Fv. 659 project.

## 4.3 Limitations of MWD technology

The MWD parameters gathered from the drilling jumbos require proper calibration based on variations due to hole length, hole diameter, drill rig, and operator. Adequate calibration of the equipment, and project-specific tuning is a important for the ability to represent actual rock mass conditions with MWD DPI. Another concern regarding the practical use of MWD, especially in real time applications, is its reliance on fast and lossless data transfer solutions. An

increasing number of modern tunneling projects are now capable of providing a wireless connection at the tunnel face. This allows for real-time processing and transfer of the drilling data to off-site operators, as well as the on-site drilling operators (van Eldert et al., 2017).

There is also a lack in industry standardization, as well as secrecy surrounding how the interpreted parameters are calculated by the different MWD software providers, which often will make it difficult to compare data from different software. The resolution of MWD data with regards to sampling frequency, is an important aspect when considering the usability of the data gathered. For applications such as fracture detection, a very high sampling frequency is required. Van Eldert (2018), also discuss the differences in sampling frequencies, wherein different projects, the sampling frequency was ranging from 2-3 cm to 10-20cm between each sample. Low sample frequency may cause the loss of important properties regarding the rock mass.

Chapter 5

# Multivariate statistical methods

The different MWD parameters represents a discrete set of values collected at equal depth intervals at each borehole. While the grouting data are a set of values collected for each borehole as a discrete time series. For the purpose of analyzing these two data sets together, converting the discrete time- and depth series for each borehole to singular values for each borehole is necessary. Furthermore, it is desirable to investigate the statistical relationship between the MWD DPI- and grouting data. It becomes apparent, that a large number of data will be included for this purpose. This, along with the relatively large number of different variables with unknown interdependencies, justifies the use of multivariate analysis.

The general goal of a statistical analysis, is to evaluate the presence of a statistical relationship between a set of *response variables* (also known as dependent or outcome variables), and *predictor variables* (also known as independent or explanatory variables) (David Hosmer and Sturdivant, 2013). The response variable will produce a certain outcome, based on its relation to the predictor variable(s). In the following chapter, different multivariate statistical methods are presented for analyzing data.

## 5.1 Simple- and multiple linear regression models

### 5.1.1 Simple linear regression

To investigate the simplest form of relationship between a response variable $Y$ and a predictor $x$, consider the linear relationship:

$$Y = \beta_0 + \beta_1 x + \epsilon \tag{5.1}$$

Where $\beta_0$ and $\beta_1$ are the intercept and slope parameters (also known as the *regression coefficients*) of the *simple linear regression model*, while $\epsilon$ is called the *random error* which associates the model with some uncertainty and keeps the model from being a simply deterministic model. An important aspect in a simple regression analysis, is estimating the regression coefficients, noted: $b_0$ and $b1$, and thus deriving the *fitted regression model* described by the regression line:

$$y = b_0 + b_1 x + e_i \tag{5.2}$$

Where $y$ is the predicted value according to the linear regression model and $e_i$ are the residual error which essentially is a reflection of the fitting error. It is expected that the fitted line lies close to the true regression line (5.1) when a large number of data points are analyzed (Walpole et al., 2011).

### 5.1.2 Multiple linear regression

Multiple Linear Regression (MLR) becomes a relevant approach when more than one variable is considered in the model (multivariate). In the case of $k$-number of independent variable: $x_1, x_2, x_3, ..., x_k$, the estimated response variable $y$ is given by the regression equation:

$$y = b_0 + b_1 x_1 + ... + b_k x_k \tag{5.3}$$

Here, similarly to linear regression (equation 5.2), $b_k$ are estimated from the data using least squares approximation.

### 5.1.3 Correlation

The strength of relationships between one response variable and one (or more) predictor variables can be established through *correlation analysis*, which seeks to derive a singular value

named the *correlation coefficient*, quantifying the statistical strength of the relationship. Widely used correlation coefficients in regression modeling, are the *Pearson correlation coefficient* - $r_p$, *Spearman correlation coefficient* - $r_s$ and the *sample coefficient of determination* or simply *R-squared* - $r^2$ (Walpole et al., 2011).

## Pearson correlation coefficient

One common method for quantifying the strength of any linear dependency, is by establishing the *Person correlation coefficient* $r_p$. The basic purpose is to draw a line through some $x$ and $y$ scattered data, so that the total distance between the line and all the scattered data are kept as small as possible. Establishing the coefficient $r_p$ between two arbitrary variables $x$ and $y$, is defined by:

$$r_p = \frac{\sum_{i=1}^{n} x_i y_i}{\sqrt{\sum_{i=1}^{n} x_i^2 \sum_{i=1}^{n} y_i^2}} \tag{5.4}$$

Equation 5.4 implies that when the plotted points lie close to a straight line, $r_p$ will be high (closer to 1.0 or -1.0) and vice versa (Walpole et al., 2011). The interpretation of correlation coefficients is somewhat different depending on which context and data they are representing, but a general "rule of thumb" approach can be seen in table 5.1.

| Correlation coefficient | Interpretation |
|---|---|
| 1.0 to 0.9 or -0.9 to -1.0 | Very high correlation |
| 0.7 to 0.9 or -0.9 to -0.7 | High correlation |
| 0.5 to 0.7 or -0.7 to -0,5 | Moderate correlation |
| 0.3 to 0.5 or -0.5 to -0.3 | Low correlation |
| 0.0 to 0.3 or -0.3 to 0.0 | Negligible to very low correlation |

**Table 5.1:** General basis for interpreting correlation coefficients.

## Spearman rank correlation coefficient

Spearman rank correlation coefficient $r_s$, is an example of a *rank correlation coefficient*. The basis for finding $r_s$ is based on the same equation as for $r_p$, only with $x$ and $y$ observations *ranked* 1,2,...,$n$, by order of magnitude (Walpole et al., 2011). If no ties (similar values) are present in the ranked data, $r_s$ can be simplified to:

$$r_s = 1 - \frac{6}{n(n^2-1)} \sum_{i=1}^{n} d_i^2 \tag{5.5}$$

Where $d_i$ is given by the difference between $x_i$ and $y_i$ at each corresponding rank, and $n$ is the number of data pairs (Walpole et al., 2011). This method becomes useful when dealing with *monotonic* relationships rather than strictly linear relationships. A monotonic function is a function which either always increases or decreases, in either a linear or nonlinear way. The idea is that this non-parametric method will capture any non-linear monotonic trends between two variables. The $r_s$ value will often be similar to $r_p$ (if the relationship is linear), and can be interpreted in a similar way (see table 5.1).

### R-squared

*R-squared* or $r^2$, is a measure of how much of the variability in it's response ($y$) is explained by the model, defined by:

$$r^2 = \frac{{S_{xy}}^2}{S_{xx}S_{yy}} = \frac{SSR}{S_{yy}} \quad , \quad S_{xy} = \sum_{i=1}^{n}(x_i - \overline{x})(y_i - \overline{y}) \tag{5.6}$$

Where $SRR$ is called the *regression sum of squares*, and indicate the amount of variation explained by the $y$-variables (Walpole et al., 2011). $r^2$ values close to 1.0, means that close to $100\%$ of the total variation observed can be explained by the linear relationship between the two variables i.e. the model is able to predict with high accuracy.

T-test statistics are usually performed to check the statistical significance of the linear regression model parameters, that is its slope and intercept. Usually, the test is deemed significant at p-values < 0.05.

## 5.2 Logistic regression

Often the response/outcome variable will be discrete and categorical, taking on either two possible values or *binary* e.g. (yes, no or true, false) or a multiple set values or *dichotomous* e.g (low, medium, high). Fitting a regression model to these variables together with some continuous predictor variable (or multiple continuous variables the case of multiple logistic regression), the use of *logical regression* becomes applicable (David Hosmer and Sturdivant, 2013).

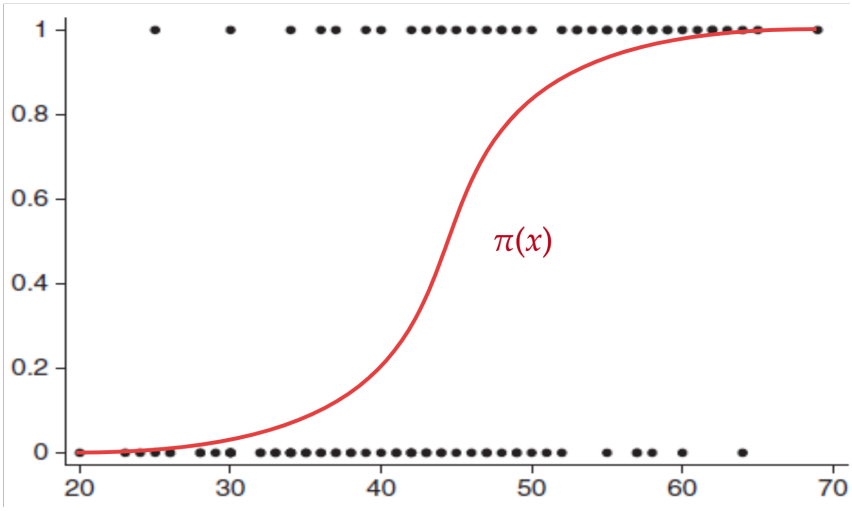


**Figure 5.1:** Example of fitting a logistic function $\pi(x)$ to a scatterplot of binary response variable (0 or 1) and continuous explanatory variables along the $x$-axis. Figure modified from David Hosmer and Sturdivant (2013).

Considering figure 5.1, the fitted regression line takes on the shape of a *logistic function*. The logistic regression function is defined by:

$$\pi(x) = \frac{e^{\beta_0+\beta_1 x}}{1 + e_0^{\beta} + \beta_1 x} \quad , \quad g(x) = \ln\left[\frac{\pi(x)}{1-\pi(x)}\right] = \beta_0 + \beta_1 x \tag{5.7}$$

The transformed logistic function $g(x)$ in equation 5.7, is also referred to as the *logit function*, it allows the regression model to be constrained to yield values between zero and one, which satisfies the binary nature of the outcome variable. Many of the same principles used in simple linear regression also translates to logistic regression, however, there are differences in terms of fitting the regression model in logistic regression. When fitting the model In linear regression, it is common to rely on the method of *least sum of squares* approximation to approximate values for $\beta_0$ and $\beta_1$, as previously stated. In logistic regression the same method does not apply, the method for estimating the parameters of a logistic regression model relies on the *likelihood function*, which derive maximum likelihood estimates that agree mostly with the observed data (David Hosmer and Sturdivant, 2013).

Testing statistical significance of logical regression models, is usually done using *chi-square distributions, Wald's test* or the *Score test*. This involves testing if the response variable is *significantly* related to the predictor variables (David Hosmer and Sturdivant, 2013).

### Multiple logistic regression

Logistic regression models can also be applied when dealing with more that *one* predictor variable, just like when considering linear regression models. Similar to equation 5.7, the logit function for multiple logistic regression becomes:

$$g(x) = \ln\left[\frac{\pi(x)}{1-\pi(x)}\right] = \beta_0 + \beta_1 x_1 + \beta_2 x_2 + ... + \beta_n x_n \tag{5.8}$$

Where $n$ is the number of predictor variables $x$, and $\beta_n$ the regression coefficients which we want to estimate through model fitting. The method for fitting involves estimating the $\beta$-coefficients, using likelihood functions as previously described. Testing for statistical significance for multiple logistical regression models is essentially the same as previously stated as for the univariate models (David Hosmer and Sturdivant, 2013).

## 5.2.1 Logistic regression as a predictive tool

Logical regression modeling is widely used as a machine learning application, more precisely, it is used as a *supervised binary classification tool*, to help predict some binary outcome variable using continuous predictor variables. For implementing logical regression as a binary classifier, *scikit learn's* `linear_model.LogisticRegression()`, Python module can be used (Pedregosa et al., 2011).

The basic idea is to fit logistic model based on some *training data*, which is represented by the $n$-number of predictor variables $x$ (also referred to as *features*), together with its corresponding response variables - $y$ (also referred to as *target*). The trained model is then used to predict values that are compared to the *test data* (Albon, 2018). Usually, the dataset is split in two, in which 75% is used as training data ($x$ and $y$ variables) to train the model, then the remaining 25% of data is used as test data (data the model has not seen before) to evaluate the performance of the model. Where a good model is a model that is able to accurately predict a large portion of the test data. The test data is not involved in actual training of the model, and is important to establish a benchmark for the overall performance of the model.

| | |
|---|---|
| **0**'s correctly predicted *(True negative)* | **0**'s wrongly predicted*(False positive)* |
| **1**'s wrongly predicted*(False negative)* | **1**'s correctly predicted *(True positive)* |

**Table 5.2:** Concussion matrix, showing the number of correct and wrong predictions for each case. Blue cells indicate correct predictions.

According to (Albon, 2018), the fitted models predictive power can be evaluated by investigating multiple metrics, such as: *confusion matrix*, *recall*, *precision*, and *accuracy*.

- A *confusion matrix* will give some information on the accuracy of the model in terms of which observation in the test data that were accurately predicted, and likewise which observations were wrongfully predicted; In the same way as presented in table 5.2, blue cells (main diagonal) are indicating the number of correct predictions.
- The *precision* metric relates to the confusion matrix and shows what percentages each instant (1 or 0) that were accurately predicted. Top right and lower left are also called type I and type II errors, both representing unwanted prediction outcomes. Both false negatives or false positives could represent the most unwanted prediction outcome depending on the target variable.
- The *accuracy* metric is given as a value between 0 and 1, where values closer to 1 are better, indicating the models overall prediction accuracy.
- *Recall* is a measure of the model's ability or "confidence" in correctly predicting positive targets (i.e. 1's). With a high recall metric, the model is highly confident in predicting the target in question.

Another useful method for evaluating the overall quality of a binary classifier, which includes logistic regression, is the *Receiving Operating Characteristic curve* (*ROC* curve) (Albon, 2018). This curve visualizes the performance of the model by showing the rate of which the model makes wrongly predicted 0's (False positive) and correctly predicted 1's (True positive) (i.e. right top and bottom values in the concussion matrix 5.2). An example of a ROC curve can be seen in figure 5.2. The orange stapled line shows the linear trend of a random predictor i.e. a model which does prediction based on pure guessing. The gray line illustrates the perfect predictor, which predicts with 100% accuracy. The blue line is the ROC curve representing the model, the closer it aligns with the gray line and the more it deviates from the orange line, the better predictive performance of the model.

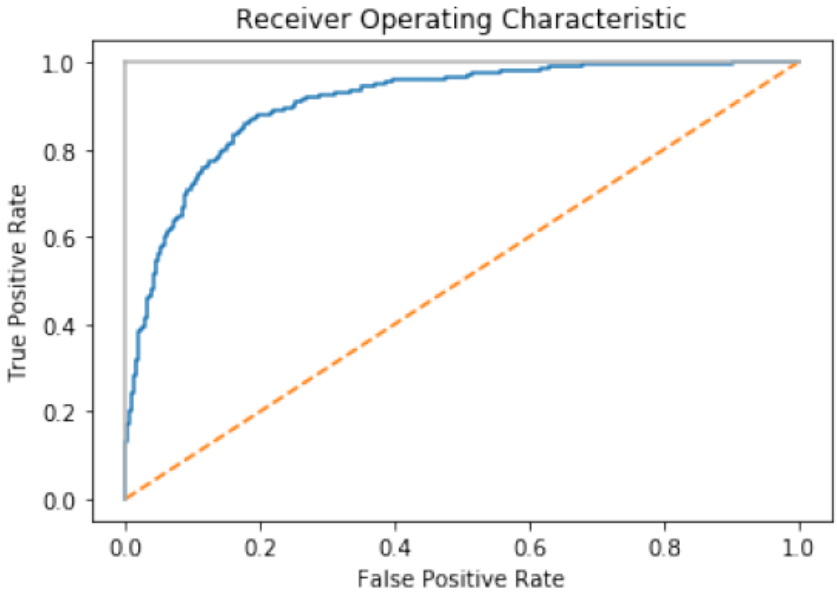


**Figure 5.2:** ROC curve in blue, gray line indicates 100% predictive accuracy. ROC curves with large deviations from the linear trend line (orange) indicate good predictive performance of the model. Figure taken from Albon (2018).

The model parameters can then be tuned in an attempt to improve its predictive performance. Tuning binary classifiers are mainly done through *regularization*, regularization techniques prohibits the models from becoming to complex by *penalizing* or constraining them. In other words, it is a minimization technique to reduce the overall variance of the model. The main parameter for tuning regularization strength is the $C$-parameter, which establishes how strong the applied regularization is, with high values corresponding to less regularization (more complex models) and low $C$-values corresponding to stronger regularization (less complex models). Regularization will follow a specified penalty function, called *l1* and *l2* (Albon, 2018).

## Limitations of logistic regression models

Limitation of using logistic regression as binary classifier includes:

- Sensitivity to *overfitting*. Overfitting is the term used when the model becomes too complex in fitting a model according to some training data, i.e. not being able to detect underlying tendencies in the data. This effectively limits its robustness in predicting future observations. This is often due to the presence of too much noise in the predictor variables, or simply too many predictors. Regularization is a method to penalize the overfitting by minimizing the complexity of the model (Albon, 2018).

- The performance of the fitted model tends to *not perform* very well when the explanatory variables are not correlated to the response variable, and if the explanatory variables are too similar to each other i.e. highly correlated. The solution to this is often to simply remove one of the explanatory variables that are highly correlated with each other (Albon, 2018).

### 5.2.2 Cross validation for model testing

A robust method for evaluating the performance logistic regression, including any other machine learning model, is *K-fold cross-validation*. Cross-validation allows for testing a model's performance by splitting the data into *K*-number of *folds* of data into testing- and training data, and then preceding with testing based on each of the splits through iteration. E.g. test run with 5 K-Folds, this means that data will be divided into 5 parts, with 1/5 of the data set of for model training and the remaining 4/5 used for testing. This is done through iteration such that all of the data sets are tested through i.e. 5 iterations yielding 5 different performance metrics (see figure 5.3). This allows for testing the model multiple times on different parts of the data and is, therefore, often considered more robust than simply training and testing on a given portion of the data set (Müller et al., 2016).

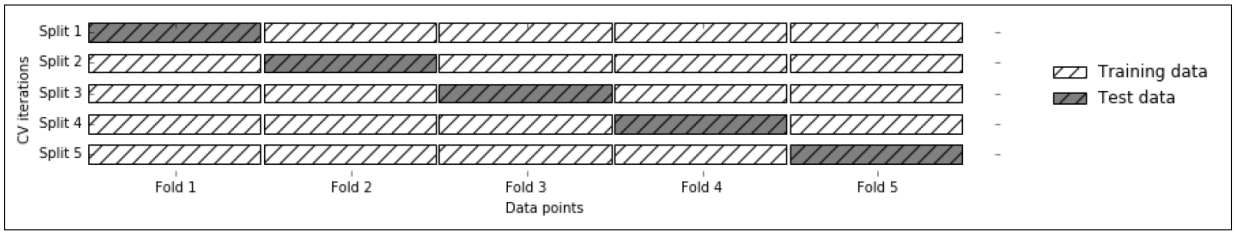


**Figure 5.3:** Example of 5-fold, where the sample data is split into 5 parts, resulting in model train/testing 5 times through iteration. Figure taken from Müller et al. (2016).

## 5.3 Principal component analysis

Principal component analysis (PCA) is a widely used statistical method for analyzing multivariate scenarios, as it has many useful appliances when dealing with many variables. The PCA utilizes algebraic transformation of initial correlated variable distribution, into uncorrelated principal components based on the original variables. The main goal is to condense the variables into new factors or components which explain a maximal portion of the total variance between the initial variables. Thus, retaining the maximal amount of information explained by the variables, while at the same time reducing the number of variables (Wackernagel, 2013). PCA has many applications, including:

- *Dimensionality reduction*, PCA can greatly reduce the number of variables that is to be used in further analysis through transformation into uncorrelated components (Barnett, 2017).
- *Data correlation*, PCA can be used to investigate the correlation matrix and loading plots to evaluate the correlation between a large number of variables.
- *Data visualization and outlier detection*, by interpreting the PCA score plots, detecting similarities and outliers among the observations is possible.

The PCA performs rotational transformation to define a new coordinate system for the original data, called *principal components*, preserving as much of the variance or *information* from the initial variables as possible. Before applying PCA, *standardization* of the initial variables is needed, which involves transforming the variables to have a mean of 0, and variance of 1. A visual example of the PCA transformation is shown in figure 5.4, in this example, the dimensionality of the initial 3-dimensional data is not reduced but preserved through three principal components. The Figure shows the rotation of initial variables into a new coordination system. The same principle can be used for higher-dimensional data (more than 3), where visualization becomes difficult. The principal components that contribute little towards variability explained can, in that case, be dropped. To help consider which principal component should be dropped, one can utilize the *scree plots*. The scree plots show the amount of variance explained within the different principal components. Figure 5.5, shows an example of a *scree plot* corresponding to figure 5.4, it can be seen that PC1 and PC2 together contribute to about 90% of the total variance explained by the model, suggesting PC3 can be dropped without loss of too much information.

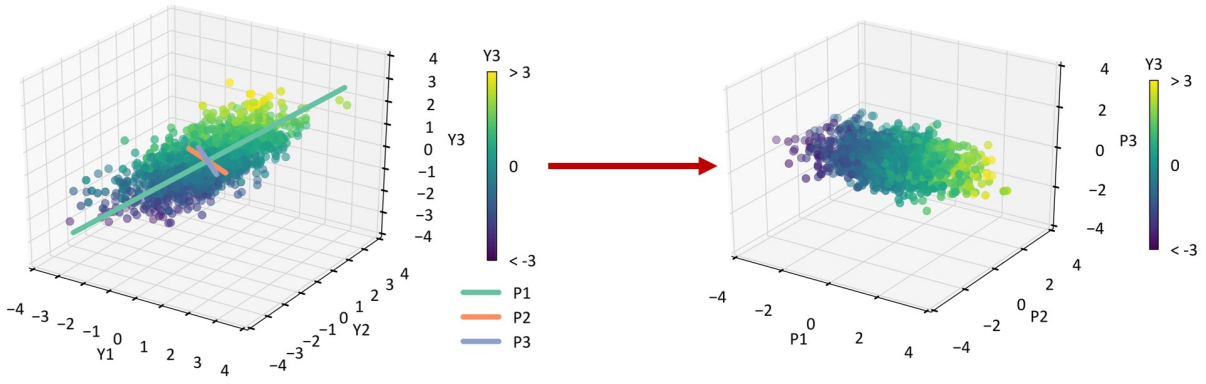


**Figure 5.4:** Figure visualizing the PCA transformation of data: from original data on the *left*, to principal components explaining the most variance in data (PC1) to least variance (PC3) on the *right*. Note the new orientation of the data, in this PCA example, dimensionality is not reduced. Figure taken from Barnett (2017).

The result of running PCA on a data set is called the *scores* (see right plot of figure 5.4). The scores are the actual results of the PCA transformation on the dataset (Bro and Smilde, 2014). The scores represent the same observations present within the original data set, after PCA transformation, and can be interpreted and visualized in many ways. A plot over the PCA scores is called a *score plot*, and will often reveal clustering and similarities within the data, and is very useful for data visualization. The principal component *loadings*, are unit vectors explaining which linear combination of variables relates to a particular principal component (Bro and Smilde, 2014). In other words, the loadings reflect how much variance each initial variable represent in terms of the different principal components, an example of loading vectors visualized in the same principal component space can be seen in figure 5.6. Loadings are useful to better understand what initial variables the different components represent. A *biplot* is essentially combining the loading vectors with the scores in the same plotting space.

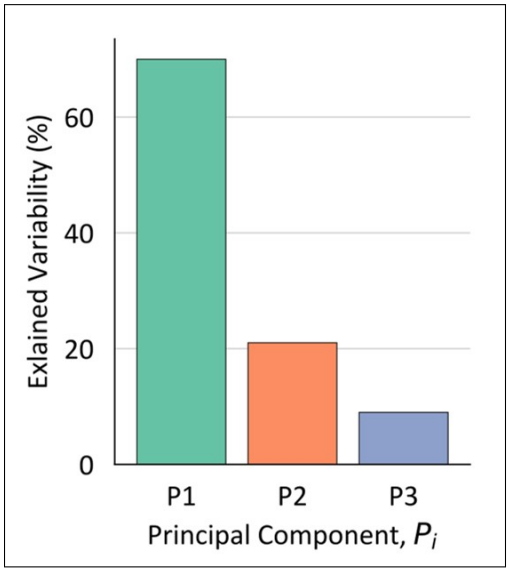


**Figure 5.5:** Example scree plot, showing the explained variance for each principal component. Figure taken from Barnett (2017).

### 5.3.1 PCA assumptions

To asses if PCA is applicable for any given dataset, some assumptions must be evaluated before moving forward with PCA. Schumacker (2015), discusses some assumptions that need to be assessed:

- As an obvious prerequisite, the dataset should consist of multiple variables with continuous values. One can argue that the full strength of PCA is realized when a large number of different variables are considered. There should also exist a certain *linear relationship* between these variables, even if the correlation is very low. This is because PCA is based around the Pearson correlation coefficients to reduce the number of variables (dimensionality reduction). To evaluate this assumption, one can check if the determinant of the *correlation matrix - M* is positive ($det(R) > 0$). Where R is the correlation matrix, a positive determinant indicates that there is some linear dependency present between the variables. In the unlikely case of perfect linear dependency (correlation of 1 between all the variables), $det(R)$ would be zero, indicating that multicollinearity is likely present i.e. the independent variables are highly correlated with each other. To evaluate if a statistical significant correlation is present, it is also suggested to check the *spherisity* by using the *Bartlett Test*. This test statistic check if the correlations are present in the correlation matrix, and if they are statistically significant ($p - value < 0.05$).

- The dataset should have *sampling adequacy*, meaning that in order for PCA to produce a reliable result, a large enough sampling space should be available. The sample adequacy is often tested using a test called KMO - *Kaiser-Meyer-Olkin*, which is a criterion for sampling adequacy. There exist different rules of thumb for what is considered "adequate" sampling, the general belief is that a KMO > 0.5-0.6 is considered adequate and reflects that there is a sufficient sample size for conducting PCA.

- The dataset should not have a significant amount of *outliers*, this is because a large number of outliers will have an irregular influence on the PCA results. However, there exist methods to detect and exclude outliers in datasets. In this thesis, *Support Vector Machines* (SVM), is used for outlier detection of the PCA results. SVM is a machine learning technique used for outlier/novelty detection, based on learning the expected distribution of any given dataset Meyer and Wien (2001). SVM needs tuning of some key parameters which have to be set properly if it is used for outlier detection, namely $gamma-$ and

$nu-$parameter. the $gamma-$parameter helps the algorithm to approximate the distribution in which to base the outlier detection on, where a value of 0 tells it to approximate the distribution. $nu$ tells the algorithm what percentage of outliers that can be expected from the dataset, a value of 0.05-0.06 is often used for outlier detection.

That being said, a violation of any of these assumptions does not reject the use of PCA as a whole. E.g. for data visualization and discovering patterns in the data. When using PCA for dimensionality reduction, these assumptions become more important, as the analysis outcome becomes more stable and reliable if the assumptions are validated. For this thesis, PCA was done using the Python library *scikit-learn*. KMO and Bartlett's test was done using the *factor-analyzer* Python module.

### 5.3.2 PCA limitations

Some limitations to consider when applying PCA, include:

- *Interpretation challenges*: Due to the process of scaling, normalizing, and transformation into principal components. The data is transformed many times, both through initial scaling of variables and the subsequent transformation of variables into principal components. This makes the final PCA result somewhat difficult to compare to the initial variables, especially when dealing with many variables.
- *Information loss*: When using a large number of variables, the transformation into principal components will result in a lot of information loss. Even though the main goal is to preserve a large portion of the *explained variance* of the original dataset, there will often be a considerable information loss due to dimensionality reduction.

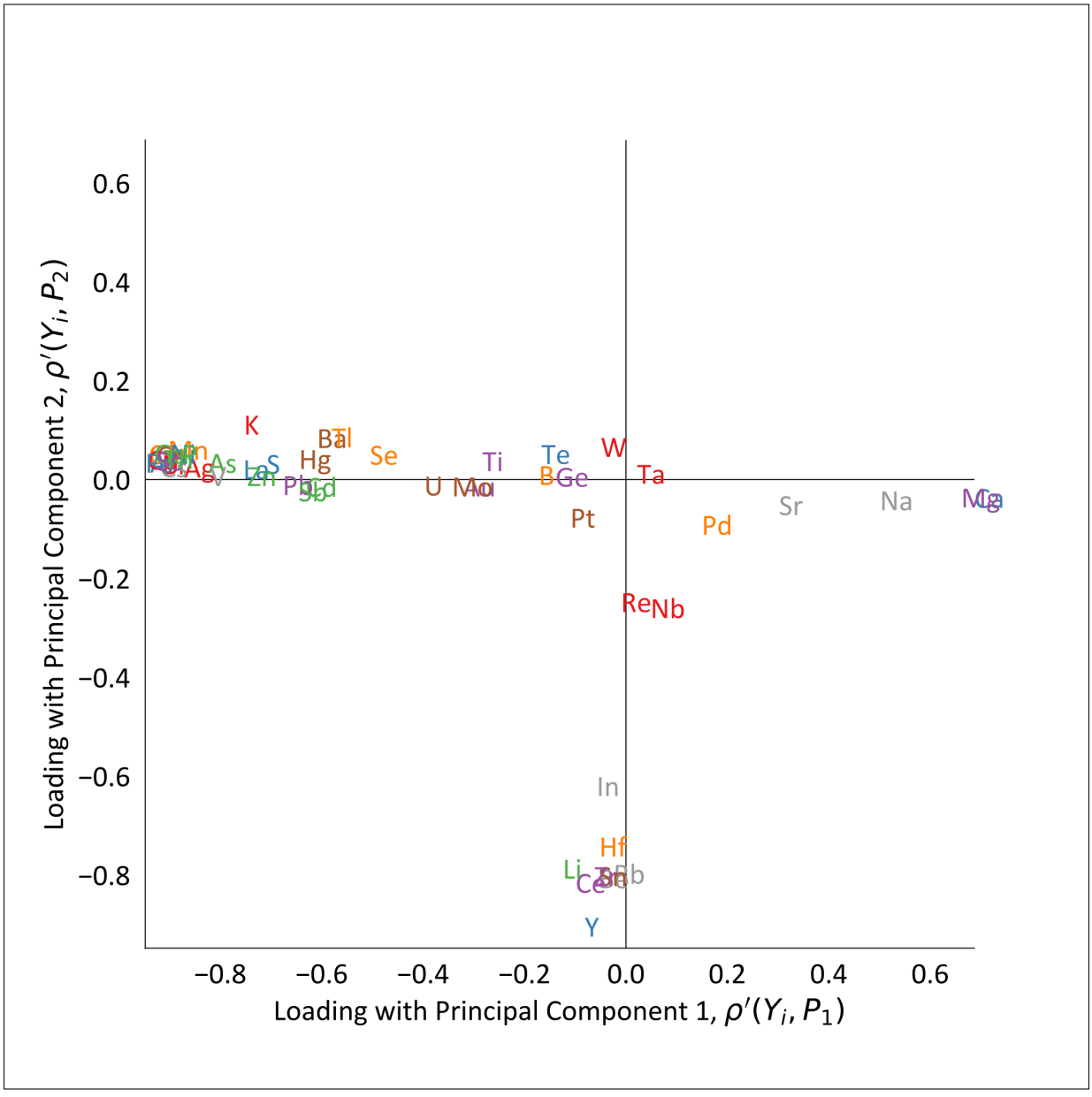


**Figure 5.6:** Example loading plot, showing the loading vector (without arrows), depicting each variables influence on the principle components (in this example being the influence from each element). Figure taken from Barnett (2017).

Chapter 6

# Project site description and methods for data gathering

## 6.1 Project description

To gather MWD- and grouting data for further data analysis, data from an ongoing (2020) infrastructure project is used, namely *Fv.659 Nordøyvegen*. The project is located in the "Møre og Romsdalen" county in northwestern Norway (see figure 6.1). It is a large infrastructure project comprising of new roads, land reclamation, three bridges, one smaller landbased tunnel, and three subsea tunnels. This will serve as mainland connection for about 2900 residents of the five islands: Lepsøya, Haramsøya, Skuløya, Fjørtoft, and Harøya. For this thesis, data from two different worksites were gathered, namely: *Longva*, which is the north-going tunnel worksite at "Nogvafjordtunnelen", and *Austnes*, which is south-going tunnel worksite at "Haramsfjordtunnelen" (see figure 6.1).

The project comprises a total of 6 contracts, of which the main contract -K5 (which also includes all the tunnels), is engaged by the turnkey contractor *Skanska Norge AS*, other smaller contracts from this project are mainly represented by smaller, local contractors. The building was started in 2017, and it's estimated to be completed by 2022. The total cost for the whole project is estimated to be around 4.9 BN NOK (NPRA, 2010).

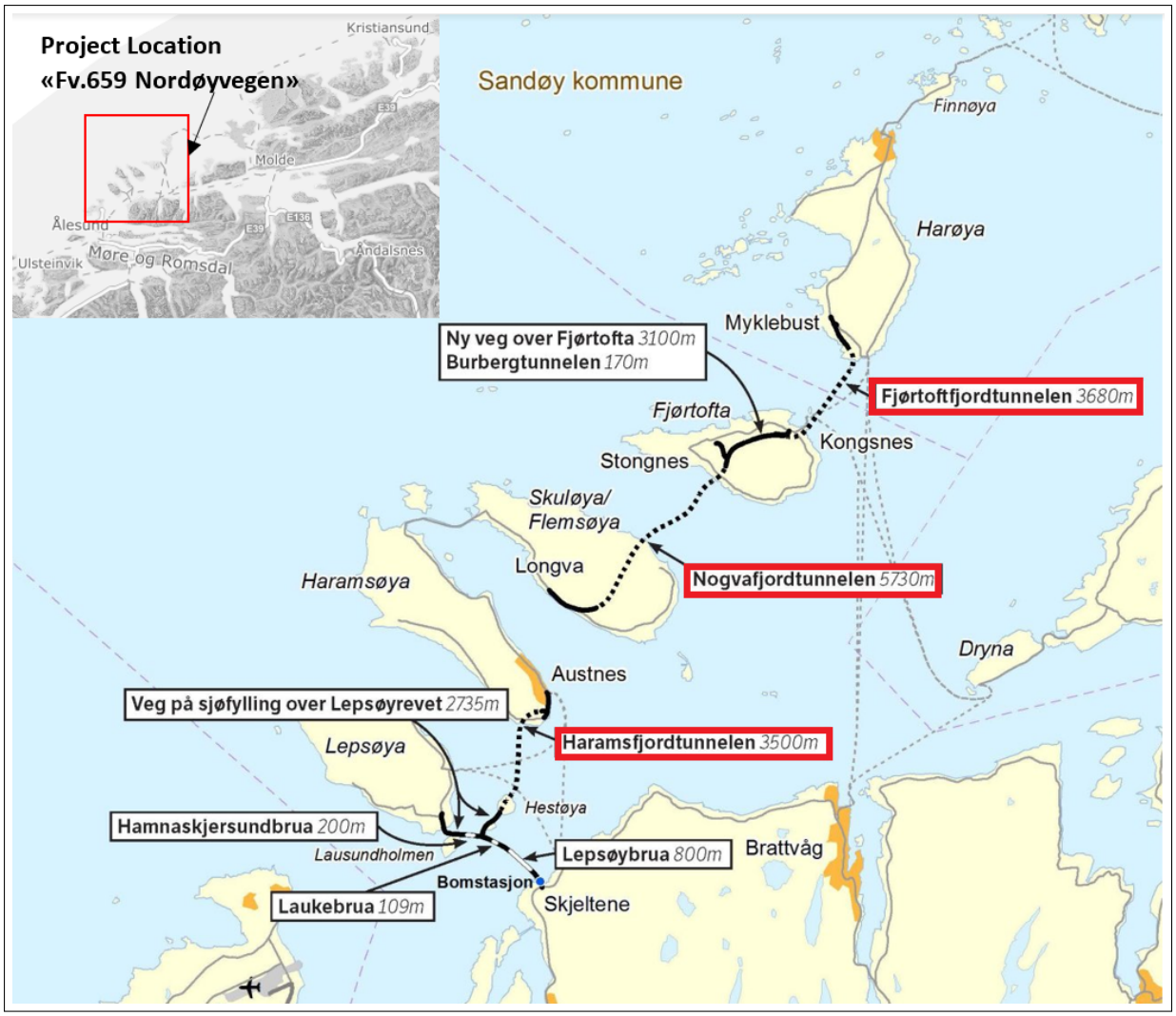


**Figure 6.1:** Location of the project Fv.659 Nordøyvegen, including location and names of the three subsea tunnels shown in red markings. Map modified from NPRA (2010).

### 6.1.1 Regional geology and engineering geology

In conjunction with the planned tunneling activity that this project included. Structural geological- and bedrock mapping was carried out as early as in June 2011, by Norwegian Geological Survey (NGU) on behalf of the Norwegian Public Roads Administration (NPRA) (Ganerød and Lutro, 2011). The bedrock geology of these islands is characteristic of the *Western Gneiss Region*. The islands were first mapped systematically by NGU in the years between 1995 and 2002, and bedrock geology in the preliminary NGU rapport is mainly based on these mappings.

The bedrock of Skuløya consists of very deformed rock which can be described as "dioritic and migmatitic gneiss". The bedrock of the three southernmost islands: Skuløya, Haramsøya, and Lepsøya also consist of "granitic gneisses" with "eclogite lenses" and sporadic introduc-

tion of "mafic intrusions" (Ganerød and Lutro, 2011). Since these rock types are so heavily deformed, it is estimated that the variation in terms of rock mass quality and rock mechanical properties of the different rock types are difficult to estimate. Problematic rock mass conditions for the tunnel construction include unfavorable sub-vertical orientation of the rock mass foliation/intrusions, which could lead to increased inflow of water where tunnel overburden is small (Ganerød and Lutro, 2011). Full bedrock geology map can be seen in figure 6.2.

In addition to the preliminary geological mapping, more detailed knowledge of the geological properties and features including soil thickness along the seabed, was gathered by geophysical mapping carried out by NGU. The geophysical methods included airborne magnetic surveying and interferometric bathymetry surveying (John F. Dehls and Rønning, 2012). The magnetic method was mainly for weakness-zone interpretation, localization, and characterization. Interferometric sonar was used to map the seabed bathymetry oriented around the 3 planned subsea tunneling paths. In addition to this, results from refraction seismic conducted prior to this mapping were used in establishing potentially problematic areas and weakness-zones. Important concluding remarks from the geophysical report, include the identification of at least three larger interpreted weakness-zones that intersects with the planned tunnel paths (see figure 6.3). One of these adverse zones was identified at the crossing between Skuløya and Fjørtoft (Nogvagjord-tunnel), two zones were identified at the crossing between Fjørtofta and Harøya (Fjørtoft-tunnel), and multiple smaller zones at the crossing between Haramsøya and Lepsøya (Haramsfjord-tunnel). The three zones are characterized as "poor quality rock mass", with seismic velocities ranging from 3400 to 4000 m/s (see figure 6.3) (John F. Dehls and Rønning, 2012). One of these interpreted weakness-zones will be used to verify the response of the MWD DPI (see section 8.1).

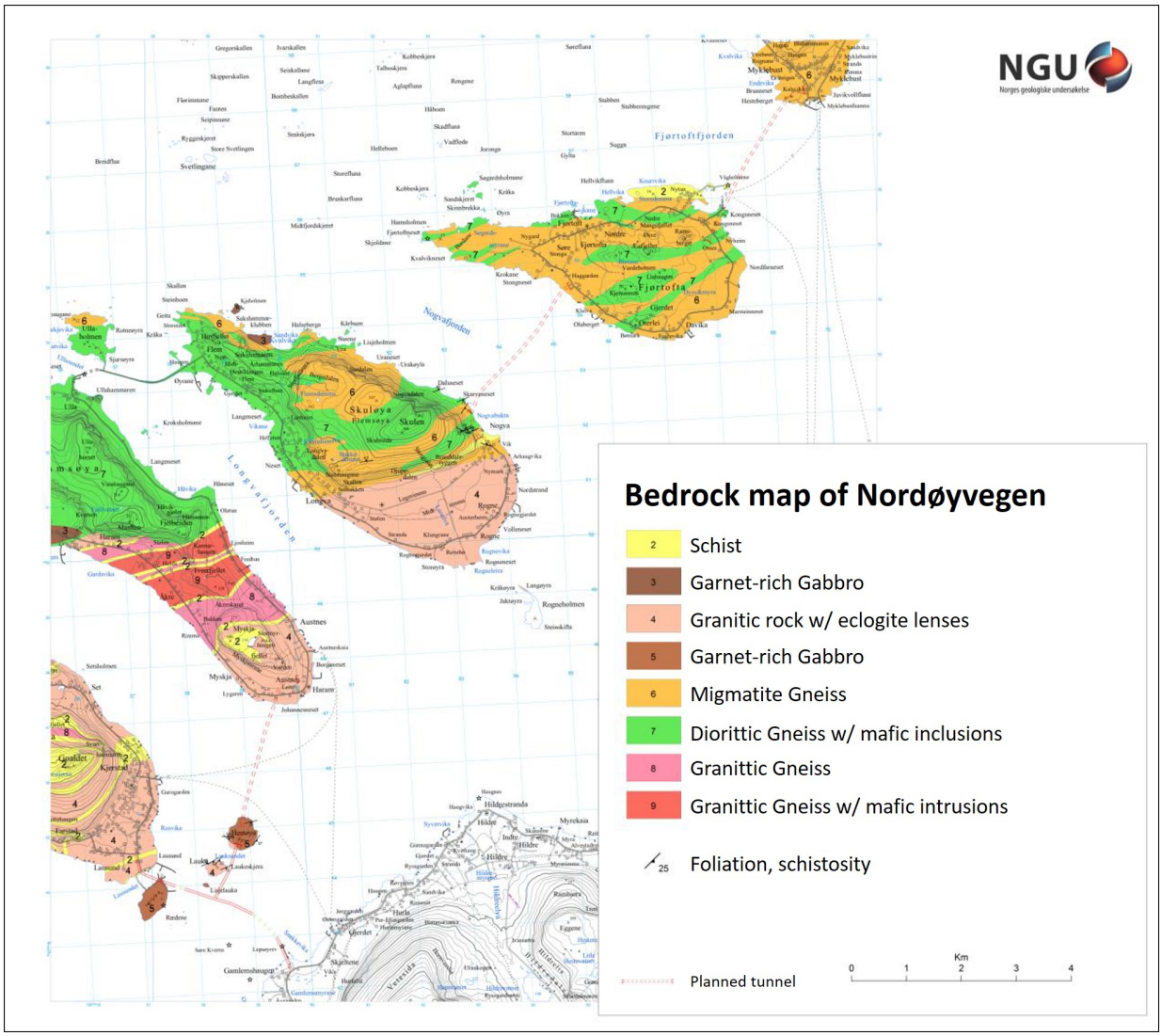


**Figure 6.2:** Bedrock geology of the area relevant to Fv.659 Nordøyvegen. Figure modified from Ganerød and Lutro (2011).

## 6.2 Data gathering, processing, and management

A database for both MWD- and grouting data was established in *Excel* for easy data entry, which was then converted to a .csv-file for further analyses. The database entries included descriptions on each hole: worksite, chainage number, hole number, and logging depth, including different columns for actual MWD DPI- and grouting data. The full database is presented in appendix A. An important aspect if the data analysis was the ability to collect as much data as possible, as well as retrieving representative data for each borehole, without missing or defective data. To combine the two data sets, both the MWD DPI- and grouting data needed to be matching their respective borehole. Data gathering and processing for both MWD and grouting data are presented in the next two subsections.

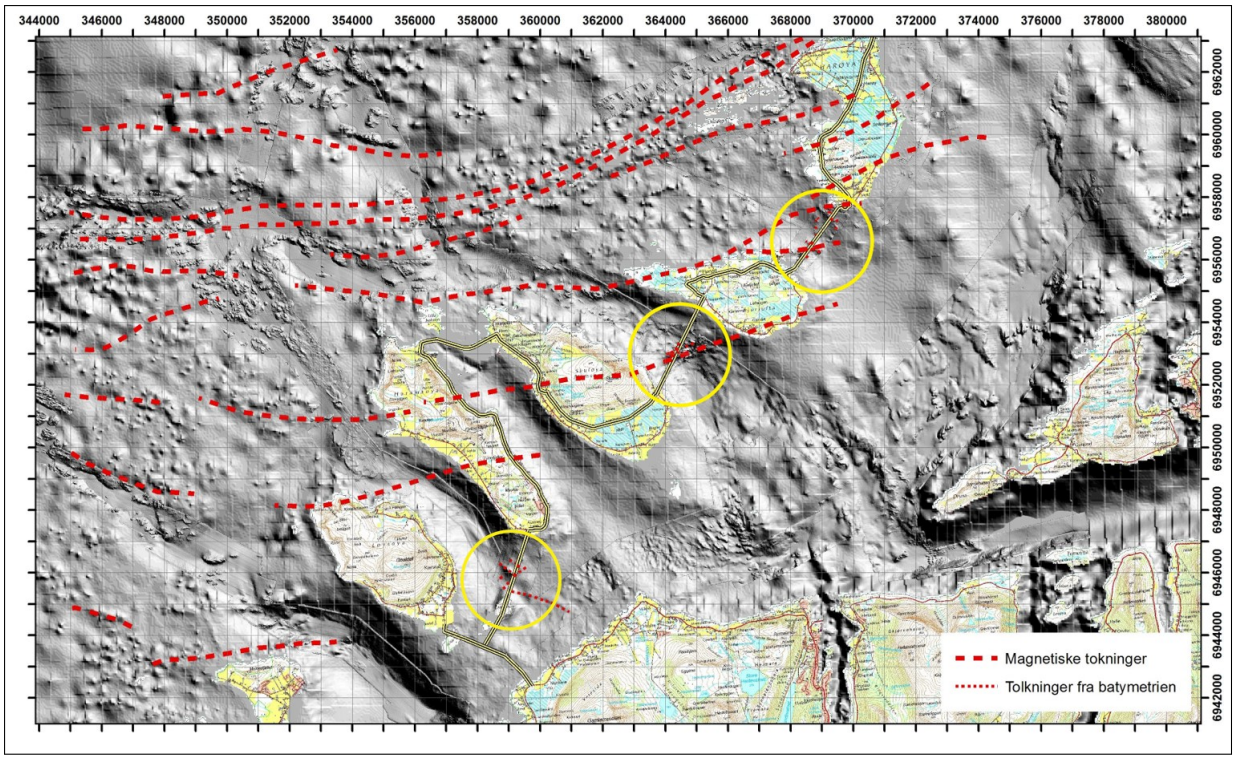


**Figure 6.3:** Schematic map illustrating positions and lateral extent of interpreted weakness-zones, intersection with planned tunneling paths are indicated with green circles. Map taken from John F. Dehls and Rønning (2012).

### 6.2.1 MWD data

The MWD data used are gathered from the Fv.659 project via the Bever Team Online (BTO) project module of Fv.659 Nordøyvegen, provided by Bever Control (Bever Control AS, 2019). BTO is a web-based solution for storing and visualizing as-built project data, which are available within the web browsing environment (see figure 6.4). BTO provides real-time monitoring of the production advance, as well as access to as-built geometry-files and drilling logs for each blast rounds and grout curtains.

The drilling logs include a hole description for each hole, including the actual MWD data logged with a typical sampling resolution of ca. $3\,\mathrm{cm}$ between each measurement. MWD logging is typically started after 0.6 m of drilling, this is done to minimize the influence of rock mass disturbed by blasting, and to avoid the unrepresentative measurements at the start of drilling. A summary of the data available in the drilling logs is shown in table 6.1.

The Excel drilling logs were organized in such a way that drilling data for each hole, were presented on different Excel-sheets. Each borehole (Excel sheet) consisted of data series with around 800 data points for each parameter (column 2 and 3, table 6.1), depending on the length

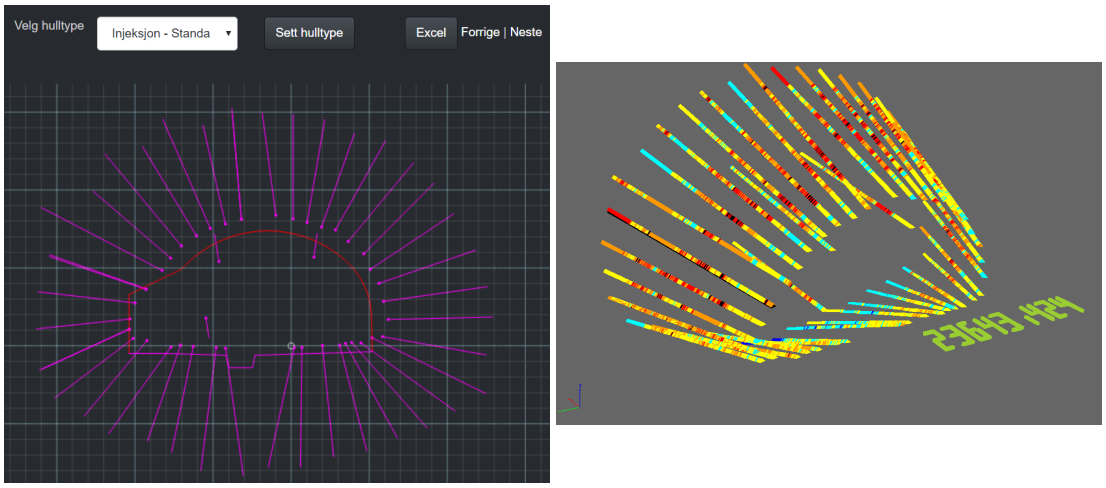


**Figure 6.4:** Snippet from BTO, left figure showing 2D presentation of a grout curtain at chainage nr. 23643. Individual or multiple borehole can be selected for export to *Excel* as drill logs. Right figure shows the same grout curtain visualized in 3D with interpreted hardness as colorized texture for each borehole.

of the borehole (which is usually between 24 and 30 meters for grouting holes). A visual inspection of the MWD data for each hole was made to ensure that the drilling logs were not lacking data. An example of a borehole with insufficient logging together with a sufficiently logged hole can be seen in figure 6.5. Boreholes with approximately > 70% missing data were *excluded* altogether for further use. The hole-numbering of the MWD data had to be compared with that of the grouting reports, to ensure that all holes were present and matched the hole numbering which was described in the grouting reports (see figure 6.6).

To ready the MWD DPI data for the data analysis, it had to be efficiently collected and processed from the Excel drilling logs. A Python script using *PyCharm* as IDE, was written to read a whole .xlsx-file, iterate through each sheet, and extract the MWD DPI data (see table 6.1, column 3). As previously stated, it was desirable to condense each borehole to a *singular value*, similar to the methods presented in Høien and Nilsen (2014). The script allows for much

| Hole description | Raw drilling parameters | Interpreted parameters |
|---|---|---|
| Tunnel chainage (nr.) | Depth (m) | Depth (m) |
| Hole type (e.g. blasthole) | Penetration (m/min) | Int. Hardness |
| Hole coordinates (X,Y,Z) | Rotation pressure (bar) | Int. Fracturing |
| Start- and stop data and time | Feeder pressure (bar) | Int. Water |
| | Hammer pressure (bar) | |
| | Rotation speed (rpm) | |

**Table 6.1:** Table of the different MWD DPI-parameters available in the drilling logs.

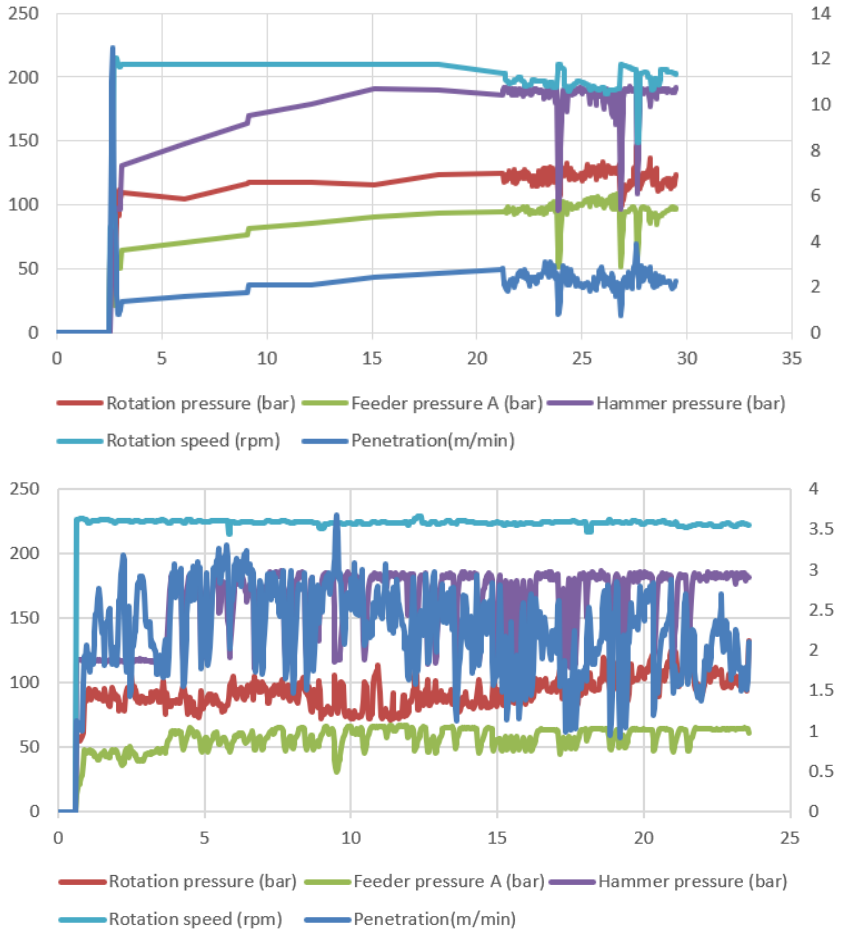


**Figure 6.5:** The top figure shows a typical drill log with lacking data, the bottom figure shows a drill log with complete data. Data example is showing MWD raw data, not DPI's. Graphs taken from the Excel drilling logs (Bever Control AS, 2019).

flexibility in terms of extracting and processing the data as wished. The output of the script provides singular descriptive values for each interpreted parameter for each borehole in a grout curtain, including: *hole number, mean, max, min, standard deviation, and quartiles*, for each interpreted parameter. The full Python source code for the MWD DPI data gathering algorithm is available in Appendix B. The processed data retrieved using the script was then inserted into the Excel database (appendix A).

Both the *mean* and *max value* from each of the MWD DPI parameters were selected to be used further in the data analysis. Mean and max values were considered to be the most representative values, in terms of representing the MWD DPI data for each borehole with a singular value. Condensing up to 900 samples per borehole, to 1 singular value, will naturally offer some limitations in regards to how well each borehole is described. It is conceivable that a mean value

would yield higher values for holes with high fracture density, but it could also potentially mask some important responses such as very large fractures in a relatively competent rock mass, and that the hole potentially could be better described by a max value. Zero values were excluded from the data in the function which provided the descriptive stats, this is because zero values in the drill logs represent voids in the dataset due to the lack of logging (as seen in figure 6.5), which occurs quite often. The data voids are neither descriptive and will potentially obscure the data analysis.

### 6.2.2 Grouting data

Grouting data are continuously monitored and logged from grouting rigs during the whole grouting procedure. The logged parameters consist of: volume, pressure, and flow against time, the logs also include start- and stop time, date, hole number, hole length, w/c, and recipe number for each hole. All these variables are stored in the grouting *log-files*, which are .txt-files of raw data taken during grouting.

The grouting-technicians are required to provide a *grouting report*, after each grouting round. The grouting report contains an overview of the cement amounts and time used, including more detailed information on each grouted borehole: stop pressure, recipes, and comments made by the rig operators. In Norwegian practice, information regarding variations in penetration rate, color of flush water, and other problems/observations made during drilling should also be registered in the full grouting rapport (Arnstein Aarset and Frogner, 2010). An example of a grouting report summary page (first page) taken from the Fv.659 project, can be seen in appendix C. Another important addition in the grouting report is the hole numbering overview (see figure 6.6), this overview is used to define the boreholes that are to be grouted. The same hole-numbering was also used in this study, to visually compare the MWD- and grouting data to match the individual holes.

For all the different worksites in this project, systematic pre-grouting is performed, with a general hole-length of 24m, and primarily standard Portland industrial cement grouts are used. Maximum grouting pressure is set at 80 bars for both the crown and invert of the tunnel. An overview of the grouting procedure used for this project is presented in appendix C. For the purpose of this research, the properties of the different grout recipes, such as w/c ratio, cement

types and, additives, are not considered.

Because Bever Control didn't have grouting data stored and available for this project, all information with regards to grouting had to be gathered from *Skanska* as they became made available from the different worksites. Preferably, the information for each grout curtain included both a grouting report and log files. The grouting logs were very important for analysis purposes, as they included all the raw data from the grouting rig: volume, flow, and pressure as time series with approx. 10 seconds sample intervals. Including general descriptions of the grouting round: tunnel site, recipe, hole number, and date. An example of a typical grouting log file can be seen in figure 6.7.

*Bever Team 3* (Bever Control AS, 2019) was initially used to import the log-files, but due to some limitations with this software, such as not being able to group and add values within same hole numbers, extract values of moment flow and problems importing log-files which have missing information, an alternate approach had to be found. After discussions with Bever Control representatives, it became clear that this was not possible to find an immediate solution to this. Due to these problems, a Python script was written to extract all the appropriate values from the

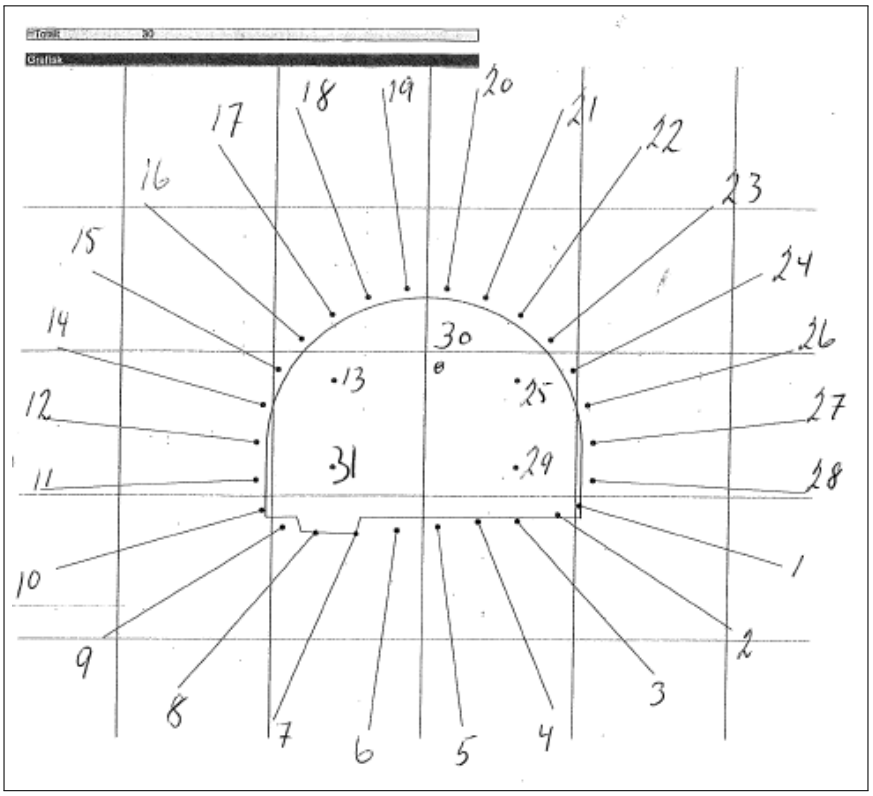


**Figure 6.6:** Example taken from a grouting report, showing hole numbering overview.

raw data in the log-files, process them accordingly, which would then allow the data to be used readily in the analysis. Full Python source code is available in Appendix B.

The grouting variables extracted from the log-files were: *total volume*, *end pressure*, *mean momentary flow* and *grouting time*. An overview on how each value was gathered is presented in table 6.2. Including these main four variables, general descriptive information, such as: grouting recipe, hole number, worksite, chainage, and date were also gathered. The output from the script was then compared with the grouting reports to verify that the data was processed and retrieved correctly by the Python script, including that the log-files were complete and not lacking any information. The finished processed grouting data could then be inserted into the main database (see appendix A).

```
Worksite;LONGVA
Section;23615
HoleNo;1
HoleLen;24.0
Stage;1
Recipe;1
Injection;1
Date;2020:01:23
Time;Pressure;Mom.Flow;Volume
HH:MM:SS;Bar;Liters/minute;Liters
10:35:56;   0.2;   0.0;      0.0
10:36:06;   0.2;   0.0;      0.0
    .        .      .         .
    .        .      .         .
    .        .      .         .
12:04:25;  59.7;  12.5;     951.4
12:04:34;  58.8;  13.3;     953.1
Checksum;1615
```

**Figure 6.7:** Snippet from an output log-file from the grouting rig.

### 6.2.3 Detection of jacking events using the PF Index

Among the different methods for detecting HJ-events described in section 3.4, it was decided to use the PF index developed by Strømsvik (2019) to locate possible HJ-event in the grouting data. The PF index was chosen as the preferred option for analyzing jacking events, because it is developed and optimized according to Norwegian tunneling conditions and grouting pressures. A prerequisite for using the PF index to detect HJ events, is a sampling frequency of one sample each 10 seconds (recall from section 3.4.1). This assumptions was validated for all grouting logs gathered from the Fv.659 project.

Similar to the methods of gathering grouting data from the log files, another Python script was written to calculate PF index for all holes. This script took the grout logs as input (.csv-files), did all the required filtering and processing of the data as described in section 3.4.1, and

outputted the graphs for each borehole which then could be visually interpreted. It was decided not to implement the full PF index algorithm for this study, but rather rely on visual interpretations of graphs consisting the flow, filtered pressure, and PF index. Since chainage 6045 did not include flow data, it was excluded in all analyses involving HJ cases. Full Python source code for calculating the PF index is available in appendix B.

Interpretation of the graphs were done using the tools for visual interpretation discussed in section 3.4.1. Figure 6.8 shows an example of a grouted hole from the Austnes worksite, depicting several characteristics of a grouting graph. Most notably, the onset of a potential jacking event can be seen at point A, this is due to the large momentary increase in flow while the pressure remains relatively constant, which is also reflected by a clear response in the PF index at the same point. The graph shows two periods of a temporary pause in the grouting procedure, this is normally done during grouting to allow the hole to "rest". This is often done after a potential jacking event has been observed, or to better facilitate that the target pressure is achieved in a controllable manner (Strømsvik and Grøv, 2017). Note also the large responses in the PF index at each point the grouting is resumed, this is because of the large momentary flow relative to the pressure happening at the start of grouting, and is not related to jacking events. The last period can be seen as stable pressure buildup while the flow remains constant, which also produces a stable response in the PF index which is as expected in this scenario. End pressure is achieved for this hole at the end.

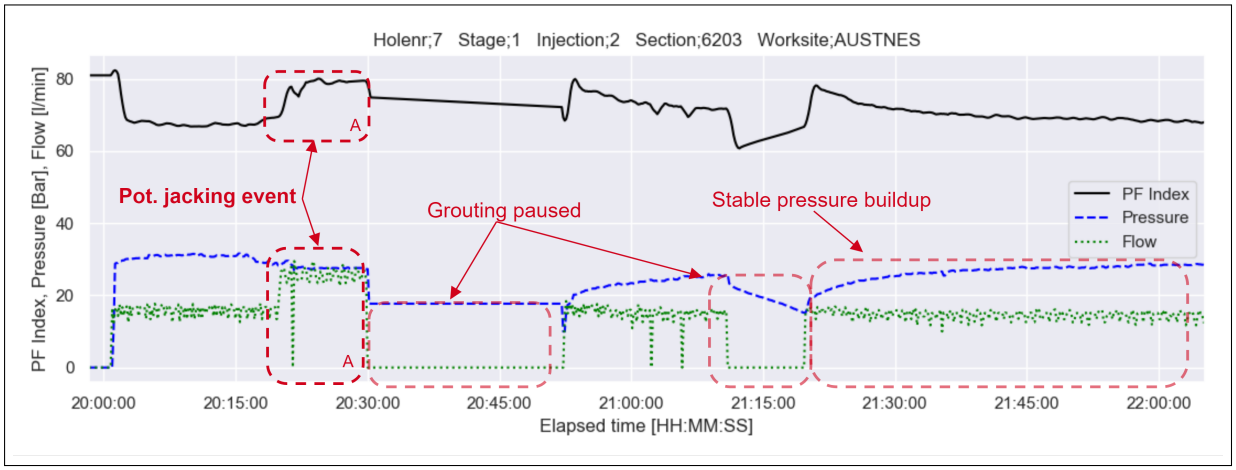


**Figure 6.8:** Interpretation example of grouting graphs. Boxes annotated 'A' show the onset position of possible HJ event.

## 6.3 Analysis of MWD and grouting data

Following is a summary of all data used further in the data analysis, along with information on how each data parameter is gathered (see table 6.2). Each borehole investigated was represented by *one value* for each variable, meaning one reading per borehole for each of the MWD DPI and grouting variables. Including this, some hypothetical assumptions on the relationships between variables are raised prior to conducting the analysis (section 6.3.1).

The full dataset consisted of 10 variables with 368 observation per variable (one per borehole), data was taken from 13 different chainages and two different worksite. A full overview of the used data is included in appendix A.

### 6.3.1 Hypothetical assumptions on MWD and grouting relationships

Some *hypothetical assumptions* are made on the presumed relationship between the variables, this is done in order to have a basis for summarizing and discussing the results. These assumptions are based on both experiences made from the litterateur review and logical reasoning. These assumptions will be discussed later in light of the research results (see section 8.6).

The assumptions are as follows:

1. It is expected that the MWD DPI parameters (FI, HI, and WI), are able to produce adequate responses according to the actual rock mass conditions.

2. Relatively high correlations between some of the different MWD DPI parameters are expected, especially FI and HI, seeing as these are dependent on partly the same input parameters. A correlation between the WI and FI is expected, since water disturbance is considered to be mainly bound to the fracture characteristics of the rock mass.

3. Considering the grouting variables, significant correlation between total volume and grouting time is expected, considering larger grout takes requires more time. Correlation between volume, time and mean flow is also expected.

4. Correlation is expected *between* MWD DPI's and grouting variables. Particularly between HI and total volume, time, and flow. It is presumed that higher overall fracturing of the rock mass (high FI values), will correspond to a systematic increase in grout con-

sumption, grouting time and mean flow rate.

5. It is expected that HJ cases will cause an increase in both time and grout consumption.

| **MWD DPI data** | |
|---|---|
| *How gathered* | *Variable* |
| Mean of all non-zero samplings across the total borehole length. | HI mean<br>FI mean<br>WI mean |
| Calculated max value of all sample points across the total borehole length. | HI max<br>FI max<br>WI max |
| **Grouting data** | |
| *How gathered* | *Variable* |
| Accumulated volume, equal to last entry in 'volume' column of grouting logs. | Total volume [l] |
| Max value of 10 last entries from the 'pressure' column of the grouting logs. | End pressure [bar] |
| Subtracting stop data and start date for each hole, then converting to minutes. | Pumptime [min] |
| Mean of all non-zero values in the mom. flow column of the grouting logs. | Mean flow [l/min] |
| By visual interpretation of PF index, flow and pressure, see section 6.2.3. | HJ detected |
| **Descriptive Data** | |
| *How gathered* | *Variable* |
| Tunnel worksite (Austnes or Longva). | Worksite |
| Relevant chainage number of the grout curtain. | Chainage number |
| Hole number taken from the grouting reports (matched with drill report). | Hole number |
| Hole depth taken from the drilling logs (not used in analyses) | Hole depth |

**Table 6.2:** Summary of all relevant MWD DPI- and grouting variables involved in the data analysis, including how they were gathered.

## 6.4 Limitations and challenges of the data gathering

The most important prerequisite for the data analysis was the availability of both MWD and grouting data for each borehole. Where information was lacking from a borehole on either MWD- or grouting-data, the same borehole had to be excluded from the analysis. Due to this fact, several had to be excluded altogether. MWD data were abundantly available, and the amount of data gathered was mainly limited by the amount of grouting log-files available. A problematic aspect regarding the grouting data, was that the log-files from the grouting rigs often were sometimes deleted altogether by the rig operators. This had a significant impact in regards to how much data was made available for analysis purposes.

Another significant challenge regarding the data gathering, was combining the two datasets (MWD and grouting) for each borehole. This is because each borehole did not have a unique standard id-number or any other feature in which they can be identified by in both datasets, this means that the hole-number indicated in the grouting logs not necessarily coincides with that of the drill reports. This complicates the process of combining the two datasets (MWD and grouting) and makes it a very time-consuming process. It also leaves room for a significant source of error because the hole distribution of the drilling logs had to be visually compared to the grouting logs to match the data. The amount and of data that could be gathered were also limited to a great extent by this issue.

Chapter 7

# Results

## 7.1 Detection of weakness-zones using MWD DPI's

To investigate the ability of the MWD DPI parameters to respond to actual geological features, it was of interest to see if the various MWD DPI's *fracturing (FI)*, *hardness (HI)* and, *water (WI)* parameters were able to produce notable responses, matching the interpreted weakness-zones as indicated by the preliminary geophysical mapping (figure 6.3). To do this, a basic visual comparison was done of the mapped MWD DPI's, as provided by BTO, with the interpreted weakness-zones (figure 6.3). Due to the limited advance of the tunnels at the time of this research, only *one* of the four weakness-zone as indicated by the geophysical mappings had been potentially intercepted by one of the advancing tunnel, namely the *Fjørtofta North* subsea tunnel.

### 7.1.1 Fjørtofta North, subsea tunnel

Figure 7.1, shows the advancing tunnel face shown in pink at the Fjørtofta tunnel. The area marked in green, indicates approximately where the interpreted weakness-zone is expected to intercept with the tunneling advance, i.e. at somewhere between chainage 32000 and 32400. Looking at a profile section of the same tunnel in figure 7.2, an apparent weakness-zone is present between approx. chainages 32100 and 32300. This is indicated by the distinct response in the DPI parameter HI, where red and darker colors indicate lower interpreted rock mass hardness.

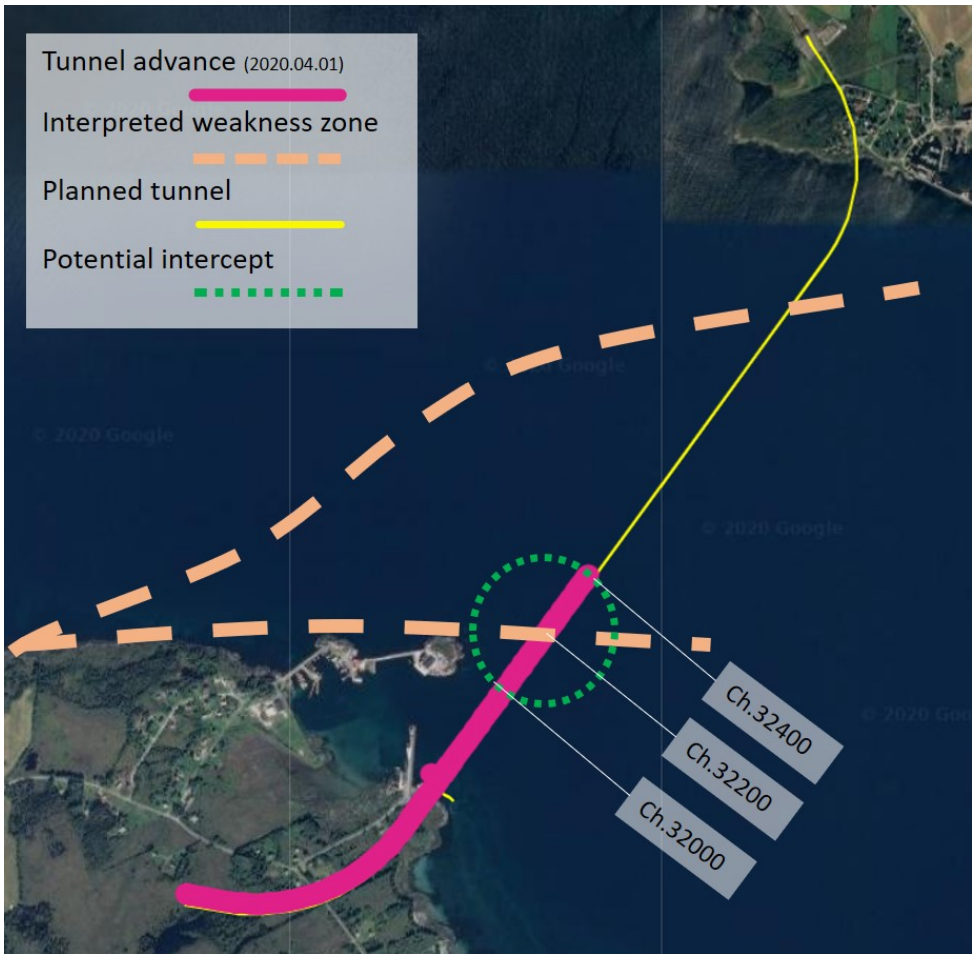


**Figure 7.1:** Map showing tunnel advance as of 1 April 2020, including interpreted weakness-zones as seen in figure 6.3. Potential intercept is estimated between ch. 32000 and 32400. Figure modified from the BTO as-built project module, showing real time tunnel advance.

A closer look at this section can be seen in figure 7.3, here all interpreted parameters are included as color gradients on fold-out tunnel geometries, all sections is taken from ch. 32100 to 32300. The response in the HI (top figure in figure 7.3) is particularly evident in this section, with a large portion of this section being classified as relatively soft rock mass. The same pattern can also be seen by the FI response, although not quite as apparent, there is a relatively higher density of yellow to red colors in this section, indicating a zone with higher fracture density. The WI parameter shows no extensive water is present at the weakness zone, however, areas indicating water disturbance seem to follow some narrow zones the same manner as the FI on the right and left side of the image (white markings in the bottom image in figure 7.1). This could indicate that "larger" water-bearing structures in the rock mass, are captured to some extent by the WI- and FI parameter.

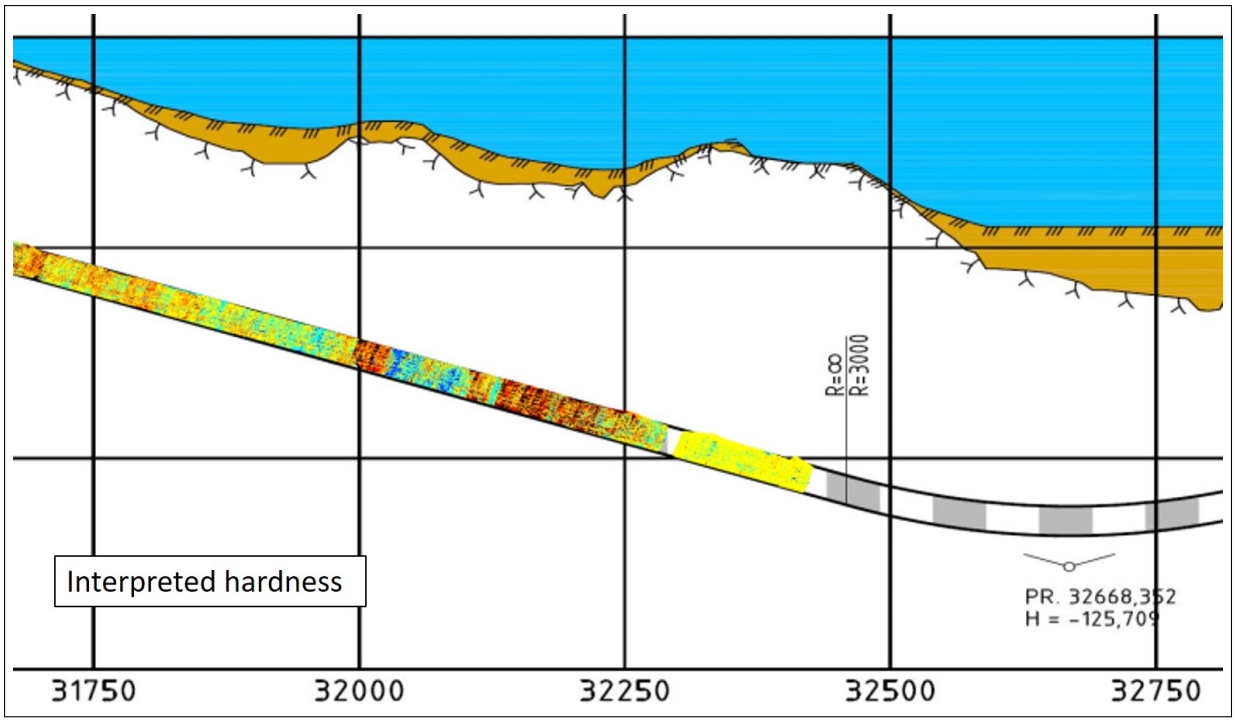


**Figure 7.2:** Profile view of Fjørtofta Nord, showing the interpreted weakness-zone intercepted by the tunnel as indicated by response in HI, marked by the red box. Figure modified from the BTO as-built module.

Judging from a visual interpretation of the MWD maps, it appears that the MWD DPI's are able to detect the interpreted weakness-zone, as indicated by the preliminary mapping. Most notably by the HI parameter, as can be clearly seen in both figure 7.2 and 7.3. There also seems to be some connection between where the WI shows indications of a water-bearing structure, and where the FI responds to a fractured structure.

Many systematic vertical and horizontal linear features can be seen from both the FI and HI DPI's. The vertical features could be an effect produced by the onset of drilling for each blasting and/or grouting rounds, while the horizontal features likely show the contour of each borehole. Keeping in mind that there is some extrapolation used in *between* each borehole, to allow for colorization of the whole tunnel contour.

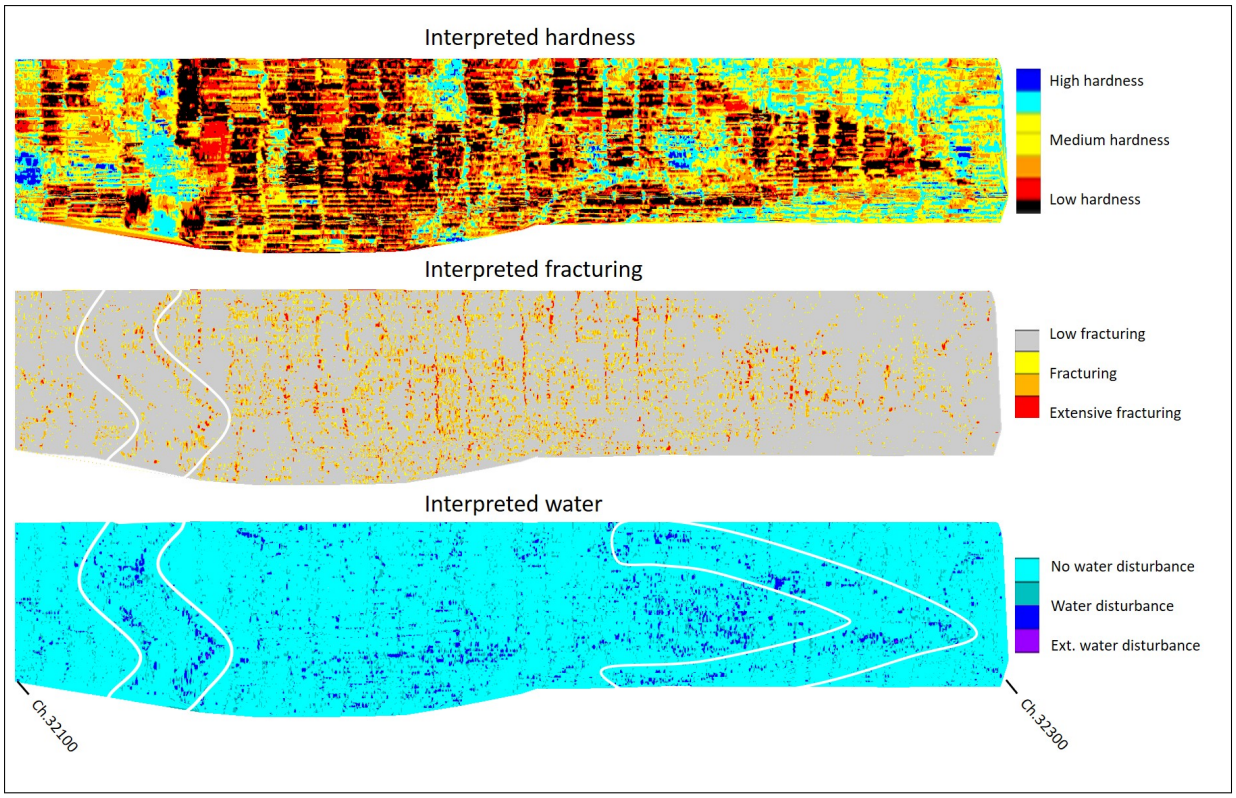


**Figure 7.3:** Images of fold-out tunnel geometries with colorized textures, comprising all MWD DPI parameters, sections taken between ch. 32100 and 32300 (200m section). Possible water bearing structures are indicated in white markings. All MWD DPI images modified from BTO as-built module.

## 7.2 Detection of hydraulic jacking

As previously described in section 6.2.3, detection of jacking events was done using the PF index. Following are the results of the visual interpretation of the PF index graphs for some boreholes exhibiting one or more indication of hydraulic jacking events. Evaluation of jacking was done for all grouting rounds, but interpretation is only presented from three different chainages in the following section (see figures 7.4, 7.5 and 7.6). A full overview of detected HJ cases can be seen in the full dataset (appendix A). Two of the presented chainages, are taken from the *Longva* worksite, and one from the *Austnes* worksite.

For data analysis purposes, holes with multiple indications detected are not explicitly presented in the full dataset. HJ events are indicated simply by binary values - *True* or *False*, i.e. potential HJ detected or no HJ detected. A summary of cases for each chainage is presented at the end of this section in table 7.4.

### 7.2.1 Chainage 5892, Austnes worksite

Figure 7.4a, shows a relatively short grouting round of about 30 minutes, with one potential HJ event as indicated by the red box. After a period of stable and constant pressure and flow conditions, the pressure drops while the flow remains constant. This also results in a clear response in the PF index. This hole achieved the target end-pressure at approx. 40 bars.

The next graph shown in figure 7.4b, shows indications of two potential HJ events in the same grouting round. In *event A*, a clear increase in flow is followed by a slight pressure increase and is therefore not characterized as an HJ event. *Event B* is seen as a momentary drop in pressure while the flow remains constant over a longer period, this is identified as a potential HJ event. Target end-pressure was achieved at approx. 90 bars, following a longer stoppage at the end of the second grouting round (not shown here).

The last graph, shown in figure 7.4c, shows on potential HJ event marked as *event A*, after a long period of relatively stable pressure and flow conditions. Just before the onset of *event A*, there is an event that gives a very clear response in the PF index. This event is interpreted as an artificial disturbance in the logging over a few samples, where the flow alternately jumps from 0 to very high levels during a smaller time period, and is not considered as a potential HJ event. This type of logging disturbance is a quite common false indicator that can be revealed by considering the sampling intervals in the raw log files. In this hole successful end-pressure at approx. 60 bars was achieved at the end of this grouting round.

| **Number of HJ events** | **0** | **1** | **2+** |
|---|---|---|---|
| **Number of holes** | 19 | 6 | 1 |
| **Percentage of holes** | 73% | 23% | 4% |

**Table 7.1:** Overview of potential HJ events detected at ch. 5892.

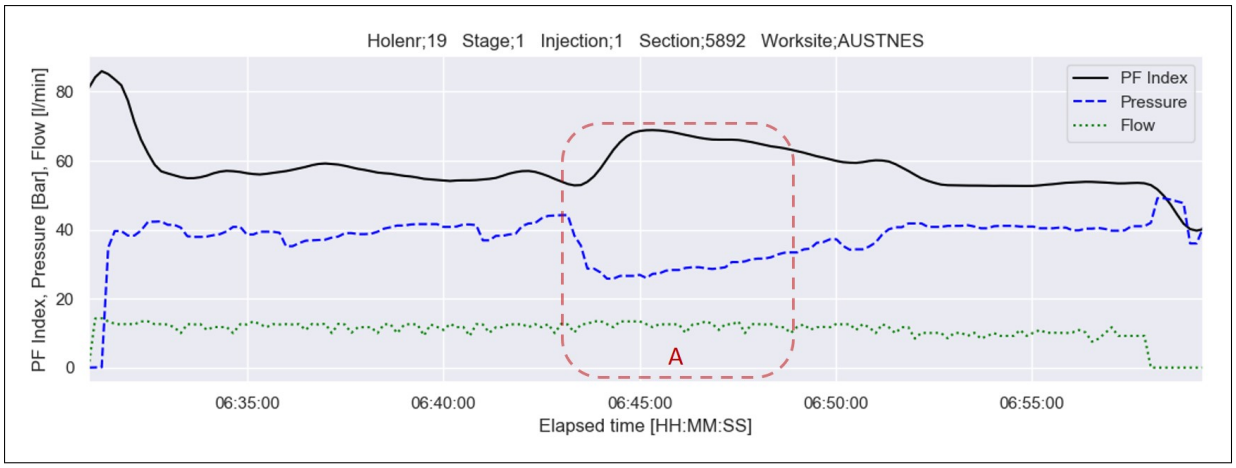


**(a)**

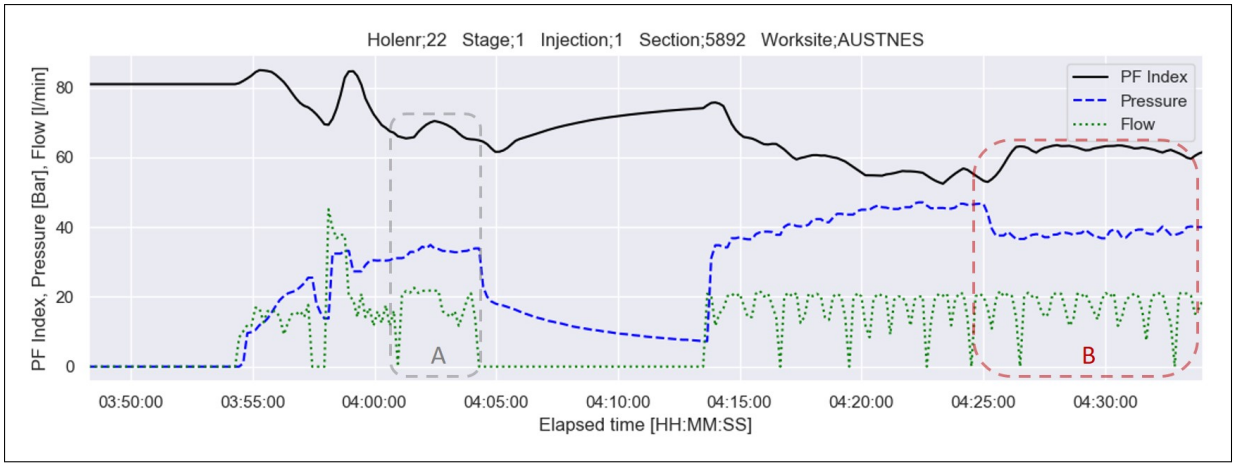


**(b)**

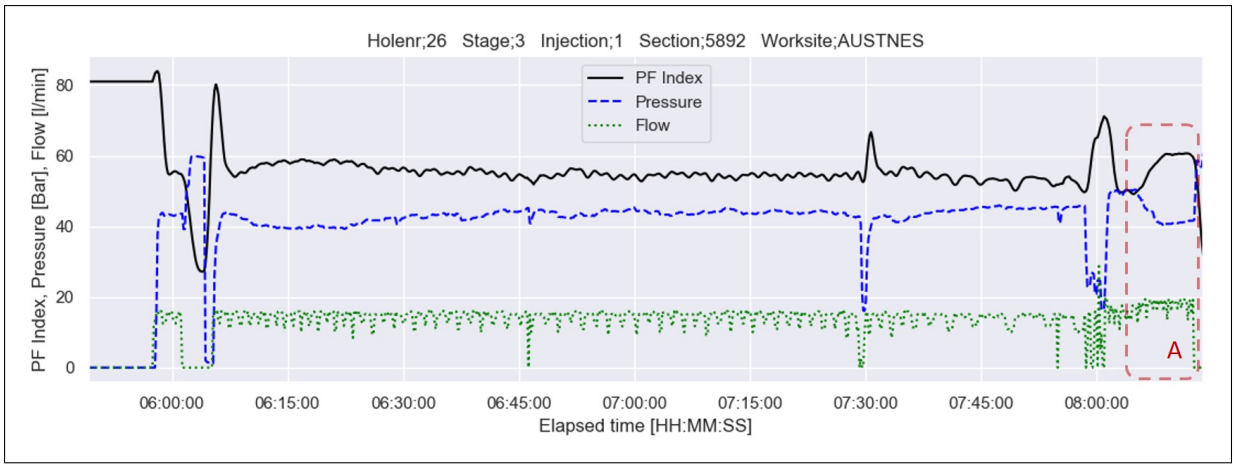


**(c)**

**Figure 7.4:** Grout pressure, flow and calculated PF index with time for three boreholes from the Austnes Worksite, ch. 5892. These are some examples where indications of HJ events were found, marked by red boxes.

### 7.2.2 Chainage 6203, Austnes worksite

In figure 7.5a, the graph depicts a very stable grout progression with very small fluctuations in both pressure and flow, and this is also reflected by the stability in PF index response, from the start of grouting (21:35), until the onset of the potential HJ event marked as *event A* (22:00). This area shows both decrease in pressure and an increase in flow, which is a strong indicator of a possible HJ event. The PF index shows a clear response to this and normalizes around the end. At this particular hole, the grouting was stopped and resumed the next day with satisfactory end-pressure achieved.

Figure 7.5b, shows the second injection round of a hole and the possible onset of an HJ event, annotated *Event A*. This HJ event is indicated by a clear drop in pressure while the flow remains constant, which also gives a corresponding response in the PF index. The event occurs after a small period of pressure increase and is followed by a short paused period. After this, relatively stable conditions are achieved with clear pressure increase with some fluctuations towards the end where end-pressure is achieved successfully.

Figure 7.5c, shows three plausible HJ events, both *events A* and *B* are relatively short-lived momentary pressure drops with constant pressure. However, because these events are short-lived with a fast regain of pressure, they are likely not related to HJ events, but rather due to other effects. *Event C* shows a pressure decrease over a longer period with constant flow, and is more likely to represent an HJ event.

| **Number of HJ events** | **0** | **1** | **2+** |
|---|---|---|---|
| **Number of holes** | 20 | 7 | 1 |
| **Percentage of holes** | 71% | 25% | 4% |

**Table 7.2:** Overview of potential HJ events detected at ch. 6203.

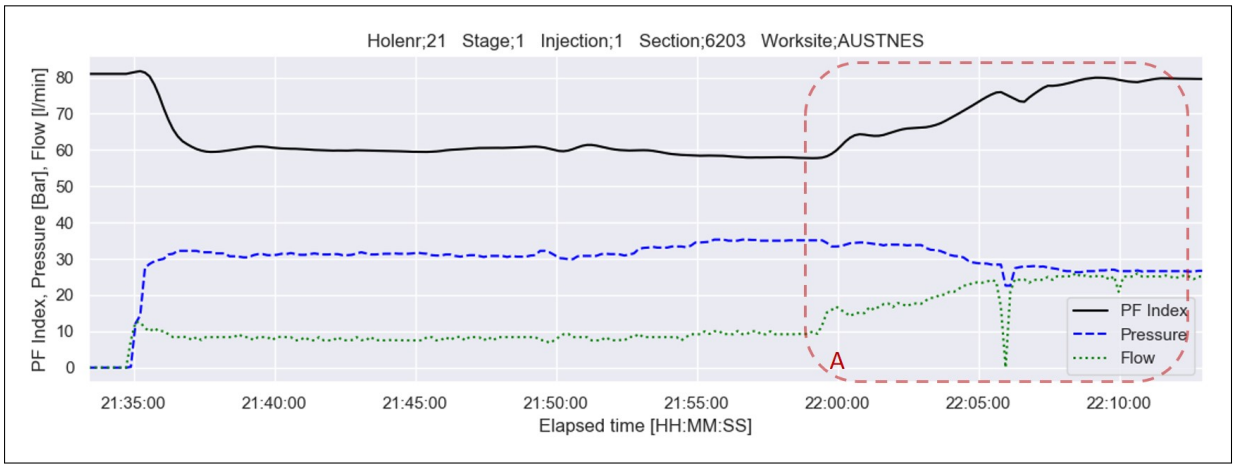


**(a)**

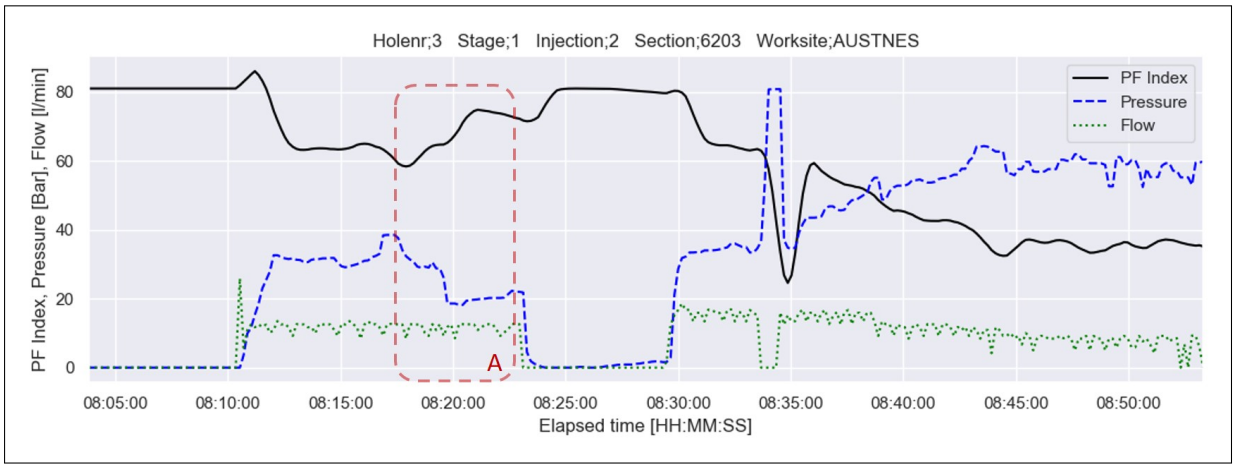


**(b)**

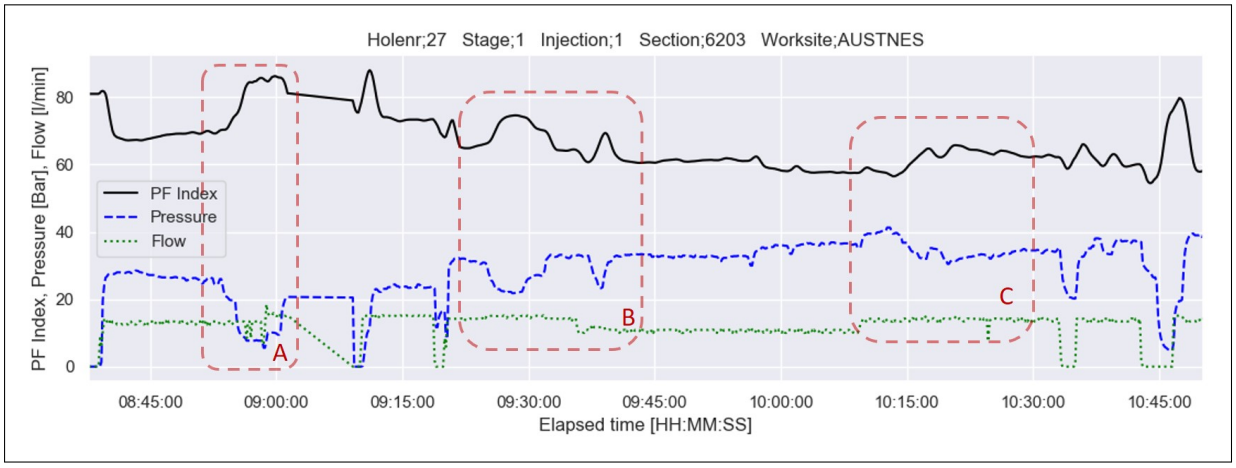


**(c)**

**Figure 7.5:** Grout pressure, flow, and calculated PF index with time for three boreholes from the Austnes Worksite, ch. 6203. These are some examples where indications of HJ events were found, marked by red boxes.

### 7.2.3 Chainage 23615, Longva worksite

Figure 7.6a, shows multiple plausible jacking events, shown here as *events A, B,* and *C*. All these events share a very steep momentary flow increase, which also signified with clear responses in PF index. However, this particular grouting exhibits high fluctuations in the flow progression, making the interpretation of actual behavior difficult. Regardless, it is reasonable to believe at least one or two of these indicators are potential HJ events. The grouting was paused at the end of this graph and resumed 30 minutes later, where stable pressure increase and end-pressure was achieved successfully.

The next graph, shown in figure 7.6b, demonstrates a potential HJ event at *event A*. Here, pressure decreases while flow remains constant and even has a slight increase, until the grouting is temporarily stopped at the end of *event A*. The PF index resonates with this event, shown by a steady increase starting from the onset of the event. This hole also had a second possible HJ event at a later grout stage not shown here. end-pressure was not achieved for this hole and was stopped by volume restrictions after multiple rounds. According to the grouting report, a special grouting component -*mauring* was used, suggesting difficult grouting conditions at this particular hole.

The last graph shown in figure 7.6b, shows a more difficult interpretive case of a potential HJ event. After a period of stable pressure increase accompanied with by a slight decrease in flow, the pressure drops momentarily while flow remains stable over a longer period. Both constant pressure and flow after a period of pressure increase, can also be considered a potential HJ event (see section 3.4.1). Despite this, a stable pressure increase was achieved without a temporary stoppage in grouting, beginning from the end of *event A*. Successful end-pressure of approximately 60 bar was achieved at the end of grouting for this hole.

| **Number of HJ events** | **0** | **1** | **2+** |
|---|---|---|---|
| **Number of holes** | 30 | 7 | 4 |
| **Percentage of holes** | 73% | 17% | 10% |

**Table 7.3:** Overview of potential HJ events detected at ch. 23615.

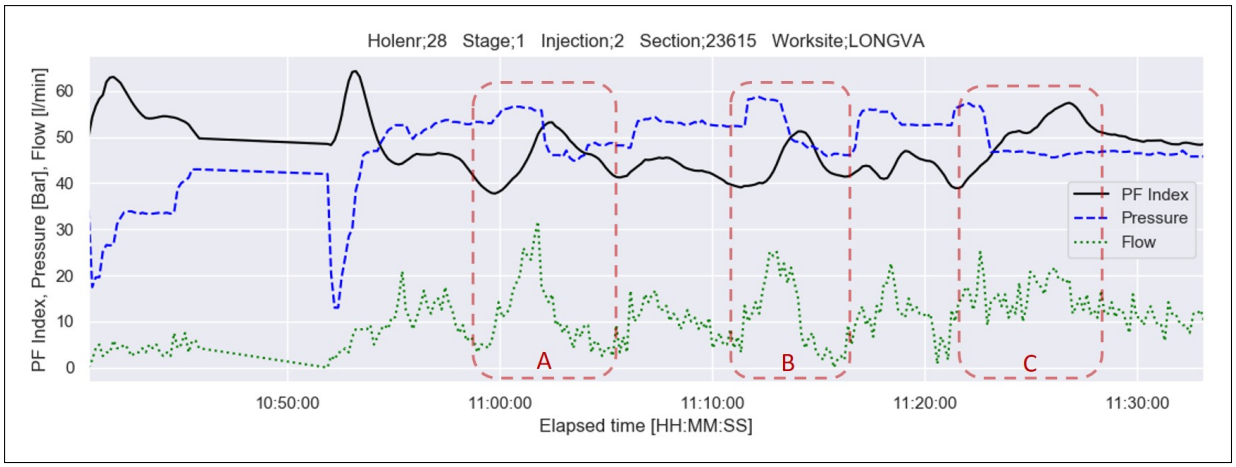


**(a)**

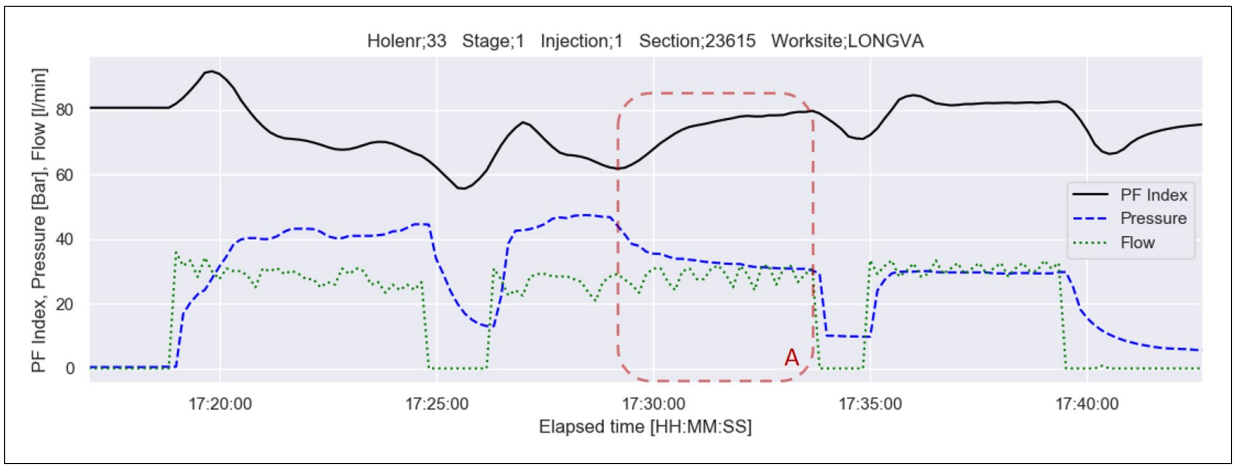


**(b)**

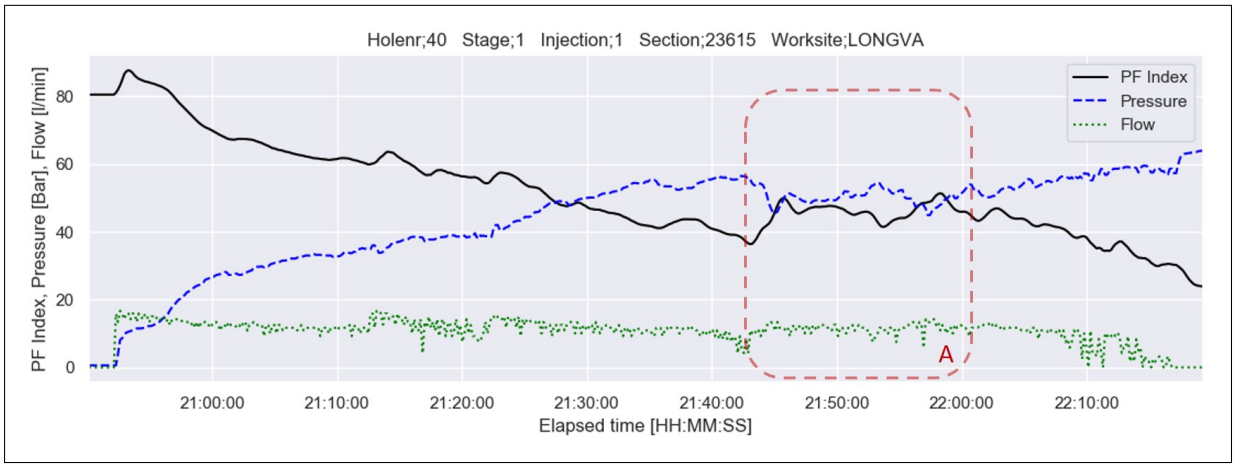


**(c)**

**Figure 7.6:** Grout pressure, flow and calculated PF index with time for three boreholes from the Longva Worksite, ch. 23615. These are some examples where indications of HJ events were found, marked by red boxes.

| Worksite | Chainage | HJ events detected | % of total holes |
|---|---|---|---|
| **Austnes** | 5506 | 5 | 25% |
| | 5523 | 7 | 25% |
| | 5856 | 3 | 15% |
| | 5892 | 7 | 27% |
| | 6203 | 8 | 27% |
| **Longva** | 23498 | 6 | 24% |
| | 23528 | 6 | 27% |
| | 23545 | 6 | 21% |
| | 23577 | 5 | 16% |
| | 23615 | 11 | 28% |
| | 23654 | 7 | 17% |
| | 23707 | 6 | 20% |

**Table 7.4:** Summary of potential HJ events detected for all analyzed chainages.

## 7.3 Principal component analysis

In this thesis, PCA was used to gain more insight and overview of the dataset. Both by visually identifying clustering and tendencies in the dataset, and to determine how these variables differ or conform with each other.

### 7.3.1 PCA on MWD DPI data

The mean value of the MWD DPI parameters: hardness, fracturing, and water were used as initial variables in this PCA analysis. The dataset used consisted of 3 columns x 369 rows of data, comprising MWD measurements for 369 boreholes across 13 different chainages. The PCA was done to compress and visualize the dataset, and to evaluate if the different chainages and worksites were fundamentally different or similar in terms of the MWD DPI parameters.

#### Assumptions

Assumptions were investigated in compliance with that presented in section 5.3.1. The correlation matrix **R**, of the three standardized MWD variables is shown in matrix 7.1. The correlation matrix shows some weak linear dependency is present between the three variables. The determinant of **R** is also positive, validating the first assumption.

$$\mathbf{R} = \begin{bmatrix} 1 & 0.08522 & 0.24713 \\ 0.08522 & 1 & 0.26394 \\ 0.24713 & 0.26394 & 1 \end{bmatrix}, \quad Det(\mathbf{R}) = 0.87311 \tag{7.1}$$

The KMO test for sample adequacy considering these DPI variables, concludes in a KMO value of $0.538$, which barely validates the assumption of sampling adequacy. Bartlett's test for sphericity indicates a statistically significant test result, with a $p - value << 0$. Outliers was filtered using the SVM-method, as described in section 5.3.1, tuned with parameters $gamma = 0.01$ and $nu = 0.05$, which seems to be appropriate for outlier detection of the PCA score results. In conclusion, all assumptions are validated, keeping in mind a low KMO test result.

## Analysis

PCA for the MWD DPI data was done reducing three variables to two principal components. A test for explained variance (scree test) gives a result of $0.469$ for principal component 1 (PC1), and $0.305$ for principal component 2 (PC2). This means that by reducing the three variables to two principal components, the PCA model is still able to account for about $77\%$ of the total information from the three initial variables. This also implies, that about $23\%$ of the total variance is left out in this analysis.

Figure 7.7, shows the score plots from the PCA analysis of both the individual chainages (7.7a), and the chainages grouped together by worksites (7.7b). Looking at the PCA score plot of the chainages (7.7a), it becomes apparent that there is generally a large variance of MWD measurements within many of the individual chainages, e.g. ch. 5523 and 23654. While other chainages exhibit more distinct and tighter clustering, e.g. ch. 6203, 23528, and 23707, indicating more constant measurements over their respective chainage. Another useful observation from this plot is the distinct differences between many of the chainages (e.g. ch. 5506 and 23707), suggesting that geological differences between chainages are captured by the MWD measurements. This observation becomes even more evident looking a figure 7.7b. In this score plot, the different chainages are grouped together by their respective worksites, and outliers removed by using the SVM-method. The score plot shows distinct clustering of both Austnes and Longva worksites (occupying different spaces of the plot), suggesting that these two worksites are distinguishable in terms of their MWD DPI measurements, which again could reflect their differences in geological domains.

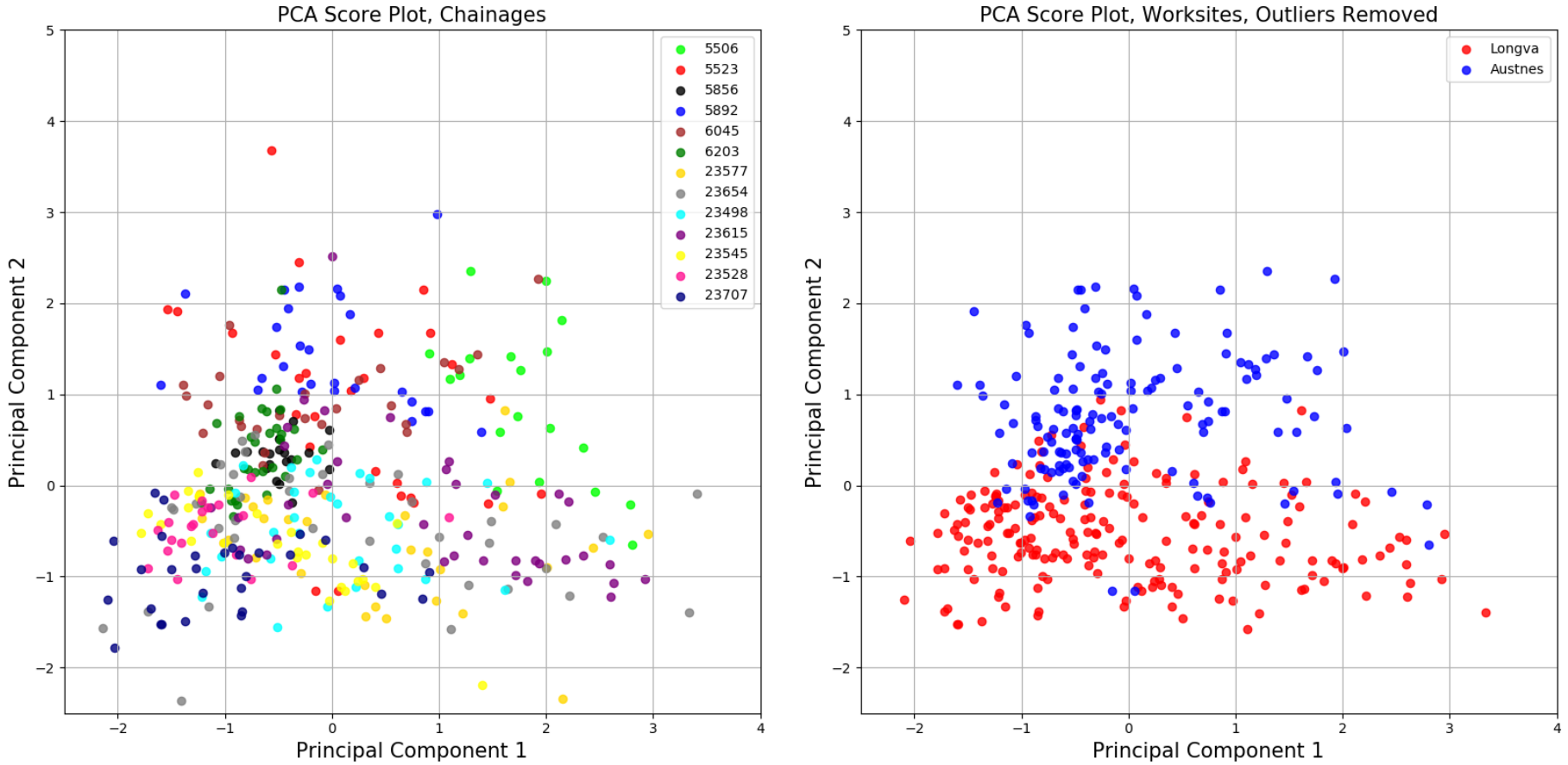


**(a)** **(b)**

**Figure 7.7:** MWD PCA score plots grouped by chainages (7.7a), and grouped by worksites Longva and Austnes (7.7b), where outlier filtering is applied.

To get more insight into what these principal components represent in terms of influence from the input variables (HI, FI and WI), the loading scores of the PCA analysis can be interpreted (as discussed in section 5.3). The individual loadings are presented in table 7.5, it shows that the water parameter (WI mean) has the strongest influence on PC1, while the hardness (HI mean) and fracturing (FI mean) parameter represent somewhat equal influences. Considering PC2, its shown that the hardness parameter has the most influence on PC2 while the water parameter has a negligible influence on PC2. This implies that the vertical axis (PC2), will be more indicative of differences in the hardness and fracturing. This also means that the clustering between worksites Longva and Austnes, as seen in figure 7.7b, are mainly due to differences in fracturing and hardness parameters from the MWD variables. This is because the separation of these two groups occurs mainly along the PC2 axis, and not PC1 where more information on the water parameter is mostly explained.

The individual loadings are also visualized in figure 7.8. Here, the loading vectors from table 7.5, are plotted as scaled vectors showed by green arrows over the score plot. The same observation as previously discussed, can be visualized here. The water parameter does not influence greatly on PC2, implying that the variation seen along PC2 is mostly influenced by the hardness and fracturing parameter.

| Principal component | HI mean | FI mean | WI mean |
|---|---|---|---|
| **1** | 0.516947 | 0.539663 | 0.664477 |
| **2** | 0.732657 | -0.680375 | -0.017415 |

**Table 7.5:** PCA loading scores for the MWD parameters.

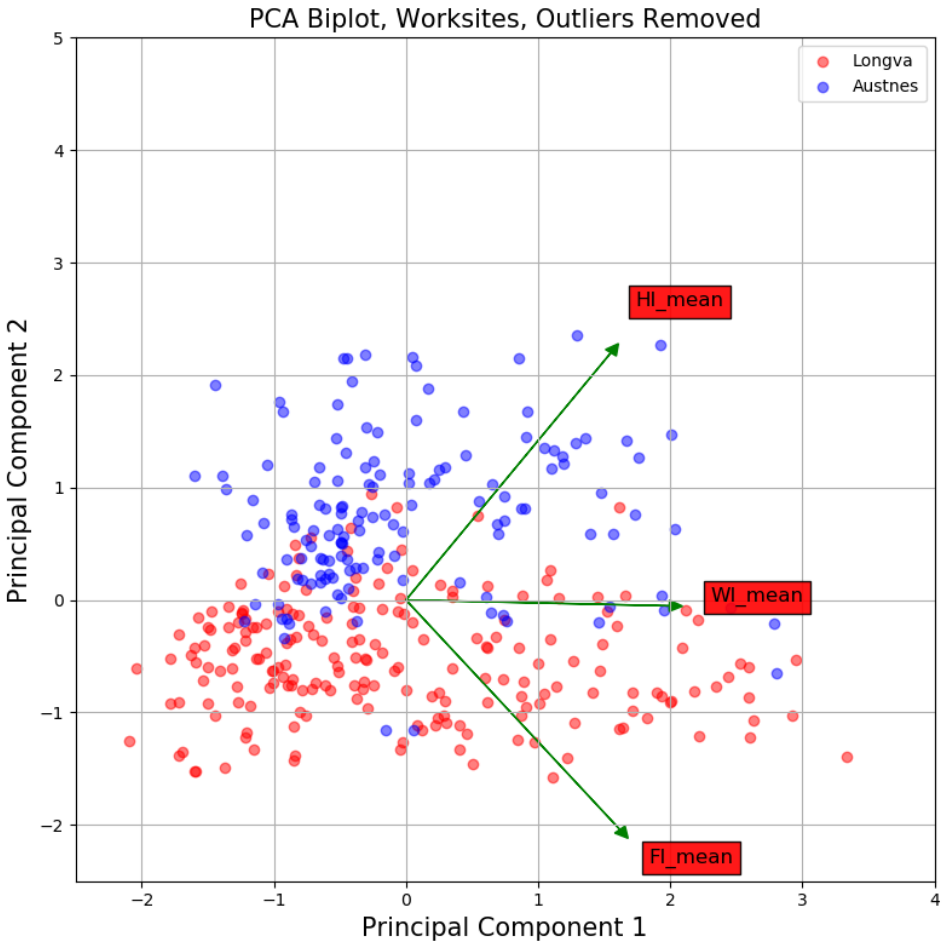


**Figure 7.8:** MWD DPI PCA biplot showing both scores grouped by worksite, and loading vectors for each input variable shown as green arrows.

### 7.3.2 PCA on grouting data

PCA was also done on the grouting variables: *total volume, end-pressure, grouting time, and mean flow* (in that order). The dataset used for this analysis consisted of 4 columns x 334 rows of data, comprising grouting measurements for 334 boreholes across 12 different chainages. The reason for this dataset being smaller than the MWD DPI dataset is because of missing grouting data for some chainages due to corrupted or lacking LOG-files. The PCA was done to compress and visualize the dataset, and to evaluate if the different chainages and worksites were fundamentally different or similar in terms of the grouting data.

## Assumptions

Assumptions for conduction PCA were investigated in compliance with methods presented in section 5.3.1. Considering first the correlation matrix **R**, of the four initial variables (7.2). The determinant of **R** is positive, validating the first assumption of linearity. Note also that the determinant is much smaller for the grouting data than for the MWD data. This is because the overall correlation within the grouting variables is larger than for the MWD parameters. Looking at the correlation matrix (7.2), there is a particularly strong correlation present between the first variable (total volume) and the third variable (grouting time), which is very much as expected, considering that more grouted volume requires more time to pump.

$$\mathbf{R} = \begin{bmatrix} 1 & 0.08342 & 0.83529 & 0.41338 \\ 0.08342 & 1 & 0.10600 & -0.05221 \\ 0.83529 & 0.10600 & 1 & 0.24284 \\ 0.41338 & -0.05221 & 0.24284 & 1 \end{bmatrix}, \quad Det(\mathbf{R}) = 0.23575 \tag{7.2}$$

The KMO test for sampling adequacy resulted in a value of $0.5147$, which barely validates the assumption of sampling adequacy. KMO is even less than for the MWD data, but with even fewer samples for the grouting data, this is as expected. The Bartlett test for sphericity resulted in a statistically significant test with a $p-value << 0.05$. Outliers was filtered using the SVM-method described in section 5.3.1, tuned with parameters $gamma = 0.01$ and $nu = 0.05$, which seems to be appropriate for outlier detection of the PCA score results. In conclusion, all assumptions are validated, again keeping in mind a low KMO test score.

## Analysis

Initially, all four principal components were considered to evaluate what percentage of variance the initial variables they account for. The explained variance between the four principal components (scree test), was: *0.513, 0.259, 0.191* and *0.036*. Dropping the last two components (PC3 and PC4), resulted in a variance explained between PC1 and PC2 of approx. $77\%$, which is about the same variance explained (with even more initial variables), compared with the MWD DPI PCA. It was decided to use two principal components for the ease of plotting, visualizing, and interpretation of the PCA results.

Figure 7.9, shows score plots from the PCA analysis. It shows the PC scores of both the individual chainages (7.9a), and the different chainages grouped together by worksite (7.9b). Looking at figure 7.9a, the clustering of individual chainages is less apparent compared with that seen of the MWD data (figure 7.7a). Some very extreme outlier measurements can be seen (e.g. ch .6203, 5892, and 23498), this is due to some holes taking in very high volumes of grout which also directly affects the grouting time. The variance in PCA scores for individual chainages seems to be relatively large for all chainages, suggesting that the general variance in grouting measurements is large. Considering figure 7.9b, there is no obvious clusters differentiating the two worksites, suggesting that both the worksites are relatively similar in terms of what grouting measurements they represent. The Longva worksite seems to have a more favored orientation of samples along the PC1 axis than the Austnes worksite, but that could be due to lack of samples for the Austnes worksite.

Table 7.6, shows the loading's each grout variable represents in terms of the principal components. It can be seen that both the *volume* and *time* has a large influence on PC1, which are also the two variables with the highest correlation. *Mean flow* is also relatively well represented in PC1, while information on *end-pressure* is not very well preserved in PC1. Likewise, considering PC2, very much information on *end-pressure* including a relatively large portion of the *mean flow* is preserved in this component. Looking at the loading vectors in figure 7.10, the influence of each variable on the two PC's is visualized. The orthogonality between time, volume, and end-pressure vectors, emphasize the lack of correlation between the variables. It should be noted that the interpretation of the loading vectors are rather limited in this PCA, seeing as no distinct clustering and groupings are present in the score plot.

| **Principal component** | **total volume** | **end-pressure** | **grouting time** | **mean flow** |
|---|---|---|---|---|
| **1** | 0.66186 | 0.09573 | 0.62691 | 0.39970 |
| **2** | -0.00985 | -0.90451 | -0.11350 | 0.41096 |

**Table 7.6:** PCA loading scores for the grouting parameters.

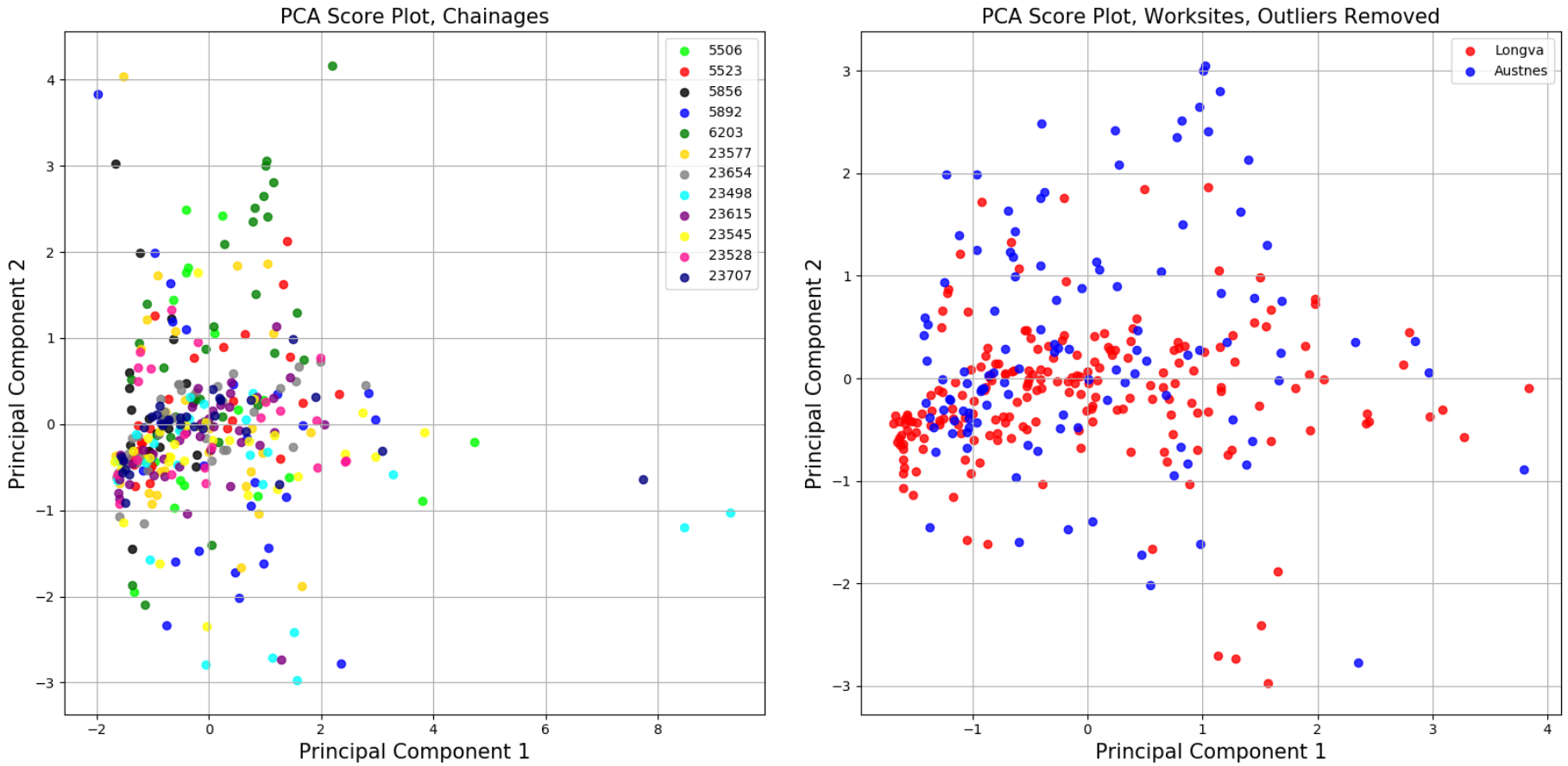


**(a)** **(b)**

**Figure 7.9:** Grouting PCA score plots grouped by chainages (7.9a), and grouped by worksites Longva and Austnes (7.9b), where outlier filtering is applied.

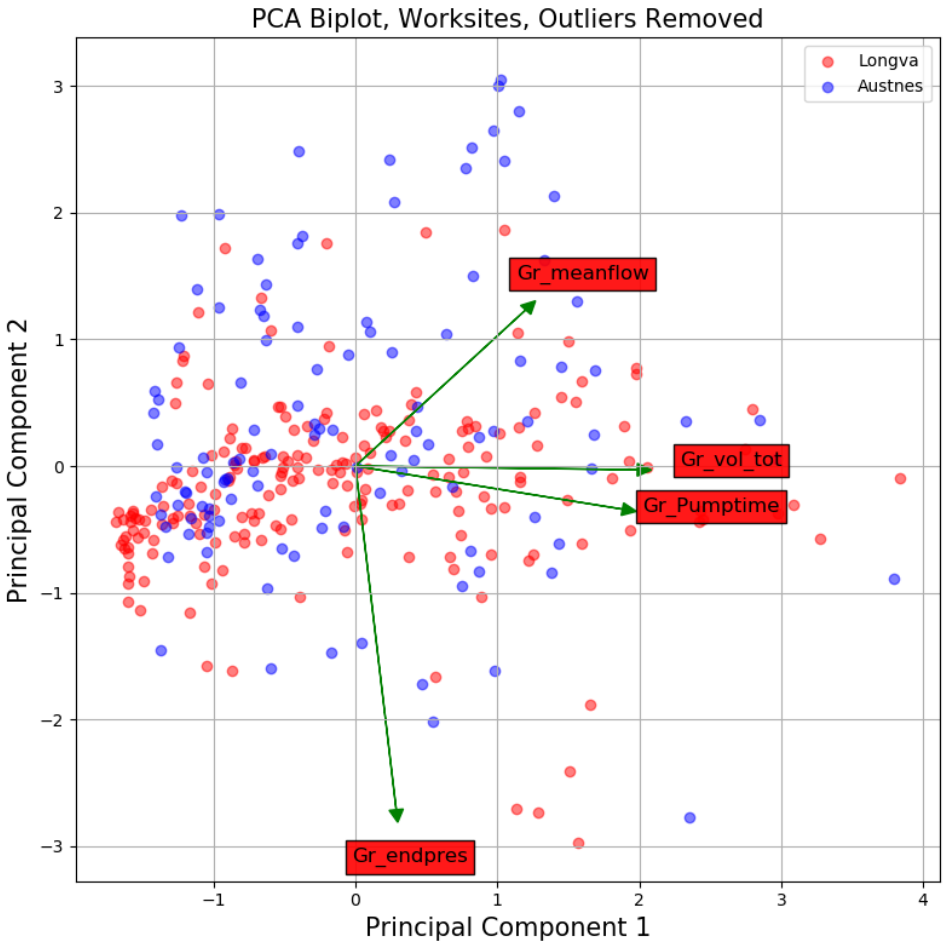


**Figure 7.10:** Grouting PCA biplot showing both scores grouped by worksite, and loading vectors for each input variable are shown as green arrows.

### 7.3.3 PCA on HJ events (grouting and MWD)

It was of interest to gain insight on the distribution of potential HJ event across both the MWD DPI- and grouting data, using the same PCA results from section 7.3.1 and 7.3.2. This was done grouping the results after potential HJ events, as previously found by using the PF index (section 7.2). Biplots are used for both cases, which enables visual interpretation of both the score orientation and evaluation of the respective loadings. Resulting plots are presented in figure 7.11.

The scattered borehole measurements of MWD DPI data, shown in figure 7.11a, shows no apparent clustering or similarities in terms of where the HJ holes orientate in the principal component space. The holes where HJ were indicated show no distinctive differences compared to the rest of the measurements. Figure 7.11b, shows a biplot over the grouting data grouped by measurements with potential HJ events. This biplot shows more distinctive tendencies in terms of where borehole with potential HJ events orientates, compared with that of the MWD biplot (figure 7.11a). There is an apparent tendency of the pot. HJ borehole to orientate further up along PC1, compered with boreholes with no HJ. Thus, suggesting that HJ events are potentially better explained by the grouting parameters *volume* and *time*.

Interestingly, there seems to be no favored orientation of the pot. HJ boreholes along the negative PC2 axis, where the information on end-pressure is mostly explained. This result points towards that the boreholes with pot. HJ events, does not tend to favor higher end-pressures. On a more general note, there seems to be a large variation and few clustering in the measurements where potential HJ events are found. But a weak tendency of HJ cases favoring *higher* volume and time consumption, can be seen.

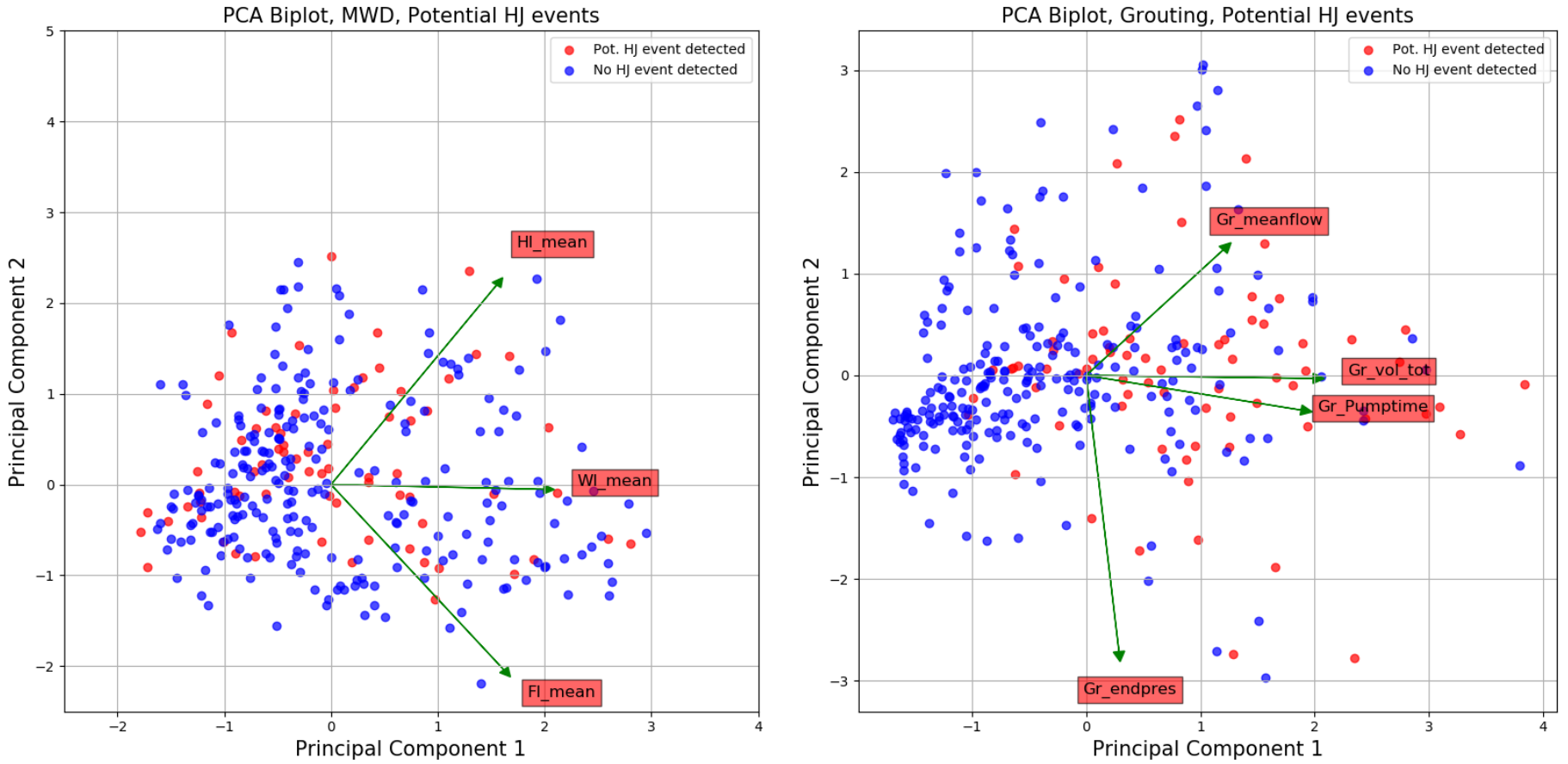


**(a)** **(b)**

**Figure 7.11:** PCA biplots of worksites indicated by holes where potential HJ events were found including remaining holes where no potential HJ events were found. The left figure is of MWD data, while the right figure is of grouting data. Outlier filtering is done using the SVM method in both cases.

## 7.4 MWD and grouting data comparative analysis

To investigate the *statistic relationship* between the MWD and grouting data, an initial correlation analysis was done followed by a comparative study on various machine learning algorithms (ML). The different ML models were evaluated in terms of their ability to train regression models, using the MWD DPI- and grouting data.

### 7.4.1 Correlation analysis

Spearman correlation coefficients were found for all numeric variables in the dataset (see table 7.7). Spearman was relied on rather than Pearson, to better detect monotonic relationships between the variables. For these variables, the Spearman correlation coefficients did not diverge significantly from the Pearson correlation coefficients, but did show higher coefficients between many of the variables (see Appendix C for Person coefficients). The correlation coefficients are presented using a heatmap matrix, shown in figure 7.12. In this heatmap, the correlation between any variable is indicated both by color and number in each cell. Each number representing the calculated Spearman correlation coefficient between each pairing of variables. Associated p-values, indicating the statistical significance of the coefficients, are shown in figure 7.13.

Looking at the correlation coefficients between the different MWD variables in figure 7.12, it becomes evident that the max values for each of the MWD DPI variables seem to be moderately correlated to each of their respective mean counterpart, with coefficients of 0.44, 0.65 and 0.66, respectively. Generally, higher correlations coefficients are seen within the max values compared to the mean values of MWD variables. Some significant correlation is seen between FI max and HI max (0.69), on the contrary, no correlation is seen between FI mean and HI mean (0.06). The low correlation between FI and HI mean can be partly explained looking at the differences between the two worksites (Austnes and Longva), as seen in figure 7.14. Together, these two worksites exhibit low correlation as previously discovered. However, looking at Longva worksite as an isolated case, a considerable higher correlation is found (0.542), compared to the Austnes worksite (0.039).

| MWD variables | Grouting variables |
|---|---|
| HI mean | Total volume |
| FI mean | Grouting time |
| WI mean | end-pressure |
| HI max | Mean flow |
| FI max | |
| WI max | |

**Table 7.7:** All MWD DPI- and grouting variables involved in the correlation analysis.

Considering the four different *grouting variables* in figure 7.12, a very strong correlation is seen between total volume and grouting time (0.89). High correlation is seen between flow and total volume (0.71), while some moderate to low correlation is seen between time and flow. Notably, end-pressure show no correlation to any of the other grouting parameters.

The most important observation that can be made from figure 7.12, is the lack of any significant correlation between any of the MWD DPI- and grouting variables. A test on statistical significance on the Spearman correlation coefficients (figure 7.13), also reveals that almost all coefficients $\leq 0.10$ are to be considered *insignificant*, as indicated by p-values > 0.05. It also shows that all the correlations discovered are can be considered statistically *significant* p-values < 0.05.

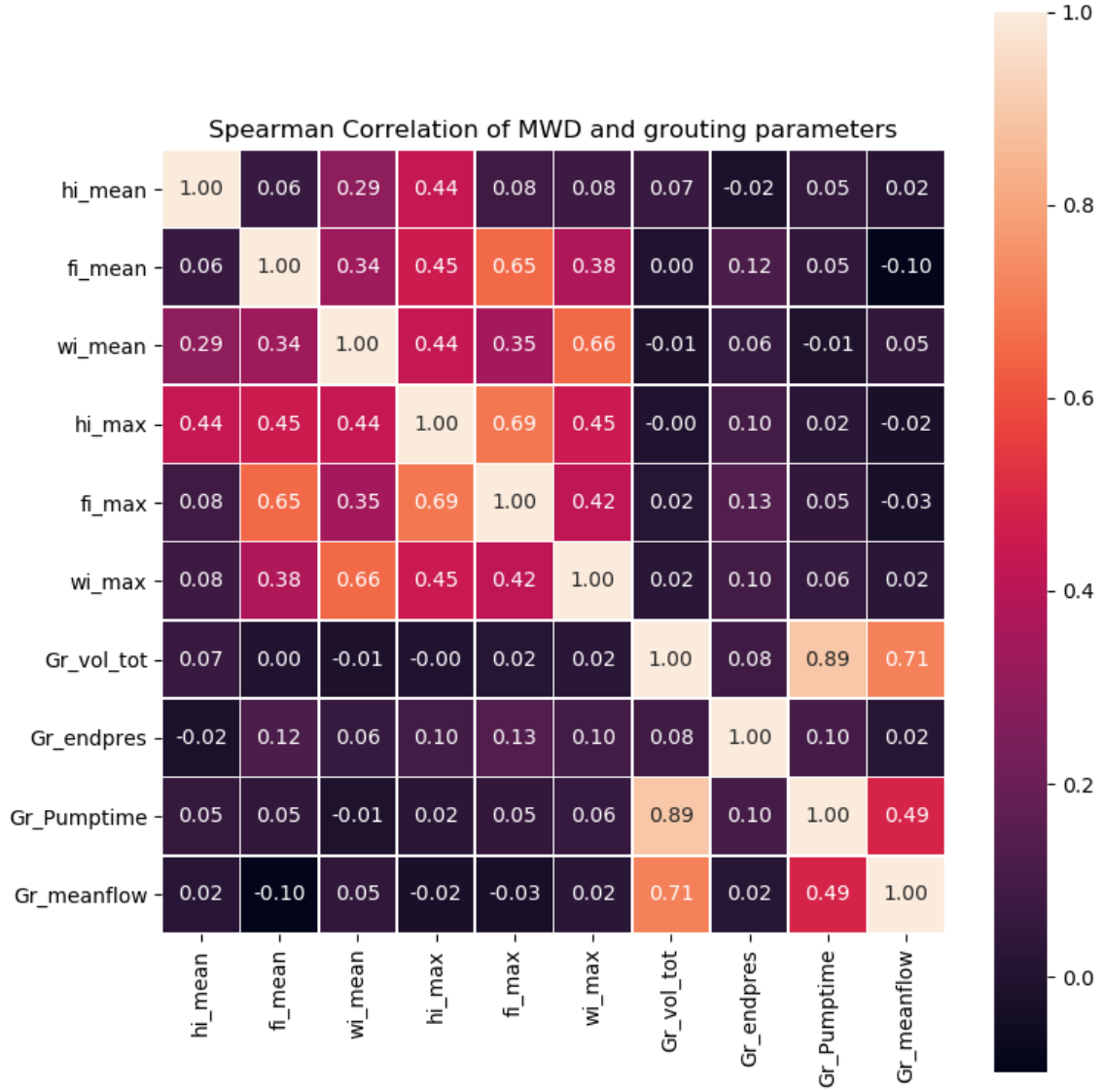


**Figure 7.12:** Heatmap showing Spearman correlation coefficients between all involved variables (see table 7.7), color gradient ranges from light (positive correlation) to dark (0 to negative correlation).


**Figure 7.13:** Heatmap showing p-values of Spearman correlation coefficients between all involved variables as in figure 7.12. Light cells depict significant correlation in terms of p-values, while light green to blue depict statistically insignificant correlations.

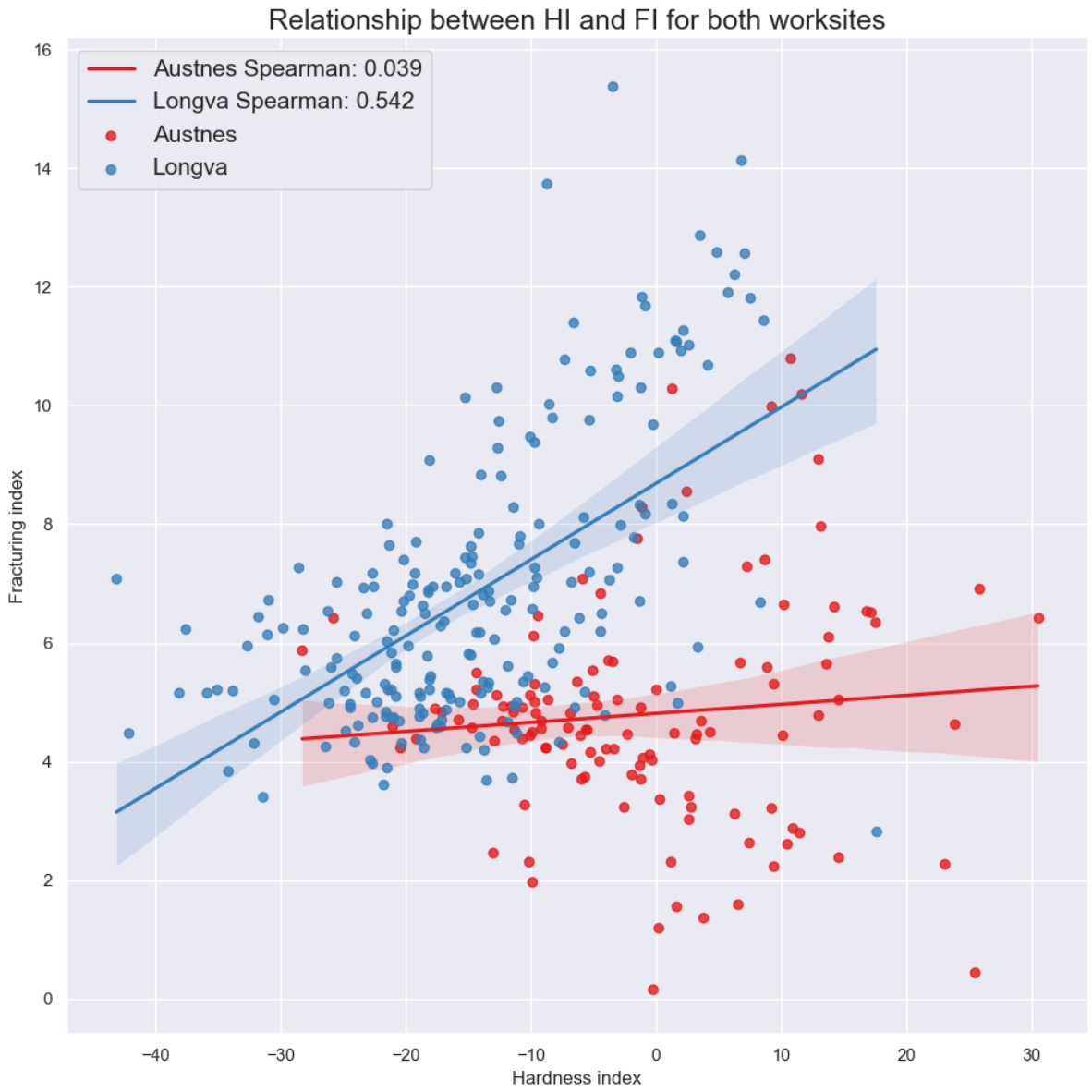


**Figure 7.14:** Scatter plot of int. hardness and fracturing grouped by the two worksites. Linear association incl. Spearman correlation coefficients between the respective groupings are annotated.

### 7.4.2 Testing ML algorithms on MWD and grouting data

Although no apparent relationships were found between the MWD DPI- and grouting parameters from the correlation analysis, it was of interest to verify this observation through other methods. To do this, various machine learning regression algorithms were tested and evaluated using *cross-validation*. The `cross_val_score` module from *sckit-learn* was used for this purpose. Python source code for the cross-validation can be seen in Code Listing 4 (Appendix B). The cross-validation method allows for testing the performance of multiple ML-algorithms (see section 5.2.2). The method returns the performance metrics for each model in terms of their predictive accuracy, which in this case, using regression models, is the $R^2$-score. The $R^2$-value serves an indication of the goodness of fit between the model's prediction and actual values (see section 5.1).

As target variables (response variables i.e. what is to be predicted), all the four grouting variables are used, to test the performance in predicting each of the four variables. Features variables used are the *mean values* of the MWD DPI parameters. namely: mean fracturing, hardness, and water. All the models used have different theoretical approach in terms of how they fit the data, and will not be discussed in detail for the purpose of this basic comparative study. The reader is referred to Pedregosa et al. (2011), Müller et al. (2016) for further reading on this subject. The regression models used in this comparative study, including their resulting $R^2$-value on each of the target variables are presented in table 7.8.

Figure 7.15, shows four plots (one for each target variable) with box plots describing the median and 95% confidence interval of each of the tested algorithms in terms of $R^2$-score. A higher positive $R^2$-value (with 1.0 being the highest), corresponds to a model that better explains the data. It becomes obvious looking at figure 7.15, that all models fail to fit the data, indicated by their negative $R^2$ for all models across all the tested target variables. It should be noted that none of the models are tuned in any way before the cross-validation, only default settings are used for all of the ML models. Never the less, using only default settings, the models are still expected to respond positively when they are able to learn and fit from the data in some way.

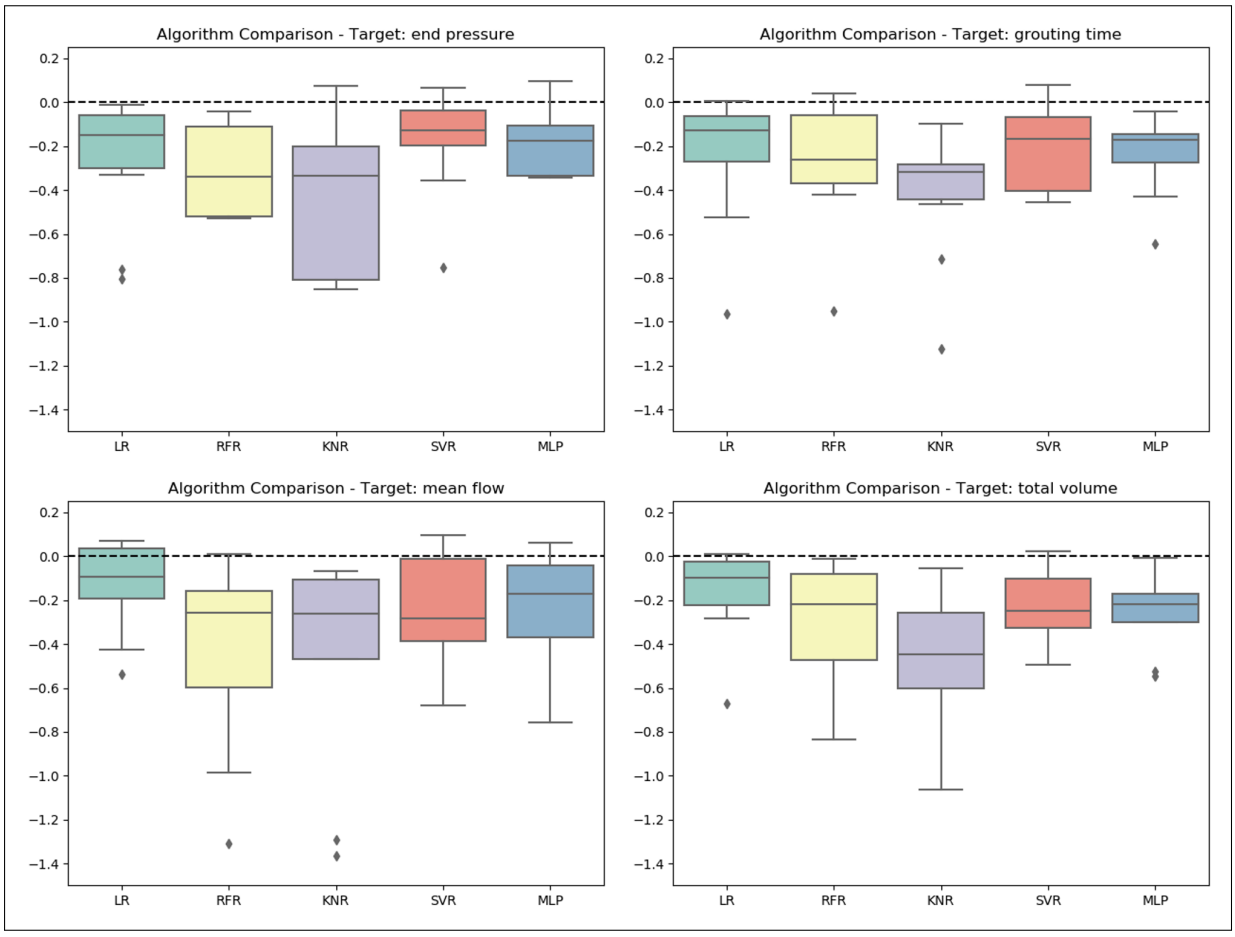


**Figure 7.15:** Box plots showing the distribution of $R^2$-values (y-axis), for each of the regression models (LR, RFR, KNR, SVR and MLP, see table 7.8), with one plot for each of the four target variables.

| **Regression model** | $R^2$**-values** | | | |
|---|---|---|---|---|
| | Volume | Time | End-pressure | Mean flow |
| Linear Regression (LR) | $-0.164$ | $-0.242$ | $-0.258$ | $-0.135$ |
| Support Vector Regression (SVR) | $-0.236$ | $-0.200$ | $-0.173$ | $-0.243$ |
| K-Neighbors Regression (KNR) | $-0.465$ | $-0.413$ | $-1.430$ | $-0.452$ |
| Random Forrest Regression (RFR) | $-0.299$ | $-0.275$ | $-1.166$ | $-0.439$ |
| Multi-layer Perception Regression (MLP) | $-0.253$ | $-0.238$ | $-0.545$ | $-0.239$ |

**Table 7.8:** Resulting mean $R^2$-values from the tested regression models on different target variables.

## 7.5 Prediction of HJ event using logistic regression

It was of interest to establish a predictive model for detecting potential HJ events from the gathered grouting data. To see if the holes where indications of HJ was found could be predicted based on the gathered grouting data alone, and possibly revealing new relationships between HJ cases and the grouting variables in the process. This was done using logistic regression as a *binary classifier*, as previously described in section 5.2.1. The data selected to predict potential HJ events as indicated by the PF index (see section 7.2), was the grouting parameters as the predictor variables or *feature variables* (i.e. what is used to predict), and potential HJ detected as the response variable or *target variable* (i.e. what is to be predicted). Both the features and target variables validate the assumptions of continuous and binary data types, respectively. The target variable is represented by Boolean values: **1** for potential HJ event detected, and **0** for no potential HJ event detected according to the PF index.

### 7.5.1 Establishing a model

In order to assess what explanatory variables or *features* to include in the model, the findings from the PCA of grouting parameters previously found in section 7.3.2, was used. By assessing the PCA result, it became apparent that the most variance was explained by the total volume and time, and to some extent the mean flow. While the end-pressure did not contribute to PC1 (recalling that differentiation between HJ events occurred mainly along PC1). Because the feature variables total volume and grouting time exhibited a very high correlation, the latter is excluded as an input variable in the logistic classifier model. The model therefore consisted of two feature variables: *total volume* and *mean flow*. Training data was set at 60% of the initial data amount, while 40% of the total data amount was used for model testing. After some model testing, the model was set with parameters $C = 0.001$ (penalizing complexity), penalty function set to $l2$ (default). The final model is established with logit parameters: $\beta_0 = -0.0156$, $\beta_1 = 0.0355$, and $\beta_2 = 0.0334$.

### 7.5.2 Evaluation of final model

Beginning with the confusion matrix (see figure 7.16), a relatively large number of the **0**-cases (no HJ-cases) were accurately predicted by the model, with 79 correct predictions. While 29 **0**-cases was wrongly predicted. On the contrary, the model was able to accurately predict 16 of the total 26 cases of **1**-cases (HJ-cases) in the test data.

| Target | Precision | Recall |
|---|---|---|
| **0** | 0.89 | 0.73 |
| **1** | 0.36 | 0.62 |
| **Accuracy** | 0.710 | |

**Table 7.9:** Classification report showing performance metrics of the model.

The performance stats of the final model are comprised in table 7.9. The stats show a much higher prediction accuracy for the **0**-cases (no HJ events) than the **1**-cases (pot. HJ event), the *recall* values, i.e. how confident the model is in its predictions. Shows a relatively fair result for the **0**-cases with a value of $0.73$, but are less confident in predicting the **1** cases, with a recall value of $0.62$. The overall model accuracy is $0.71$.

Assessing the ROC curve shown in figure 7.17, the model is clearly performing better than pure guesswork. The area under the curve (AUC) is $0.745$, where a value of 1 would represent a perfect predictor model, and a value less than 0.5 would represent a worthless predictor. The curve shows the rate of true-positives (i.e. **1**'s correctly predicted) vs. rate of false-positives (i.e. type I error, **1**'s wrongly predicted).

Taking a closer look at the actual correct predictions made by the logistic model, it seems that the model has problems distinguishing particularly the **1**-cases, with as many as 29 being wrongly predicted (false positives). Because accurately predicting the **1**-cases is considered the most important ability that the model should have, the rate of which the model predicts false-positive results (type I errors) is of particular interest. It is fair to say that this model is somewhat insufficient in predicting the potential HJ events, with respect to the gathered grouting data. Nevertheless, the model is able to fit and predict to a certain degree, using the feature variables mean flow and volume. Thus suggesting that there *might* be some relation between these feature variables, and cases of HJ.

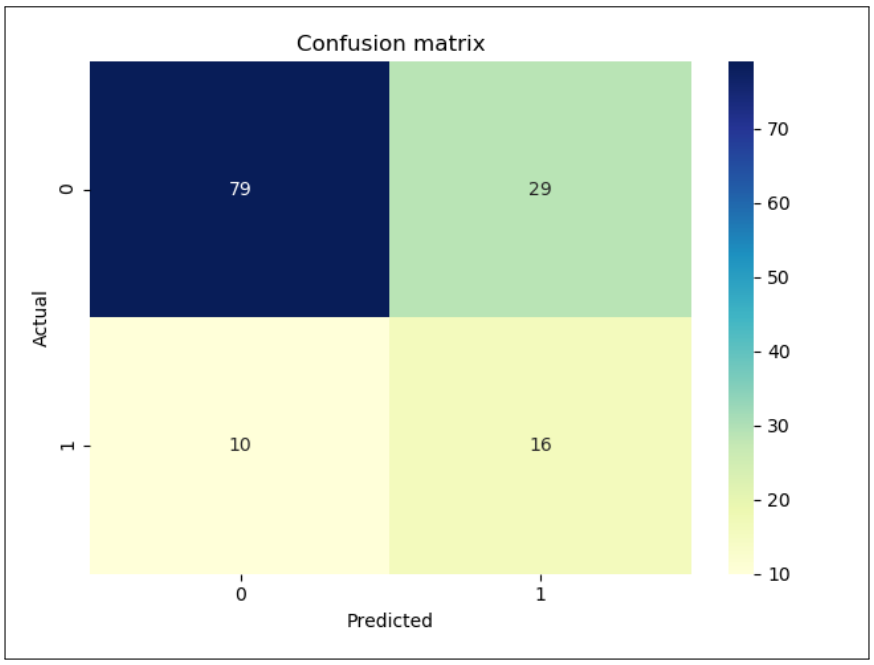


**Figure 7.16:** Confusion matrix of final model, main diagonal shows number of correct predictions for each case (79 and 16).

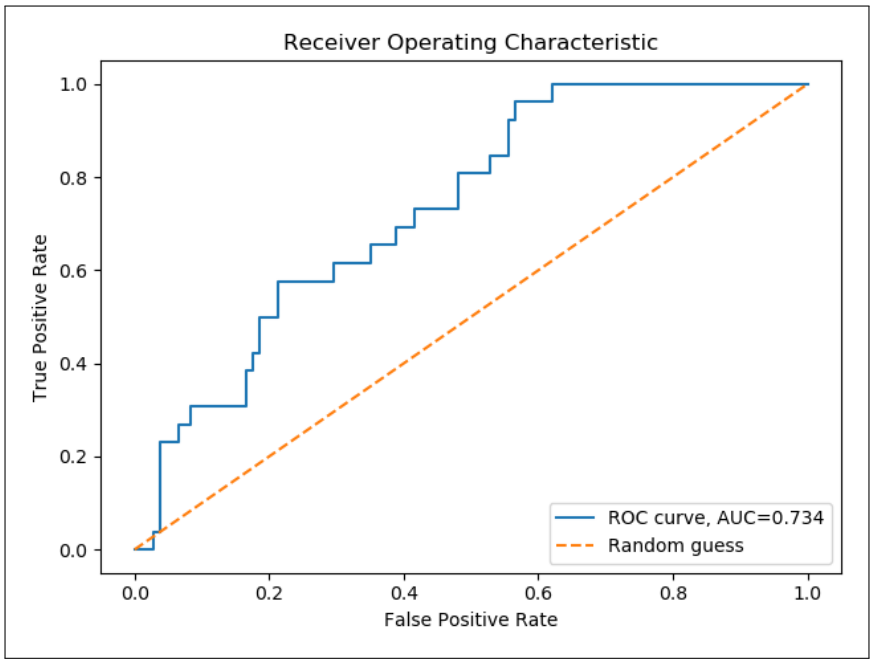


**Figure 7.17:** ROC curve showing the overall performance of the model compared to pure guesswork.

Chapter 8

# Discussion

The general usability of MWD data in establishing a grouting strategy is the question of main interest in this study. In this chapter, the research results and findings are discussed. A summarized review of the main findings is presented in section 8.6. A review of the main limitations including discussions on further work is presented at the end of this chapter.

## 8.1 Ability to detect geological features based on MWD

To verify the ability of the MWD DPI of detecting actual geological features, the response in these parameters when intersecting a prominent weakness-zone as indicated by the preliminary geophysical mapping by John F. Dehls and Rønning (2012), was analyzed. As previously stated, only one of the interpreted weakness-zones had been intersected by the tunnel advance within the time frame of this thesis, namely Fjørtofta North.

As seen from figure 7.2, the intersection of an apparent weakness-zone occurred around chainage 32100 to 32500 of the Fjørtofta North tunnel. This is similar to what was expected, judging from the weakness-zones as indicated by the geophysical mapping. In conclusion, the mapped weakness-zone, was quite clearly indicated by a response in the MWD DPI *hardness* and *fracturing*, but with a limited response in *water disturbance* (figure 7.3). Some water-bearing structures were also found by looking at both the fracturing and water disturbance textures of the fold-out tunnel geometries (figure 7.3). Considering these observations, it can be concluded that it is possible to detect large-scale geological features based on the MWD DPI's. However, this does not conclude on the MWD DPI's ability to detect smaller-scale features in the rock

mass, such as smaller fractures and water-conductive zones.

## 8.2 Using PF index to detect hydraulic jacking

To detect potential HJ events, visual interpretation of time series with PF index including corresponding flow and pressure was done. Some of the graphs, including their respective interpretations, are shown in section 7.2, the results from the HJ analysis are comprised in table 7.4. Detection of HJ events was done to supplement the data basis for this research, thus providing an additional basis for which potentially interesting relationships could be unveiled. The HJ cases are therefore used both in the PCA (section 7.3.2), and in the logistic regression (section 7.5).

Looking at table 7.4, potential HJ cases was detected in approximately 24% of holes across all chainages at the Austnes worksite, and 22% of holes across all chainages at the Longva worksite. Suggesting that a relatively even amount of HJ events has occurred at both worksites. The number of HJ events seems reasonable when considering studies on similar Norwegian tunneling projects. Strømsvik (2019), analyzed 7 different D&B tunnels in Norway for HJ events (using the PF index), and found HJ cases in approximately 23% of all grouted holes. In a master thesis done by Moe (2016), HJ events in two Norwegian railroad tunnel projects were analyzed (not with the PF index), and HJ cases were found in approximately 25% of all holes. Compared to these two comprehensive studies on HJ in Norwegian tunnel projects, it appears that a proportionate number of HJ events has occurred in all of them, between 23-25%.

As previously discussed in section 3.4.1, there are also events which exhibit similar or equal behavior to HJ events during grouting, but is rather caused by other effects. This naturally makes the indications of HJ very interpretive, and this is important to keep in mind when using the PF index. It is not possible to validate any results regarding detected HJ events, as is the case for many aspects of grouting research. The limited amount of usable data that was available for this research, made it possible to base the detection of HJ events on visual interpretation of the PF graphs. For larger datasets, it is suggested to automate the procedure by implementing the full algorithmic PF index method for HJ detection as proposed by Strømsvik et al. (2018).

## 8.3 General findings from the PCA

PCA was done to detect and visualize trends, clustering, and tendencies in the data. As well as a method for establishing which of the parameters, contributed most to the overall information explained. The PCA allowed for a deeper understanding of the data and the relationship between the different variables. Three Principal Component Analyses was done, two where the MWD DPI and grouting data were treated as isolated cases, and a third where the same grouting and MWD variables were used to investigate their relation to the HJ events.

### 8.3.1 PCA on MWD DPI data

Considering the PCA on MWD DPI's as an isolated case (figure 7.7b), some weak clustering of data points could be seen between the different chainages involved in the analysis, but overall the observation from each of the chainages seemed quite variable, with no apparent tendencies. Furthermore, the most apparent tendency became evident when the individual observations were grouped according to their respective worksites.

Grouped by *chainages*, there was a large variance of observation within many of the chainages, which also suggests that the variance in terms of rock mass quality was considerable within many of the individual chainages. This is a logical response, in that sense that the rock mass quality can change to a great deal even within the confined area of a few meters, certainly when taking into account that the "Eastern Gneissic Region", in which all these tunnels are constructed, is a geological domain which is often characterized by its high geological complexity. Looking at the PCA grouped by *worksites*, the clustering of the individual tunnel worksites became apparent, clearly showcasing the overall differences in rock mass characteristics between these two areas. This also supports the ability of the MWD data in differentiating the overall geological characteristics between two areas.

From the PCA biplot in figure 7.8, the importance of the MWD parameters fracturing and hardness in differentiating the two worksites clustering, became evident. This clearly shows that the differences between these two worksites are due to overall differences in the rock mass characteristics, that are captured by these two parameters. This further supports the ability of the MWD interpreted parameters *fracturing* and *hardness*, to quantify geological conditions relatively. The resulting clustering also suggests that the worksite *Austnes* was consistent with

overall higher rock mass quality (in terms of fracturing and hardness) than the *Longva* worksite. Suggesting that even though both the tunnel worksites are consistent with the same geological domain according to the bedrock geology (granitic rock with eclogite lenses, see figure 6.2), the relative rock mass characteristics of this region can change greatly within the same geological unit.

It should also be stated that the validity of all these observations, only holds if reliable calibrations are assumed for all the drilling jumbos. Meaning that what is indicated by the data is representative of the actual rock mass conditions at the different worksites, and not due to false effects such as equipment not being calibrated properly.

### 8.3.2 PCA on grouting data

Considering the PCA on grouting data as an isolated case, less apparent clustering could be seen from the score plot grouped after chainages (figure 7.9a), compared to the MWD DPI PCA results. No apparent clustering or tendencies was differentiating the two worksites (figure 7.9a), as was seen by the PCA on MWD DPI's. The most interesting perspective resulting from this observation, is that the clear difference in rock mass quality as indicated by the MWD PCA result, did not translate to any notable differences in terms of grouting parameters between the two worksites, as may would have been expected. Another observation from the grouting PCA is that the similarities in total volume and grouting time became evident (which was also found in the correlation analysis), including the orthogonality (i.e. no correlation) between end-pressure and grouting time/total volume. Most of the total variance in this dataset was caused by the total volume, time and to a certain extent mean flow, while the end-pressure provided a lesser amount of variance explained on PC1. This is as expected considering that the end-pressure is set at a predetermined value (40, 60, or 80 bar), and reached successfully for most of the grouted holes. Other than this, the PCA on grouting parameters was rather inconclusive, and did maybe suffer to some extent by the lack of data (especially from the Austnes worksite). As was also indicated by the KMO test ($0.5147$), which barely validated the assumption on sampling adequacy.

### 8.3.3 Evaluation of potential HJ events (grouting and MWD data)

PCA was also done using results from the two preceding PCA's, grouped after observation (holes) where indications of HJ events were found and not. No clear tendencies or clusters were discovered from the MWD PCA biplot (figure 7.11a), while a certain tendency of HJ cases to orientate further away along the PC1 compared to the observations with no indications of HJ, was found for the grouting PCA. The latter observation suggesting that holes with HJ events indicated, have a weak affinity towards higher values of the interdependent variables *time* and *total volume*, and to a certain extent *flow*. This observation is also in conjunction with the general belief that hydraulic jacking causes higher grout takes and increased time consumption of grouting (Stille, 2015; Strømsvik, 2019).

## 8.4 Relationship between MWD and grouting variables

Investigating the statistical relationships between the MWD DPI- and grouting variables represents an integral part of this study. As the result from this would help gain a deeper understanding of how the MWD parameters could potentially relate to the grouting parameters. For this purpose, a correlation analysis comprising all the MWD DPI data and the grouting data was conducted (see section 7.4). Subsequently, a comparative study using *cross-validation* of various different machine learning models was done (section 5.2.2).

### 8.4.1 Correlation analysis

A correlation analysis was conducted to measure the strength, direction, and statistical significance of any association between the different variables. The main emphasis was put on the relationship between the MWD- and grouting variables. Results from the correlation analysis visualized as a heatmap matrix can be seen in figure 7.12, while their corresponding p-values are presented in figure 7.13. The main results from the correlation analysis were as follows:

- Some weak to moderate correlations were found within the MWD DPI's of the dataset. The highest correlation was found between the max and mean values of each variable ($0.44$, $0.65$, $0.66$). Generally, high correlations were found within the max values than the mean values of MWD DPI's. Notably, no correlation was found between the mean of fracturing and hardness, when both worksites were analyzed together ($0.06$), but a moderate correlation was found between the same variables when only data from Longva

worksite was considered ($0.542$, see figure 7.14).

- Within the four grouting variables of the dataset, a very high correlation was found between time and grouted volume ($0.89$). A considerable correlation was also found between total volume and mean flow ($0.71$), while a moderate correlation was found between mean flow and grout time ($0.49$). No correlations were found between the remaining pairings.

- Between both the MWD DPI- and grouting data, *no correlations* were found.

Since both of the interpreted parameters, FI and HI, are both partially derived from the same normalized penetration rate parameter from the raw MWD data, as previously explained in section 4.2. It would also be reasonable to believe that a fractured and weak rock mass would produce a somewhat equal, or at the very least comparable response in these two parameters, including that these two exhibits some correlation. The two variables were shown to be uncorrelated when the full dataset was used, as seen from the correlation map (figure 7.12). However, the correlation is deemed *insignificant*, judging by its corresponding low p-value = 0.238 (see figure 7.13). As figure 7.14 suggests, there is a large difference in correlation between the two worksites (0.06 and 0.542), contributed by an observable high sampling variance at the Austnes worksite. This could be because its geological domain being more fluctuating and varying, compared to that of the Longva worksite. As was also seen previously in the MWD PCA (section 7.7). Figure 7.14, also suggests that there is generally a higher degree of fracturing and harder rock mass (lower hardness index) at the Longva worksite, compared to Austnes worksite, which resonates well with the results from the MWD PCA biplot (7.8).

The most important finding obtained from the correlation analysis is the lack of any linear or non-parametric relationships between any of the MWD DPI- and grouting variables. An initial hypothesis for this research was an observable dependency between grout consumption and particularly the fracturing parameter (FI). Even though no correlation was found between these variables, it is still believed that the overall grout take is largely dependent on the fracturing of the rock mass, as established by many researchers Stille (2015); Gunnar Gustafson (2012). As an initial approach for a PhD on grouting parameters and HJ events, done byStrømsvik (2019), the correlation between MWD and grouting was investigated. However, no correlation was found in this research either, and the approach was discarded after a few months. The PhD

study also suggested that the MWD parameters were insufficient in detecting and describing smaller fractures and water-conductive zones, similar to the results of this study

The lack of correlation could be due to how the fracturing parameter was gathered. To investigate a large number of boreholes across many chainages, the mean and max value 0f the 700-900 samplings *per* borehole was taken. It is conceivable that the information loss was too great in terms of establishing accurate and representative estimates for these DPI's when considering that up to 900 samplings were compressed to a singular value for each borehole. Another matter which obscures the interpretation of the FI is fracture infilling. Fracture infilling such as clay, will often significantly reduce permittivity of an otherwise fractured rock mass. It is not possible to establish whether fracture filling is present or not based solely on the FI DPI. Suggestions for alternative methods for establishing the MWD DPI data, is discussed later in section 8.7.2.

It should also be stated that correlation coefficients were also established for the Longva and Austnes as isolated datasets, in the same manner as done in figure 7.14. However, still no significant correlations between the MWD DPI's and grouting variables were found using this approach.

### 8.4.2 Testing ML algorithms on MWD and grouting data

Even though no inherent relationships were found between any of the MWD DPI's- or grouting variables, it was of interest to check the performance of some machine learning algorithms. To see if the ML models could detect any relationship between these variables, and produce an appropriate predictive response. To do this, four different target variables (all grouting variables) with corresponding mean MWD DPI variables as feature variables: FI mean, HI mean, and WI mean was used in five different ML regression models (see table 7.8). The performance of each model was evaluated through *cross-validation*.

As figure 7.15 shows, none of the used models are adequate in establishing a relation between the two sets of variables. This further supports the previous observation that no inherent relationship exists between the two variable groups.

Although few studies on the relationship between geology in terms of MWD DPI- and grouting data are conducted, Strømsvik (2019) and Høien and Nilsen (2014), offers some perspective on this subject.

In the first study conducted by Strømsvik (2019), grout consumption is compared with engineering geological mapping reports from a Norwegian tunneling project, relying mainly on the Q-system (rock mass classification system). This study also concludes with no obvious relationship between grout consumption and geological conditions. However, a limitation in this study, was that the Q-values were obtained *after* the grouting procedure was done. This could have altered the rock mass conditions on-site, in terms of some of the input parameters to the Q-system.

In another study by Høien and Nilsen (2014), the grouting performance of an urban tunnel was evaluated in terms of gathered MWD DPI variables. In this particular study, a distinct relationship was discovered between the mapped water leakages and the water disturbance factor (WI), while some rather indistinct relationships were found between *grouted volume* and the DPI factors *water and fracturing* (WI, FI), for some sections of the tunnel. It should also be stated that this research was conducted with MWD DPI provided by another software (GPM+ Tunnel, Rockma AB, 2011), which is not necessarily comparable to the MWD DPI provided by *Bever Control*.

It is also important to keep in mind that *correlation does not imply causation*. This means that any relationship found by either means of simple correlation analysis or more complex machine learning models, high correlation or predictive accuracy does not necessarily mean that the used variables are inherently related by nature. This also implies that one must be careful to assume a causational relationship beyond a strictly statistical relationship when interpreting these results. A critical point is that the statistical measures presented do not explain *why* or *how* the data are related, this means that there must also exist some sound logical reasoning behind them.

## 8.5 Prediction of HJ events using logistic regression

Logistic regression was used as a binary classifier for predicting potential HJ events based on the grouting data. The goal of this exercise was to investigate the predictive power of a classifier in accurately predicting HJ-cases in the dataset, relying only on the gathered grouting variables. And potentially gaining a deeper understanding of the relationship between HJ cases and the grouting variables.

The final model was able to predict 79 of the 108 **1**-cases in the test data, and 16 of the total 26 **1**-cases in the dataset. With an overall accuracy of $0.710$. The ROC-curve was established with an AUC of $0.734$, which is an improvement compared to pure guesswork ($0.5$). This in itself does not qualify the binary classifier as a good predictive model, which was not the purpose of this model. Nevertheless, the results signalize that the classifier model is able to detect a logistic relationship between the variables grouted volume, mean flow, and cases of HJ. This also supports the findings of Strømsvik (2019), where holes with HJ events were found to be correlated to an higher grout consumption.

As could be seen, it is not sufficient to base the detection of HJ event in grouted holes, solely on a predictive model such as logistic regression. However, applying ML methods on entire *grouting logs* time series to predict HJ events, could potentially return positive results. But this problem was not treated in this study. For computerized detection of HJ events, it is suggested to implement the PF index algorithm (Strømsvik et al., 2018).

## 8.6 Review of raised assumptions

To provide a critical and summarized review of the results, the raised assumptions from section 6.3.1, are discussed in light of the results, and previous discussions.

**Assumption 1**: *It is expected that the MWD DPI parameters (FI, HI and WI), are able to produce adequate responses according to the actual rock mass conditions.*
Based on the findings from the weakness-zone analysis and the PCA on MWD DPI variables, this assumption has been *validated*. The weakness-zone could be detected from the MWD DPI maps with quite high accuracy, based on the extent of the weakness-zone indicated by previous geophysical mappings. The two analyzed worksites: Austnes and Longva, exhibited consistent differences in terms of MWD DPI variables HI and FI. Further supporting the ability of the DPI's to relatively distinguish different rock mass characteristics. However, the ability to detect *small scale features* of the rock mass is still inconclusive, based on the research results.

**Assumption 2**: *It is expected that the different MWD DPI variables exhibit relatively high correlations, notably between: FI and HI, including FI and WI.*
The results from the correlation analysis and PCA only *partly validated* this assumption. Although no Significant correlation between FI and HI was found when both worksites were considered (figure 7.12), a moderate correlation was found between these variables at the Longva worksite (figure 7.14). The PCA result of the MWD variables of both worksites, revealed orthogonality between the parameters HI and FI, also suggesting that no correlations were found between these two. On the contrary, some weak correlation was found between both FI, HI, and the water disturbance, WI.

**Assumption 3**: *Significant correlation between total volume and grouting time is expected since larger grout takes requires more time. Correlation between volume, time and mean flow is also expected.*
The PCA and correlation analysis on the grouting variables validated this assumption. As expected, a high correlation was seen between grouting time and total volume. A moderate correlation was also seen between total volume and mean flow.

**Assumption 4**: *Correlation is expected to be found between MWD DPI's and grouting variables.*

This assumption was *rejected*, based on the findings from the correlation- and ML analysis. No apparent correlations could be derived from this dataset. Contrary to these results, it is still believed that relationships between MWD and grouting parameters could be established through alternative approaches, and prove a valuable resource in establishing grouting strategies. This will be discussed further under section 8.7.

**Assumption 5**: *It is expected that HJ cases will cause increases in both time and grout consumption.*

This assumption was *validated* through the results from PCA on grouting variables grouped by HJ events (figure 7.11a). The observations with HJ cases were scattered further up PC1, which is dominated by both the volume and time parameter. The results from the logistic classifier also support this assumption to some extent. The ability to predict HJ cases with an accuracy $0.710$, reflects the model's ability to detect some relationship between observations with HJ events and the grouting variables volume and flow.

## 8.7 Review of research limitations and future work

Although most of the limitations are addressed in each appropriate section, a summary of the most important research limitations is presented in the following section. Including some recommendations regarding future work, presented at the end.

### 8.7.1 Research limitations

Because of the data-oriented nature of this research, data gathering and processing represent a great deal of the research limitations. The following comprises a review of the most important limitations in this study, including suggestions on how they could be improved for the benefit of future research. Detailed discussion on data limitations were presented previously in section 6.4.

The *amount of data* was greatly limited by difficulties in matching the hole numbering from the grouting reports and that of the drilling reports; including limited access to grouting log-files, due to files being deleted by the grouting technicians. For future applications, it is suggested to implement a unique hole ID for each borehole, which is used both for the individual drilled holes and the grouted holes. This would allow for greater certainty in matching MWD- and grouting data, and would help facilitate a larger amount of data to be used for research and analysis. This feature would also improve the *certainty* in conducting research on both MWD- and grouting variables. An improved system for data management of as-built data, including that all project data is systematically saved and store for later use, will not only be beneficial for future research but also to evaluate the grouting procedure *after* grouting.

A considerable limitation that is relevant for all the gathered data, whether it is MWD- or grouting data, is the reliance on accurate calibration of all the used equipment, i.e. drilling jumbos and grouting rigs. Incorrect or irregular calibration of equipment will produce skewed responses between different worksites, which are not representative of actual rock mass conditions. This represents a considerable pitfall to this study, which was not possible to evaluate based on the available information.

### 8.7.2 Recommendations for future work

Although no correlation was found according to the main research question, there are still questions that remain unanswered by this research. Further research is needed to better understand the relationship between MWD- and grouting data.

It is firmly believed that a more profound relationship between these variable groups could be found by alternate approaches to establishing representative values for MWD DPI data. A better understanding in how the different MWD DPI parameters respond to especially water-bearing/conductive fractures, and from that deriving a value for each hole in terms of "fracture conductivity". It is also suggested that the MWD DPI responses is compared to its corresponding engineering geological mapping, similar to methods used by Høien and Nilsen (2014), to give a better understanding in the MWD DPI's responses to variations in the rock mass.

Furthermore, to better explain the fracturing parameter (FI) with a singular value, more knowledge on how the fracturing translates to overall permittivity is needed. One possible suggestion, is to derive a method for establishing a "fracture density" for each hole, based on *optical televiewer imaging* (OTW). This would lead to a better understanding of what response is produced by the fracturing parameter when fractures of different apertures are crossed by the drill bit (as indicated by the OTW), similar to methods described by Khorzoughi et al. (2018). This would allow for better estimates by establishing more insight on the actual rock mass conditions, and understanding which FI thresholds correspond to actual high resistivity (open) or closed fractures. Understanding the MWD DPI responses to different rock mass characteristics, could be the key to establish a relationship between MWD DPI and grouting parameters. Including deeper insight in terms of grouting applications.

Seeing as the ability of the MWD DPI's to produce detailed information on the rock mass characteristics ahead of the tunnel face, is of utmost importance when seeking to establish a method for utilizing this data in a grouting context. This study verified the ability of MWD to detect large scale features of the rock mass, such as weakness-zones. However, to utilize the MWD data in a grouting context, *highly* detailed information is needed. It could be argued that the sampling frequency of today's drilling equipment (approx. one sample every $3\,\mathrm{cm}$, at best), is inadequate for establishing detailed data on the *fracturing characteristics*, which is the most

important aspect when considering the groutability of the rock mass.

When both MWD data of high quality (high sampling frequency, robust DPI pre-processing, and minor loss of data), and a deeper understanding in the MWD response to various rock mass characteristics have been established. This high-quality MWD data could then be used with greater confidence in various machine learning applications. More specifically, this involves learning models based on detailed and representative data on the rock mass conditions ahead of the tunnel face. In turn, this could allow for accurate predictions of variables related to grouting, e.g. penetrability, volume, flow, and susceptibility to jacking events. These predictions could then be used as supplementary guidelines for the grouting technicians.

Chapter 9

# Conclusions

The main objective for this thesis, was to evaluate the relationship between the MWD and grouting variables, and in the process, achieving an increased understanding of how these these descriptive parameters may relate to each other. This was done in order to detect possibilities of using the MWD DPI data as a supplementary tool in the grouting procedure. This thesis also investigated several data analytical approaches to establish deeper understanding on the different MWD DPI- and grouting variables.

Main conclusions from the research results are summarized in the following list:

1. Results from MWD DPI study, suggest that it is possible to detect large scale features in the rock mass, such as weakness zones, based on the MWD DPI mapping. It should be emphasized that, based on these results, there is still uncertainty in the MWD DPI's ability to detect and respond to small scale features of the rock mass, including the overall water conductivity.

2. It was found that differences in rock mass between two different tunnels was shown through differences in the measured MWD DPI's *fracturing* and *hardness*. Thus, suggesting these two parameters could be used to relatively differentiate between rock masses.

3. It was experienced that the PF index could be used as a visual tool in detecting potential HJ cases from the grouting logs. Furthermore, results from this study indicate that approximately 23% of the grouted holes were influence by hydraulic jacking, suggesting that this phenomenon is relatively common in Norwegian grouting practice. There was

also found a logistical relationship between the cases of HJ jacking and grouted volume, time, and flow. Supporting the assumed relationship between grouting time/volume and HJ cases.

4. Considering the main research question, no significant correlation was found between any of the MWD DPI variables and the grouting variables, using the data from 13 different grout curtains comprising approximately 330 holes. However, moderate to strong correlations were found within the respective MWD DPI- and grouting data groups. Thus suggesting that inter-correlation are present *within* the two different groups, but not *between* the two data groups.

The main findings of this study indicate that no apparent relationships exist between these variable groups. However, it is still believed that the abundantly available MWD data, could still prove useful for grouting purposes in future applications. The ability of the MWD DPI's to establish detailed information on the rock mass characteristics ahead of the tunnel face, is of utmost importance when seeking to establish a method for utilizing this data in a grouting context. This study verified the ability of MWD DPI to detect large scale features of the rock mass, such as weakness-zones. Regardless, to utilize the MWD data in a grouting context, there is a need for *highly* detailed information on the rock mass ahead of the tunnel face. It could be argued that the industry standard MWD technology of today, is inadequate in describing the rock mass at a high enough level detail for it to prove useful for grouting applications. Based on the results from this thesis, it is suggested that further research is done to gain deeper understanding on the presumed relationship between MWD- and grouting parameters.

# Bibliography


Albon, C. (2018). *Machine learning with python cookbook: Practical solutions from preprocessing to deep learning*. O'Reilly Media, Inc.

Arnstein Aarset, Hans Olav Hognestad, J. I. F. A. K. L. B. E. G. and Frogner, E. (2010). Praktisk Berginjeksjon for Undergrunnsanlegg. Technical report, Norsk Forening for Fjellsprengningsteknikk.

Arnulf Hansen, Knut Garshol, R. B. and Grøv, E. (2017). The Principles of Norwegian Tunnelling. Technical report, Norsk Forening for Fjellsprengningsteknikk.

Atlas Copco/Epirock (2019). Underground Manager. `https://software.miningandconstruction.com/underground-manager`. Accessed: 15.11.2019.

Barnett, R. M. (2017). Principal Component Analysis. *Geostatistics Lessons; Deutsch, JL.*

Barr, M. V. (1985). *Instrumented horizontal drilling for tunnelling site investigation*. PhD thesis, University of London.

Barton, N. and Quadros, E. (2019). Understanding the need for pre-injection from permeability measurements: What is the connection? *Journal of Rock Mechanics and Geotechnical Engineering*, 11(3):576–597.

Bever Control AS (2019). Bever Team Online. Accessed: 14.11.2019.

Bjørn Nilsen and Arild Palmström (2000). *Engineering Geology and Rock Engineering - Handbook No 2*. NBG - Norwegian Group for Rock Mechanics.

Brantberger, M., Stille, H., and Eriksson, M. (2000). Controlling grout spreading in tunnel grouting — analyses and developments of the gin-method. *Tunnelling and Underground Space Technology*, 15(4):343 – 352.

Bro, R. and Smilde, A. K. (2014). Principal Component Analysis. *Analytical Methods*, 6(9):2812–2831.

Caine, J. S., Evans, J. P., and Forster, C. B. (1996). Fault zone architecture and permeability structure. *Geology*, 24(11):1025–1028.

David Hosmer, S. L. and Sturdivant, R. (2013). *Applied logistic regression*, volume 398. John Wiley & Sons.

Eklund, D. and Stille, H. (2008). Penetrability due to filtration tendency of cement-based grouts. *Tunnelling and Underground Space Technology*, 23(4):389 – 398.

Eriksson, M. and Stille, H. (2003). A Method for Measuring and Evaluating the Penetrability of Grouts. *Geotechnical Special Publication*, pages 1326–1337.

Ganerød, G. V. and Lutro, O. (2011). Berggrunnsgeologisk og strukturgeologisk kartlegging i forbindelse med prosjektet Fv. 650 Nordøyvegen, Møre og Romsdal. Technical report, NGU.

Ghosh, R. (2017). *Assessment of rock mass quality and its effects on charge ability using drill monitoring technique*. PhD thesis, Luleå tekniska universitet.

Grøv, E., Funehag, J., and Janson, T. (2014). Rock mass grouting in Sweden and Norway A matter of cultural differences or factual causes? *Geotechnical News*, 32:41–51.

Gunnar Gustafson (2012). *Hydrogeology for Rock Engineers*. BeFo - Rock Engineering Research Foundation.

Høien, A. H. and Nilsen, B. (2014). Rock mass grouting in the løren tunnel: case study with the main focus on the groutability and feasibility of drill parameter interpretation. *Rock Mechanics and Rock Engineering*, 47(3):967–983.

Holmøy, K. and Nilsen, B. (2014). Significance of geological parameters for predicting water inflow in hard rock tunnels. *Rock Mechanics and Rock Engineering*, 47.

Holmøy, K., Strømsvik, H., and Rise, T. (2015). State of the art for sementbasert forinjeksjon. *SINTEF Byggforsk*, 47.

Jakobsen, P. D. and van Oosterhout, D. (2018). Kort Innføring i Borparametertolkning for Anleggsdrift. Technical Report 2, NFF – Utviklingskomiteen.

Jalaleddin Rafi, H. S. and Johansson, F. (2017). Jacking of rocks fractures during pre-grouting in scandinavian tunneling projects–a study of the effects from chosen grouting pressure. *BeFo. Rock Engineering Research foundation*.

John F. Dehls, O. O. and Rønning, J. S. (2012). Magnetisk og batymetrisk kartlegging ved vegprosjektet Fv. 659 Nordøyvegen, Møre og Romsdal. Technical report, NGU.

Kettle, C. and Katterbach, M. (2015). Practical application of the gin concept (part 1). *Geotechnical News*.

Khan, R., Kuru, E., Tremblay, B., Saasen, A., et al. (2004). An investigation of the extensional viscosity of polymer based fluids as a possible mechanism of internal cake formation. In *SPE international symposium and exhibition on formation damage control*. Society of Petroleum Engineers.

Khorzoughi, M. B., Hall, R., and Apel, D. (2018). Rock fracture density characterization using measurement while drilling (MWD) techniques. *International Journal of Mining Science and Technology*, 28(6):859–864.

Kjell I. Davik, Alf Kveen, T. å. O. A. R. K. and Heimli, P. (2002). Berginjeksjon. Technical report, Norsk Forening for Fjellsprengningsteknikk.

Klüver, B. H. and Kveen, A. (2004). Berginjeksjon i praksis. Technical report, Statens Vegvesen.

Kobayashi, S., Stille, H., Gustafson, G., and Stille, B. (2008). Real time grouting control method. Development and application using Äspö HRL data. Technical report, Swedish Nuclear Fuel and Waste Management Co.

Lombardi, G. (2003). Grouting of Rock Masses. pages 164–197.

Lombardi, G. and Deere, D. (1993). Grouting design and control using the GIN principle. *Water Power & Dam Construction*.

M. Holmberg, M. Tsuji, B. S. and Stille, H. (2012). Evaluation of Pre-grouting For the City Line Project Using the RTGC Method. *International Society for Rock Mechanics and Rock Engineering*.

Meyer, D. and Wien, F. (2001). Support Vector Machines. *Porting R to Darwin/X11 and Mac OS X*, 1:23.

Moe, S. (2016). Hydraulisk jekking ved høytrykksinjeksjon av berg. Master's thesis, NTNU.

Müller, A. C., Guido, S., et al. (2016). *Introduction to machine learning with Python: a guide for data scientists*. O'Reilly Media, Inc.

Munier, R., Stenberg, L., Stanfors, R., Hermanson, J., and Triumf, C.-A. (2003). Geological site descriptive model. a strategy for the model development during site investigations. Technical report, Swedish Nuclear Fuel and Waste Management Co.

Navarro, J., Sanchidrián, J., Segarra, P., Castedo, R., Paredes, C., and López, L. (2018). On the mutual relations of drill monitoring variables and the drill control system in tunneling operations. *Tunnelling and Underground Space Technology*, 72:294–304.

NPRA (2010). Fv. 659 Nordøyvegen. `https://www.vegvesen.no/Fylkesveg/fv659nordoyvegen`. Accessed: 15.01.2020.

Pedregosa, F., Varoquaux, G., Gramfort, A., Michel, V., Thirion, B., Grisel, O., Blondel, M., Prettenhofer, P., Weiss, R., Dubourg, V., Vanderplas, J., Passos, A., Cournapeau, D., Brucher, M., Perrot, M., and Duchesnay, E. (2011). Scikit-learn: Machine Learning in Python. *Journal of Machine Learning Research*, 12:2825–2830.

Rockma System AB (2011). GPM+ Tunnel. `https://www.rockma.com/system/contact/`. Accessed: 14.11.2019.

Rolf Christiansson, Isabelle Olofsson, D. M. M. H. and Carlsson, A. (2014). Application of the observational method in the Äspö expansion project. pages 1447–1452.

Sandvik (2019). iSure. `https://www.rocktechnology.sandvik/en/products/underground-drill-rigs-and-bolters/underground-equipment-support/isure/`. Accessed: 15.11.2019.

Schumacker, R. E. (2015). *Using R with multivariate statistics*. Sage Publications.

Scwarz, L. G. and Krizek, R. J. (2000). Evolving morphology of early age microfine cement grout. In *Proceedings of Sessions of Geo-Denver 2000 - Advances in Grouting and Ground Modification, GSP 104*, volume 292, pages 181–295.

Segui, J. and Higgins, M. (2002). Blast design using measurement while drilling parameters. *Fragblast*, 6(3-4):287–299.

Stille, H. (2012). Rock Grouting In Tunnel Construction - Models And Design. In editor, T., editor, *ISRM International Symposium - EUROCK 2012*, volume 4 of *5*, page 19, Stockholm, Sweden. ISRM, International Society for Rock Mechanics and Rock Engineering.

Stille, H. (2015). *Rock grouting: theories and applications*. Befo, Rock Engineering Research Foundation.

Strømsvik, H. (2019). The significance of hydraulic jacking for grout consumption during high pressure pre-grouting in norwegian tunnelling. *Tunnelling and Underground Space Technology*, 90:357–368.

Strømsvik, H. and Grøv, E. (2017). Interpretation of Pressure and Flow during Pre-Grouting in Hard Rock Tunneling. In *Grouting 2017*, pages 285–294.

Strømsvik, H., Morud, J. C., and Grøv, E. (2018). Development of an algorithm to detect hydraulic jacking in high pressure rock mass grouting and introduction of the pf index. *Tunnelling and Underground Space Technology*, 81:16–25.

Strømsvik, H. (2019). *Assessment of High Pressure Pre-Excavation Rock Mass Grouting in Norwegian Tunnelling*. PhD thesis, NTNU.

Van Eldert, J. (2018). *Analysis of Excavation Damage, Rock Mass Characterisation and Rock Support Design using Drilling Monitoring*. PhD thesis, Luleå tekniska universitet.

van Eldert, J., Schunnesson, H., and Johansson, D. (2017). The History and Future of Rock Mass Characterisation by Drilling in Drifting: From sledgehammer to PC-tablet. In *26th International Symposium on Mine Planning and Equipment Selection, Luleå, Sweden, August 29-31, 2017*, pages 99–106. Luleå tekniska universitet.

van Eldert, J., Schunnesson, H., Johansson, D., and Saiang, D. (2019). Application of Measurement While Drilling Technology to Predict Rock Mass Quality and Rock Support for Tunnelling. *Rock Mechanics and Rock Engineering*, pages 1–10.

Vezhapparambu, V., Eidsvik, J., and Ellefmo, S. (2018). Rock classification using multivariate analysis of measurement while drilling data: Towards a better sampling strategy. *Minerals*, 8(9):384.

Wackernagel, H. (2013). *Multivariate geostatistics: an introduction with applications*. Springer Science & Business Media.

Walpole, R. E., Myers, R. H., Myers, S., and Ye, K. (2011). *Probability and Statistics for Engineers and Scientists , 9th*. Pearson.

# Appendices

## A Full MWD DPI- and grouting dataset

| | worksite | chainage | hole_id | hole_depth | hi_mean | fi_mean | wi_mean | hi_max | fi_max | wi_max | Gr_vol | Gr_endpres | Gr_time | Gr_meanflow | HJ_detected |
|---|---|---|---|---|---|---|---|---|---|---|---|---|---|---|---|
| 0 | Austnes | 5506 | 5506_1 | 23.999 | 1.209170 | 10.280930 | 2.532740 | 39.11316 | 35.049740 | 10.56515 | 1001.3 | 66.50 | 2:11:38 | 14.233305 | True |
| 1 | Austnes | 5506 | 5506_2 | 23.985 | 9.194560 | 9.991990 | 2.049380 | 37.71006 | 28.750140 | 6.19756 | 4142.7 | 67.50 | 11:35:47 | 7.627690 | False |
| 2 | Austnes | 5506 | 5506_3 | 23.993 | 12.919590 | 9.105810 | 1.995750 | 53.43641 | 26.794130 | 7.97140 | 1433.6 | 30.80 | 2:15:40 | 11.290466 | False |
| 3 | Austnes | 5506 | 5506_4 | 23.980 | 10.704680 | 10.796540 | 2.114100 | 56.49632 | 27.787310 | 8.17776 | 1196.6 | 61.20 | 2:06:20 | 7.614469 | False |
| 4 | Austnes | 5506 | 5506_5 | 23.993 | 8.644370 | 7.403370 | 2.193090 | 52.30747 | 34.661020 | 19.99814 | 1883.5 | 69.70 | 4:29:09 | 6.200890 | True |
| 5 | Austnes | 5506 | 5506_6 | 23.999 | 11.634810 | 10.202340 | 1.532040 | 55.42387 | 46.475560 | 8.19077 | 14.1 | 82.50 | 0:25:52 | 1.205970 | False |
| 6 | Austnes | 5506 | 5506_7 | 23.982 | 13.154980 | 7.966930 | 1.714710 | 45.96993 | 24.470580 | 10.99512 | 1948.6 | 66.90 | 6:20:39 | 7.390424 | False |
| 7 | Austnes | 5506 | 5506_8 | 24.004 | 17.137290 | 6.509670 | 1.791300 | 111.66973 | 46.062970 | 6.11779 | 448.2 | 70.70 | 1:56:45 | 3.866014 | True |
| 8 | Austnes | 5506 | 5506_9 | 23.731 | 8.804520 | 5.588220 | 1.781400 | 44.83992 | 34.342780 | 11.49967 | 1237.1 | 45.00 | 2:59:39 | 7.300189 | True |
| 9 | Austnes | 5506 | 5506_10 | 23.975 | 16.778590 | 6.539030 | 1.500280 | 51.02813 | 17.922180 | 7.59776 | 717.6 | 38.90 | 1:15:09 | 10.233183 | False |
| 10 | Austnes | 5506 | 5506_11 | 23.979 | 17.499930 | 6.344890 | 2.070370 | 61.53278 | 28.156600 | 20.62389 | 5503.1 | 60.20 | 12:10:18 | 10.104512 | False |
| 11 | Austnes | 5506 | 5506_12 | 15.561 | 25.791210 | 6.913520 | 1.799110 | 63.84284 | 29.663650 | 10.57366 | 222.3 | 65.50 | 0:40:36 | 5.290650 | False |
| 12 | Austnes | 5506 | 5506_13 | 25.492 | 23.829620 | 4.636290 | 1.602060 | 55.32447 | 16.909150 | 10.37057 | 549.6 | 39.20 | 1:51:51 | 6.289313 | True |
| 13 | Austnes | 5506 | 5506_16 | 23.987 | 30.498230 | 6.429280 | 1.616910 | 70.73870 | 20.868790 | 11.86651 | 1791.8 | 60.50 | 3:38:39 | 11.320786 | False |
| 14 | Austnes | 5506 | 5506_17 | 23.979 | 13.545760 | 5.643600 | 1.470710 | 44.56870 | 15.959890 | 6.84139 | 712.7 | 39.80 | 1:06:23 | 10.290881 | False |
| 15 | Austnes | 5506 | 5506_18 | 23.992 | 9.405130 | 5.315100 | 2.323990 | 50.70096 | 25.729190 | 21.40367 | 438.0 | 67.70 | 2:01:39 | 5.206200 | False |
| 16 | Austnes | 5506 | 5506_32 | 24.005 | 7.240480 | 7.282910 | 1.898130 | 77.13987 | 21.622200 | 5.31995 | 43.0 | 65.90 | 0:07:40 | 5.587500 | False |
| 17 | Austnes | 5506 | 5506_33 | 23.985 | 14.214300 | 6.619620 | 1.496760 | 43.70116 | 21.178560 | 7.81214 | 409.1 | 71.70 | 1:31:28 | 7.558884 | False |
| 18 | Austnes | 5506 | 5506_34 | 23.980 | 2.440090 | 8.558890 | 1.815560 | 36.74090 | 21.038740 | 7.80054 | 513.8 | 33.70 | 0:37:29 | 13.572124 | False |
| 19 | Austnes | 5523 | 5523_1 | 29.490 | 0.153460 | 1.193820 | 0.796560 | 32.18154 | 19.269220 | 4.15055 | 2633.0 | 60.00 | 4:55:59 | 11.256492 | False |
| 20 | Austnes | 5523 | 5523_2 | 29.480 | 1.574190 | 1.565410 | 0.757990 | 31.18157 | 14.848760 | 5.96673 | 583.1 | 55.80 | 0:58:04 | 11.695852 | False |
| 21 | Austnes | 5523 | 5523_3 | 23.993 | 25.452440 | 0.440500 | 0.842970 | 40.82592 | 11.384470 | 4.06191 | 2243.7 | 47.80 | 6:10:14 | 8.071432 | True |
| 22 | Austnes | 5523 | 5523_4 | 23.496 | 14.531460 | 2.386910 | 1.065470 | 44.47186 | 17.996450 | 5.96503 | 212.0 | 64.20 | 0:58:01 | 3.769217 | False |
| 23 | Austnes | 5523 | 5523_5 | 23.477 | 1.174860 | 2.314150 | 1.036460 | 36.43109 | 26.141430 | 4.68611 | 1293.2 | 51.40 | 2:17:20 | 10.378078 | True |
| 24 | Austnes | 5523 | 5523_6 | 23.505 | -28.268810 | 5.883920 | 1.986460 | 16.30621 | 34.838760 | 12.06607 | 26.3 | 60.80 | 0:39:53 | 1.883333 | False |
| 25 | Austnes | 5523 | 5523_7 | 23.996 | -9.863890 | 6.121170 | 1.950190 | 39.09559 | 35.205200 | 9.38567 | 2354.6 | 65.50 | 4:42:26 | 7.943887 | True |
| 26 | Austnes | 5523 | 5523_8 | 23.987 | -1.131660 | 8.288630 | 1.915300 | 39.85940 | 48.430060 | 10.64657 | 1458.4 | 60.90 | 2:57:32 | 8.476879 | False |
| 27 | Austnes | 5523 | 5523_9 | 19.508 | -10.104120 | 5.127540 | 1.952060 | 51.60145 | 29.343320 | 15.28536 | 2284.7 | 37.90 | 5:25:30 | 9.556402 | False |
| 28 | Austnes | 5523 | 5523_10 | 23.497 | -5.853540 | 7.079810 | 1.725440 | 40.74712 | 31.836090 | 9.52193 | 2584.3 | 35.70 | 4:01:16 | 13.000891 | True |
| 29 | Austnes | 5523 | 5523_11 | 23.486 | -25.818330 | 6.426060 | 1.971830 | 29.40437 | 29.260300 | 16.06403 | 1613.4 | 54.10 | 1:53:54 | 14.173520 | False |
| 30 | Austnes | 5523 | 5523_14 | 29.482 | 3.143130 | 4.381080 | 1.560050 | 84.27127 | 36.982900 | 10.91521 | 626.6 | 60.70 | 1:00:09 | 10.596775 | True |
| 31 | Austnes | 5523 | 5523_15 | 23.494 | -4.448270 | 6.836460 | 1.617880 | 52.72147 | 31.058600 | 7.02400 | 70.1 | 62.40 | 0:13:35 | 5.021687 | False |
| 32 | Austnes | 5523 | 5523_16 | 23.483 | 10.195900 | 6.646430 | 1.845320 | 53.75599 | 27.400060 | 24.82154 | 245.2 | 59.90 | 0:31:07 | 9.148734 | False |
| 33 | Austnes | 5523 | 5523_17 | 23.496 | 13.776210 | 6.111780 | 1.542310 | 54.93369 | 22.760280 | 6.63115 | 230.2 | 62.40 | 0:54:57 | 3.990634 | False |
| 34 | Austnes | 5523 | 5523_18 | 23.496 | 10.082620 | 4.443860 | 1.149630 | 43.29483 | 18.834570 | 7.06726 | 114.1 | 61.50 | 0:19:21 | 6.279487 | False |
| 35 | Austnes | 5523 | 5523_19 | 23.499 | 6.741990 | 5.678220 | 1.118040 | 112.44936 | 56.303520 | 6.46711 | 115.5 | 65.80 | 0:30:33 | 1.990517 | False |
| 36 | Austnes | 5523 | 5523_20 | 23.487 | 14.553050 | 5.051150 | 1.544550 | 64.49162 | 22.966830 | 8.36201 | 305.9 | 60.40 | 0:57:13 | 5.125872 | False |
| 37 | Austnes | 5523 | 5523_21 | 23.474 | 4.304180 | 4.492370 | 1.085400 | 35.41105 | 20.768510 | 5.15385 | 108.1 | 61.20 | 0:23:34 | 4.232168 | False |
| 38 | Austnes | 5523 | 5523_22 | 30.394 | 9.380620 | 2.243240 | 2.156650 | 53.72855 | 21.153790 | 27.14358 | 80.4 | 68.00 | 0:18:23 | 5.983117 | False |
| 39 | Austnes | 5523 | 5523_23 | 23.480 | 12.991780 | 4.789990 | 1.267330 | 67.91149 | 40.422350 | 7.18169 | 3474.3 | 57.10 | 6:09:24 | 10.822162 | True |
| 40 | Austnes | 5523 | 5523_24 | 23.494 | 3.226070 | 4.471350 | 1.071260 | 86.81121 | 59.278470 | 7.05775 | 1106.8 | 63.10 | 2:15:35 | 12.630343 | False |
| 41 | Austnes | 5523 | 5523_25 | 23.487 | -1.258920 | 4.912690 | 1.122620 | 41.98079 | 20.475510 | 5.57606 | 1026.7 | 66.30 | 2:15:00 | 11.514978 | True |
| 42 | Austnes | 5523 | 5523_27 | 21.030 | 2.614760 | 3.426230 | 1.103020 | 59.13809 | 30.132840 | 7.86453 | 43.2 | 59.30 | 0:09:08 | 4.816071 | False |
| 43 | Austnes | 5523 | 5523_28 | 23.499 | -0.024740 | 5.227170 | 1.161050 | 32.73629 | 21.945020 | 6.23680 | 116.6 | 59.70 | 0:56:41 | 2.019648 | False |
| 44 | Austnes | 5523 | 5523_29 | 23.492 | -1.515580 | 7.759980 | 2.407360 | 47.15607 | 26.895810 | 17.32058 | 231.4 | 42.20 | 1:04:44 | 6.173043 | False |

Continued on next page

| | worksite | chainage | hole_id | hole_depth | hi_mean | fi_mean | wi_mean | hi_max | fi_max | wi_max | Gr_vol | Gr_endpres | Gr_time | Gr_meanflow | HJ_detected |
|---|---|---|---|---|---|---|---|---|---|---|---|---|---|---|---|
| 45 | Austnes | 5523 | 5523_30 | 23.485 | -9.497390 | 6.456710 | 1.971110 | 35.52610 | 23.859530 | 17.88044 | 75.7 | 62.30 | 0:36:12 | 2.018349 | False |
| 46 | Austnes | 5523 | 5523_31 | 23.473 | -3.453940 | 5.682160 | 1.161580 | 34.53745 | 19.252310 | 9.66616 | 203.8 | 65.40 | 1:17:36 | 2.515665 | False |
| 47 | Austnes | 5856 | 5856_1 | 23.981 | -11.313740 | 4.545960 | 1.446090 | 31.39699 | 22.852570 | 4.99159 | 865.7 | 66.80 | 1:36:34 | 7.812708 | False |
| 48 | Austnes | 5856 | 5856_2 | 23.999 | -8.837270 | 4.238590 | 1.369600 | 16.50739 | 22.792530 | 7.12667 | 238.3 | 61.90 | 0:38:59 | 6.114468 | False |
| 49 | Austnes | 5856 | 5856_3 | 24.002 | -6.007960 | 3.713230 | 1.367460 | 32.77337 | 16.493850 | 6.48948 | 76.0 | 60.40 | 0:11:00 | 6.677612 | False |
| 50 | Austnes | 5856 | 5856_4 | 23.986 | -6.113140 | 4.444680 | 1.604220 | 39.12859 | 19.383750 | 22.85873 | 75.3 | 65.20 | 0:12:09 | 6.159459 | False |
| 51 | Austnes | 5856 | 5856_5 | 23.987 | -9.206130 | 4.558050 | 1.322040 | 27.83770 | 23.474590 | 6.41899 | 810.2 | 65.60 | 2:22:38 | 5.645093 | True |
| 52 | Austnes | 5856 | 5856_6 | 29.478 | -9.934790 | 4.498100 | 1.395520 | 27.83770 | 23.474590 | 6.41899 | 599.4 | 62.40 | 0:52:56 | 11.018495 | True |
| 53 | Austnes | 5856 | 5856_7 | 23.990 | -12.799190 | 5.121620 | 1.344870 | 46.85620 | 21.091690 | 8.21745 | 199.4 | 49.60 | 0:16:18 | 11.670707 | False |
| 54 | Austnes | 5856 | 5856_8 | 24.002 | -14.403270 | 5.497760 | 1.422240 | 24.31892 | 22.481640 | 7.77781 | 65.6 | 54.10 | 0:23:16 | 2.781560 | False |
| 55 | Austnes | 5856 | 5856_9 | 24.003 | -14.759860 | 4.573220 | 1.485480 | 25.24137 | 16.791950 | 8.08210 | 25.0 | 76.30 | 0:12:08 | 1.810811 | False |
| 56 | Austnes | 5856 | 5856_14 | 23.984 | -6.335630 | 5.348910 | 1.019640 | 25.07506 | 18.024020 | 8.21040 | 263.0 | 50.00 | 0:11:13 | 2.257881 | False |
| 57 | Austnes | 5856 | 5856_15 | 24.000 | -9.721460 | 5.019140 | 1.189500 | 24.85595 | 18.386330 | 3.50780 | 573.0 | 45.00 | 1:48:38 | 5.788744 | False |
| 58 | Austnes | 5856 | 5856_16 | 23.992 | -8.670110 | 5.047880 | 1.307600 | 15.49724 | 17.648660 | 6.03330 | 276.0 | 62.00 | 0:21:35 | 13.043511 | False |
| 59 | Austnes | 5856 | 5856_17 | 23.976 | -7.553430 | 5.669460 | 1.440220 | 36.83755 | 21.325140 | 6.83980 | 320.0 | 63.70 | NaN | NaN | False |
| 60 | Austnes | 5856 | 5856_18 | 23.999 | -10.103710 | 4.444320 | 1.255910 | 26.07930 | 21.015540 | 4.53740 | 320.0 | 60.00 | 0:47:21 | 6.623509 | True |
| 61 | Austnes | 5856 | 5856_19 | 23.999 | -8.837270 | 4.238590 | 1.369600 | 16.50739 | 22.792530 | 7.12670 | 42.0 | 60.00 | 0:14:01 | 2.700000 | False |
| 62 | Austnes | 5856 | 5856_20 | 23.977 | -6.811220 | 3.970610 | 1.450900 | 19.73772 | 15.504190 | 6.42530 | 129.0 | 33.00 | 0:15:22 | 6.761175 | False |
| 63 | Austnes | 5856 | 5856_22 | 29.484 | -12.400000 | 4.603630 | 1.331110 | 33.80769 | 21.256720 | 8.74350 | 94.0 | 60.00 | NaN | NaN | False |
| 64 | Austnes | 5856 | 5856_23 | 23.978 | -12.905950 | 4.346620 | 1.025430 | 31.80692 | 17.509950 | 4.68740 | 25.0 | 15.00 | 0:05:33 | 4.097143 | False |
| 65 | Austnes | 5856 | 5856_24 | 23.989 | -9.204540 | 4.686290 | 1.069060 | 33.26406 | 18.423800 | 5.78480 | 270.0 | 64.00 | 0:31:11 | 8.589894 | False |
| 66 | Austnes | 5856 | 5856_25 | 29.479 | -5.065310 | 5.545920 | 1.225130 | 29.52562 | 26.560010 | 8.43600 | 300.0 | 63.00 | 0:55:58 | 5.332641 | False |
| 67 | Austnes | 5856 | 5856_26 | 23.983 | -10.716180 | 4.382390 | 1.085640 | 14.52707 | 15.425570 | 5.39600 | 11.0 | 50.00 | 0:03:17 | 4.261905 | False |
| 68 | Austnes | 5892 | 5892_1 | 23.505 | 6.507940 | 1.603990 | 1.462360 | 37.60539 | 16.800530 | 6.25836 | 3594.5 | 99.90 | 5:23:00 | 8.819823 | True |
| 69 | Austnes | 5892 | 5892_2 | 23.477 | -1.344900 | 3.939420 | 1.568020 | 32.98139 | 18.859180 | 5.65914 | 1801.5 | 74.10 | 2:44:46 | 10.845986 | False |
| 70 | Austnes | 5892 | 5892_3 | 23.370 | 3.540490 | 4.690220 | 1.278280 | 35.94885 | 16.820690 | 5.19842 | 679.9 | 84.90 | 1:05:59 | 9.310930 | False |
| 71 | Austnes | 5892 | 5892_4 | 14.931 | -0.230520 | 0.168590 | 2.214300 | 2.84473 | 3.907070 | 25.68012 | 1588.3 | 84.00 | 4:16:31 | 8.570575 | True |
| 72 | Austnes | 5892 | 5892_5 | 23.489 | -2.583070 | 3.236990 | 1.207780 | 19.60834 | 17.315880 | 15.05720 | 225.2 | 84.40 | 0:56:02 | 7.300686 | False |
| 73 | Austnes | 5892 | 5892_6 | 23.485 | -9.930100 | 1.973020 | 0.941310 | 23.28227 | 14.746030 | 12.70843 | 2206.1 | 74.90 | 2:32:06 | 8.154663 | False |
| 74 | Austnes | 5892 | 5892_7 | 23.475 | -1.045690 | 4.076700 | 1.300730 | 26.16489 | 17.109830 | 6.52621 | 177.9 | 92.20 | 0:53:24 | 4.968796 | False |
| 75 | Austnes | 5892 | 5892_8 | 23.504 | -0.503110 | 4.129830 | 0.959360 | 27.23633 | 21.956270 | 5.69015 | 2409.1 | 72.80 | 4:35:46 | 8.770993 | False |
| 76 | Austnes | 5892 | 5892_9 | 23.503 | 2.788690 | 3.239970 | 1.370400 | 32.17226 | 13.595350 | 12.47096 | 4935.0 | 61.00 | 5:54:13 | 10.562845 | False |
| 77 | Austnes | 5892 | 5892_10 | 23.507 | 23.042810 | 2.268840 | 1.801630 | 43.22766 | 14.686510 | 37.53916 | 4100.5 | 57.60 | 6:44:48 | 11.765398 | False |
| 78 | Austnes | 5892 | 5892_11 | 23.484 | 10.434140 | 2.607750 | 1.055300 | 39.02823 | 16.594280 | 3.85184 | 1307.3 | 91.80 | 2:32:38 | 9.409518 | False |
| 79 | Austnes | 5892 | 5892_12 | 23.493 | 2.585640 | 3.032880 | 1.352440 | 36.19185 | 18.205470 | 7.13103 | 1191.8 | 94.40 | 1:53:10 | 18.115116 | False |
| 80 | Austnes | 5892 | 5892_13 | 23.486 | 10.933960 | 2.872280 | 1.392410 | 40.62447 | 18.844250 | 5.82650 | 267.7 | 60.60 | 0:42:32 | 6.650423 | False |
| 81 | Austnes | 5892 | 5892_14 | 23.491 | 9.212410 | 3.212310 | 1.460460 | 39.45597 | 19.501570 | 10.70620 | 1835.6 | 67.70 | 2:17:18 | 17.482325 | True |
| 82 | Austnes | 5892 | 5892_15 | 23.478 | 6.225940 | 3.124050 | 1.049020 | 40.20195 | 17.349660 | 6.71379 | 52.5 | 67.10 | 0:10:25 | 5.073437 | False |
| 83 | Austnes | 5892 | 5892_16 | 23.501 | 7.381240 | 2.639120 | 1.180210 | 44.31775 | 33.281050 | 6.53095 | 303.6 | 30.90 | 1:24:29 | 5.727200 | False |
| 84 | Austnes | 5892 | 5892_17 | 23.493 | -10.179800 | 2.322050 | 2.708080 | 27.53766 | 15.701250 | 25.06155 | 16.3 | 0.00 | 0:14:09 | 1.279167 | False |
| 85 | Austnes | 5892 | 5892_18 | 23.503 | -3.099160 | 5.042940 | 2.497990 | 36.71686 | 18.368910 | 25.77655 | 610.1 | 42.10 | 1:46:48 | 5.690796 | False |
| 86 | Austnes | 5892 | 5892_19 | 23.570 | -3.371350 | 4.227730 | 2.267070 | 23.58275 | 18.855100 | 16.46665 | 308.2 | 42.60 | 0:28:26 | 10.804070 | False |
| 87 | Austnes | 5892 | 5892_20 | 23.504 | 1.384960 | 4.491310 | 1.872200 | 34.34413 | 18.840320 | 13.45039 | 981.0 | 41.50 | 2:24:45 | 4.539910 | False |
| 88 | Austnes | 5892 | 5892_21 | 21.046 | -13.017350 | 2.473420 | 2.773710 | 36.42496 | 19.487300 | 10.87284 | 218.3 | 63.00 | 0:57:03 | 3.842690 | True |
| 89 | Austnes | 5892 | 5892_22 | 23.498 | -2.296440 | 4.467660 | 2.172260 | 32.18809 | 19.045560 | 37.80778 | 1058.5 | 91.20 | 1:52:42 | 12.031579 | True |

Continued on next page

| | worksite | chainage | hole_id | hole_depth | hi_mean | fi_mean | wi_mean | hi_max | fi_max | wi_max | Gr_vol | Gr_endpres | Gr_time | Gr_meanflow | HJ_detected |
|---|---|---|---|---|---|---|---|---|---|---|---|---|---|---|---|
| 90 | Austnes | 5892 | 5892_23 | 23.506 | -1.238370 | 3.717130 | 1.435480 | 25.14669 | 20.930790 | 10.23608 | 1402.7 | 68.00 | 2:50:48 | 11.819306 | True |
| 91 | Austnes | 5892 | 5892_24 | 23.476 | -0.323260 | 4.024550 | 1.669130 | 34.63026 | 15.743520 | 15.16257 | 1297.0 | 60.80 | 1:55:47 | 12.860316 | False |
| 92 | Austnes | 5892 | 5892_25 | 23.482 | 0.300180 | 3.377400 | 1.245630 | 29.97987 | 19.802530 | 6.81665 | 942.1 | 66.20 | 2:28:25 | 6.326777 | False |
| 93 | Austnes | 5892 | 5892_26 | 23.498 | 3.794210 | 1.363190 | 0.774740 | 40.55666 | 33.346060 | 14.89051 | 2829.4 | 63.90 | 4:25:54 | 11.109984 | True |
| 94 | Austnes | 6045 | 6045_1 | 23.502 | -4.024330 | 2.866970 | 1.015010 | 23.17708 | 16.069213 | 7.78000 | 1260.2 | 63.00 | 2:37:20 | NaN | False |
| 95 | Austnes | 6045 | 6045_2 | 23.489 | -10.469200 | 3.402380 | 1.293910 | 24.05560 | 19.652280 | 8.49000 | 503.2 | 61.40 | 0:48:59 | NaN | False |
| 96 | Austnes | 6045 | 6045_3 | 23.501 | -8.647540 | 2.640430 | 0.967110 | 26.17539 | 19.027550 | 5.76768 | 1001.2 | 59.00 | 1:26:29 | NaN | False |
| 97 | Austnes | 6045 | 6045_4 | 23.480 | 2.146170 | 2.197840 | 0.999240 | 26.97472 | 18.296250 | 5.10170 | 1813.0 | 59.00 | 2:14:56 | NaN | False |
| 98 | Austnes | 6045 | 6045_5 | 23.489 | -15.170400 | 3.865140 | 1.519790 | 23.86079 | 19.125290 | 8.80384 | 3999.2 | 51.90 | 5:16:32 | NaN | False |
| 99 | Austnes | 6045 | 6045_6 | 23.493 | -14.038450 | 2.892130 | 1.220170 | 11.39831 | 16.267050 | 7.22589 | 1017.7 | 62.00 | 1:21:07 | NaN | False |
| 100 | Austnes | 6045 | 6045_7 | 22.631 | -11.405140 | 2.945490 | 1.390500 | 15.09373 | 23.007700 | 10.15864 | 1019.7 | 55.60 | 1:36:09 | NaN | False |
| 101 | Austnes | 6045 | 6045_8 | 23.478 | -10.869090 | 2.497520 | 1.225150 | 33.57691 | 16.240570 | 7.48541 | 2702.8 | 61.90 | 3:46:51 | NaN | False |
| 102 | Austnes | 6045 | 6045_9 | 23.483 | -10.979310 | 1.700000 | 1.186750 | 10.93971 | 14.441060 | 12.40248 | 3335.0 | 58.40 | 3:11:44 | NaN | False |
| 103 | Austnes | 6045 | 6045_10 | 29.490 | -3.133650 | 3.686790 | 1.459190 | 31.36678 | 18.955670 | 10.64849 | 341.6 | 58.00 | 0:57:59 | NaN | False |
| 104 | Austnes | 6045 | 6045_11 | 23.502 | -12.484780 | 3.967770 | 1.429330 | 36.13909 | 25.404120 | 18.00423 | 2056.0 | 58.80 | 2:02:03 | NaN | False |
| 105 | Austnes | 6045 | 6045_12 | 23.496 | -5.548610 | 4.006230 | 1.297460 | 19.46186 | 17.688280 | 7.50915 | 921.6 | 56.40 | 1:47:40 | NaN | False |
| 106 | Austnes | 6045 | 6045_13 | 23.479 | 16.410510 | 3.244340 | 2.581850 | 136.92592 | 54.759200 | 15.11842 | 500.6 | 32.70 | 0:31:44 | NaN | False |
| 107 | Austnes | 6045 | 6045_14 | 23.506 | -1.759260 | 5.073100 | 1.906720 | 48.14970 | 22.935750 | 13.21582 | 2182.3 | 57.10 | 2:30:21 | NaN | False |
| 108 | Austnes | 6045 | 6045_15 | 29.493 | -0.639880 | 4.595530 | 1.845840 | 29.29396 | 16.771990 | 19.55445 | 1682.8 | 57.50 | 1:53:45 | NaN | False |
| 109 | Austnes | 6045 | 6045_16 | 23.483 | -2.388330 | 4.815540 | 1.240470 | 56.37435 | 47.080500 | 6.39046 | 986.4 | 45.70 | 1:14:15 | NaN | False |
| 110 | Austnes | 6045 | 6045_17 | 23.506 | -2.300960 | 4.406720 | 1.531620 | 38.83983 | 34.225550 | 25.61954 | 111.2 | 46.10 | 0:15:53 | NaN | False |
| 111 | Austnes | 6045 | 6045_18 | 23.487 | 4.089020 | 4.164240 | 2.249810 | 51.24193 | 20.882090 | 14.18217 | 148.8 | 39.80 | 0:21:20 | NaN | False |
| 112 | Austnes | 6045 | 6045_19 | 23.495 | 3.088490 | 3.354100 | 2.565390 | 30.18365 | 15.969540 | 16.19742 | 201.0 | 46.10 | 0:25:04 | NaN | False |
| 113 | Austnes | 6045 | 6045_20 | 29.497 | -6.971630 | 4.230130 | 2.230910 | 43.51517 | 22.206630 | 16.06788 | 82.0 | 43.70 | 0:16:49 | NaN | False |
| 114 | Austnes | 6045 | 6045_21 | 23.476 | 6.639520 | 4.458990 | 2.013100 | 48.20578 | 25.511730 | 14.55968 | 107.2 | 61.40 | 0:32:49 | NaN | False |
| 115 | Austnes | 6045 | 6045_22 | 23.492 | -0.848970 | 3.607730 | 1.790010 | 58.61753 | 26.141120 | 14.72140 | 60.7 | 62.30 | 0:05:49 | NaN | False |
| 116 | Austnes | 6045 | 6045_23 | 23.496 | -1.090050 | 3.065290 | 2.051840 | 51.23907 | 30.530630 | 24.10306 | 68.1 | 62.10 | 0:12:37 | NaN | False |
| 117 | Austnes | 6045 | 6045_24 | 23.506 | -10.199800 | 3.294730 | 1.881640 | 13.06025 | 16.540630 | 14.20324 | 877.4 | 56.80 | 1:25:44 | NaN | False |
| 118 | Austnes | 6045 | 6045_25 | 29.497 | -7.512990 | 4.143450 | 1.175800 | 26.83076 | 18.733220 | 8.22345 | 2917.5 | 55.90 | 2:43:48 | NaN | False |
| 119 | Austnes | 6045 | 6045_26 | 23.486 | -13.210720 | 5.242730 | 1.620530 | 71.52769 | 38.218850 | 14.16854 | 1.7 | 61.60 | 0:03:52 | NaN | False |
| 120 | Austnes | 6203 | 6203_1 | 23.384 | -9.652980 | 4.821030 | 1.418620 | 63.08564 | 39.311560 | 13.90191 | 2000.9 | 27.40 | 3:58:32 | 12.168728 | False |
| 121 | Austnes | 6203 | 6203_2 | 23.471 | -9.762070 | 5.310870 | 1.090590 | 50.91589 | 45.129420 | 5.20831 | 494.9 | 48.00 | 1:38:28 | 4.252656 | False |
| 122 | Austnes | 6203 | 6203_3 | 23.497 | -3.803360 | 5.707530 | 1.255950 | 17.99526 | 15.652360 | 10.91141 | 1067.9 | 81.30 | 1:53:45 | 7.599682 | True |
| 123 | Austnes | 6203 | 6203_4 | 23.489 | -17.139860 | 4.843090 | 1.219940 | 15.40577 | 21.200770 | 6.80610 | 656.1 | 60.30 | 1:18:24 | 4.645226 | False |
| 124 | Austnes | 6203 | 6203_5 | 23.497 | -20.483490 | 4.241460 | 1.184900 | 8.78658 | 18.036690 | 6.10231 | 2008.1 | 27.50 | 3:03:40 | 29.914523 | False |
| 125 | Austnes | 6203 | 6203_6 | 23.500 | -15.812070 | 4.715670 | 1.010590 | 10.62032 | 19.963420 | 6.93028 | 1247.3 | 44.90 | 2:39:15 | 7.930537 | False |
| 126 | Austnes | 6203 | 6203_7 | 23.498 | -14.639400 | 4.967470 | 1.060650 | 15.46994 | 21.580680 | 4.70967 | 2000.1 | 31.70 | 2:46:41 | 13.501416 | True |
| 127 | Austnes | 6203 | 6203_8 | 23.485 | -11.423910 | 4.838680 | 1.095730 | 26.00880 | 22.627120 | 7.63649 | 2008.8 | 31.60 | 1:47:10 | 18.782841 | False |
| 128 | Austnes | 6203 | 6203_9 | 23.498 | -21.100100 | 4.593820 | 1.377440 | 40.23068 | 28.198760 | 17.82220 | 2104.9 | 30.00 | 1:55:41 | 18.133442 | False |
| 129 | Austnes | 6203 | 6203_10 | 23.487 | -14.416460 | 5.216460 | 1.290880 | 26.68781 | 21.757660 | 8.86696 | 2240.1 | 63.00 | 3:07:19 | 18.861587 | True |
| 130 | Austnes | 6203 | 6203_11 | 23.481 | -19.202170 | 4.392620 | 1.339090 | 24.50290 | 19.469770 | 9.25971 | 2062.3 | 59.90 | 2:08:04 | 16.651375 | False |
| 131 | Austnes | 6203 | 6203_12 | 29.499 | -12.334690 | 4.689990 | 1.174400 | 24.28419 | 14.989650 | 6.15209 | 2188.0 | 59.50 | 2:23:44 | -15.892030 | False |
| 132 | Austnes | 6203 | 6203_13 | 23.490 | -10.733700 | 4.917140 | 1.262530 | 28.06705 | 15.421200 | 7.46496 | 2406.1 | 34.30 | 2:33:26 | 14.380039 | False |
| 133 | Austnes | 6203 | 6203_14 | 29.494 | -10.503120 | 3.284180 | 1.135950 | 6.38000 | 11.077830 | 22.41394 | 2016.6 | 57.70 | 3:49:55 | 8.448052 | False |
| 134 | Austnes | 6203 | 6203_15 | 23.511 | -4.703980 | 4.946630 | 1.119880 | 33.12181 | 19.066530 | 7.58365 | 2027.7 | 36.70 | 1:34:56 | 20.575872 | False |

Continued on next page

| | worksite | chainage | hole_id | hole_depth | hi_mean | fi_mean | wi_mean | hi_max | fi_max | wi_max | Gr_vol | Gr_endpres | Gr_time | Gr_meanflow | HJ_detected |
|---|---|---|---|---|---|---|---|---|---|---|---|---|---|---|---|
| 135 | Austnes | 6203 | 6203_16 | 23.488 | -4.012020 | 4.210920 | 1.121580 | 24.92606 | 15.070370 | 7.64399 | 81.7 | 49.20 | 0:28:22 | 2.953216 | False |
| 136 | Austnes | 6203 | 6203_17 | 23.503 | -5.289490 | 4.157190 | 0.975260 | 45.53546 | 14.914630 | 5.88287 | 150.8 | 41.60 | 0:21:19 | 7.004651 | False |
| 137 | Austnes | 6203 | 6203_18 | 23.483 | -7.543060 | 4.298230 | 1.246080 | 27.93332 | 15.984290 | 8.38459 | 914.0 | 44.60 | 3:43:53 | 5.102127 | False |
| 138 | Austnes | 6203 | 6203_19 | 23.494 | -7.016110 | 4.580930 | 1.044320 | 23.91517 | 18.235500 | 5.12072 | 613.4 | 54.50 | 2:23:27 | 3.285897 | True |
| 139 | Austnes | 6203 | 6203_20 | 23.484 | -1.982600 | 3.780690 | 1.203030 | 35.77485 | 15.860340 | 5.68934 | 1.8 | 44.30 | 0:59:21 | 4.053030 | False |
| 140 | Austnes | 6203 | 6203_21 | 23.596 | -5.756840 | 3.738420 | 1.363080 | 14.17129 | 11.483300 | 4.75906 | 1377.0 | 37.70 | 1:47:11 | 12.866979 | True |
| 141 | Austnes | 6203 | 6203_22 | 29.480 | 11.464120 | 2.803500 | 0.962100 | 45.02155 | 17.414230 | 5.19550 | 1463.3 | 62.40 | 1:50:37 | 9.648913 | False |
| 142 | Austnes | 6203 | 6203_23 | 23.476 | -4.510360 | 4.007960 | 1.140140 | 20.08059 | 16.576530 | 7.13016 | 483.0 | 63.90 | 0:40:38 | 12.648704 | False |
| 143 | Austnes | 6203 | 6203_24 | 23.486 | -5.654060 | 4.530490 | 1.318100 | 44.26567 | 20.170580 | 12.63895 | 1421.6 | 62.60 | 2:36:45 | 6.618285 | False |
| 144 | Austnes | 6203 | 6203_25 | 29.476 | -5.511590 | 4.529710 | 1.189260 | 85.60776 | 33.623750 | 9.10539 | 2476.0 | 52.30 | 3:15:47 | 16.503984 | True |
| 145 | Austnes | 6203 | 6203_26 | 23.487 | -6.839770 | 4.812620 | 1.027710 | 28.52435 | 28.615610 | 8.74335 | 272.4 | 59.90 | 1:08:03 | 4.527532 | False |
| 146 | Austnes | 6203 | 6203_27 | 23.497 | -17.676000 | 4.893270 | 1.240180 | 21.45205 | 20.149820 | 6.45596 | 2208.5 | 41.50 | 3:17:59 | 9.940787 | True |
| 147 | Austnes | 6203 | 6203_28 | 23.506 | -12.205230 | 4.933210 | 1.398160 | 26.75976 | 23.661000 | 7.57368 | 2250.1 | 60.10 | 3:39:41 | -17.523598 | False |
| 148 | Austnes | 6203 | 6203_29 | 23.481 | -4.977480 | 5.107890 | 1.093900 | 30.46654 | 23.781820 | 5.09380 | 2132.2 | 30.20 | 3:20:31 | 10.609040 | True |
| 149 | Austnes | 6203 | 6203_30 | 23.502 | -11.637380 | 4.938260 | 1.157870 | 18.11525 | 18.780750 | 5.19328 | 958.4 | 60.10 | 1:12:30 | 9.735152 | False |
| 150 | Longva | 23545 | 23545_1 | 23.681 | -8.536670 | 10.017900 | 1.043400 | 36.82570 | 29.464150 | 5.98208 | 1416.7 | 66.70 | 5:22:43 | 4.259232 | False |
| 151 | Longva | 23545 | 23545_2 | 23.684 | -14.160740 | 7.163320 | 1.020920 | 14.74458 | 26.659780 | 6.25509 | 2442.3 | 72.00 | 3:53:12 | 8.821911 | False |
| 152 | Longva | 23545 | 23545_3 | 23.705 | -8.780510 | 13.732450 | 1.174650 | 27.93597 | 42.645600 | 6.70456 | 1092.7 | 59.20 | 2:27:02 | 6.392838 | True |
| 153 | Longva | 23545 | 23545_4 | 23.680 | -8.282650 | 9.802130 | 0.976330 | 33.92083 | 32.309080 | 5.98969 | 4114.1 | 62.80 | 6:18:56 | 7.321801 | False |
| 154 | Longva | 23545 | 23545_5 | 23.685 | -13.982150 | 8.844380 | 1.176130 | 37.18347 | 36.068620 | 6.64603 | 399.8 | 64.30 | 1:29:12 | 5.357117 | False |
| 155 | Longva | 23545 | 23545_6 | 23.701 | -20.538660 | 4.685770 | 0.724000 | 36.07736 | 32.650090 | 8.22020 | 161.3 | 61.40 | 0:31:33 | 4.936649 | False |
| 156 | Longva | 23545 | 23545_7 | 23.547 | -18.280620 | 5.781970 | 1.495600 | 44.94639 | 33.795720 | 18.65103 | 74.6 | 60.70 | 0:25:56 | 2.508917 | False |
| 157 | Longva | 23545 | 23545_8 | 23.689 | -19.806980 | 5.960040 | 1.030130 | 6.53611 | 16.184340 | 10.87789 | 5722.3 | 68.00 | 6:15:00 | 14.882697 | True |
| 158 | Longva | 23545 | 23545_9 | 23.677 | -20.322240 | 6.540040 | 1.878640 | 35.73167 | 48.797000 | 21.96358 | 658.6 | 97.30 | 1:19:24 | 9.315744 | False |
| 159 | Longva | 23545 | 23545_10 | 23.702 | -13.861540 | 5.348790 | 0.968250 | 39.54653 | 21.007700 | 11.51166 | 528.7 | 62.20 | 1:32:49 | 8.031667 | False |
| 160 | Longva | 23545 | 23545_11 | 23.694 | -15.756820 | 5.013870 | 0.876960 | 5.69611 | 14.787560 | 7.20594 | 742.7 | 38.50 | 2:06:28 | 9.702153 | False |
| 161 | Longva | 23545 | 23545_12 | 23.692 | -14.965800 | 5.822990 | 1.126580 | 34.61111 | 32.913950 | 8.01559 | 266.3 | 61.80 | 1:04:02 | 2.944255 | False |
| 162 | Longva | 23545 | 23545_13 | 23.674 | -13.428480 | 5.337840 | 0.670000 | 12.35458 | 23.886130 | 6.70808 | 2189.5 | 65.50 | 3:42:49 | 10.693892 | True |
| 163 | Longva | 23545 | 23545_14 | 23.689 | -23.202450 | 5.167450 | 1.038030 | 46.94375 | 40.023550 | 6.82126 | 3788.9 | 61.20 | 6:45:00 | 11.939213 | True |
| 164 | Longva | 23545 | 23545_15 | 29.676 | -10.935350 | 7.795630 | 1.129890 | 72.09778 | 33.000100 | 18.78497 | 1689.2 | 65.00 | 1:58:35 | 14.374945 | False |
| 165 | Longva | 23545 | 23545_16 | 23.595 | -18.798260 | 4.378360 | 1.089780 | 11.95639 | 16.633650 | 8.05579 | 1722.1 | 61.70 | 4:09:34 | 6.848357 | False |
| 166 | Longva | 23545 | 23545_17 | 23.604 | -18.967330 | 4.759580 | 0.954440 | 98.21667 | 68.358960 | 7.45577 | 520.4 | 61.50 | 1:44:52 | 4.976115 | False |
| 167 | Longva | 23545 | 23545_18 | 23.686 | -24.105050 | 4.330300 | 0.997840 | 3.79416 | 11.353840 | 6.67193 | 2469.6 | 65.10 | 6:27:30 | 6.048387 | False |
| 168 | Longva | 23545 | 23545_19 | 23.702 | -24.811930 | 4.521930 | 0.847430 | 12.30806 | 19.930760 | 6.21563 | 3.8 | 70.50 | 0:11:40 | 0.729167 | False |
| 169 | Longva | 23545 | 23545_20 | 11.955 | -5.774050 | 8.123200 | 1.440710 | 31.81028 | 25.056340 | 6.46365 | 1.9 | 61.70 | 0:13:48 | 0.882353 | False |
| 170 | Longva | 23545 | 23545_21 | 23.704 | -14.776010 | 7.461650 | 1.192140 | 25.60097 | 22.779340 | 7.12596 | 1.5 | 59.80 | 0:02:59 | 0.080000 | False |
| 171 | Longva | 23545 | 23545_22 | 23.705 | -14.806530 | 7.339430 | 1.153910 | 28.49694 | 26.086540 | 6.87106 | 517.1 | 65.60 | 1:01:34 | 5.535484 | False |
| 172 | Longva | 23545 | 23545_23 | 29.581 | -15.276950 | 7.442090 | 1.144230 | 24.14597 | 23.115030 | 7.84058 | 1364.6 | 67.20 | 2:05:52 | 10.467275 | True |
| 173 | Longva | 23545 | 23545_24 | 23.603 | -11.444470 | 8.291170 | 1.127450 | 33.75069 | 28.302070 | 6.28043 | 534.7 | 67.50 | 1:22:51 | 7.479642 | False |
| 174 | Longva | 23545 | 23545_25 | 23.603 | -10.117920 | 9.470290 | 1.061890 | 38.70056 | 29.426870 | 5.97883 | 1422.3 | 63.00 | 2:03:37 | 6.977168 | False |
| 175 | Longva | 23545 | 23545_26 | 23.470 | -12.547750 | 9.733510 | 0.889100 | 7.07750 | 22.234300 | 10.25653 | 319.4 | 60.40 | 0:56:56 | 5.322112 | False |
| 176 | Longva | 23545 | 23545_27 | 23.589 | -12.711780 | 9.296410 | 1.089600 | 30.78986 | 29.379420 | 9.03218 | 171.1 | 79.40 | 1:27:02 | 3.076093 | False |
| 177 | Longva | 23545 | 23545_28 | 23.685 | -14.085500 | 4.434620 | 0.919200 | 62.24875 | 36.274970 | 14.24656 | 3962.0 | 63.90 | 8:15:54 | 8.971313 | True |
| 178 | Longva | 23528 | 23528_1 | 23.573 | -9.815910 | 6.959400 | 2.153750 | 63.22292 | 60.646620 | 20.49989 | 794.5 | 72.30 | 1:15:42 | 10.469451 | False |
| 179 | Longva | 23528 | 23528_2 | 23.604 | -10.595210 | 5.344780 | 1.027100 | 38.66667 | 27.274800 | 6.82830 | 2053.7 | 64.80 | 2:19:20 | 13.938850 | False |

Continued on next page

| | worksite | chainage | hole_id | hole_depth | hi_mean | fi_mean | wi_mean | hi_max | fi_max | wi_max | Gr_vol | Gr_endpres | Gr_time | Gr_meanflow | HJ_detected |
|---|---|---|---|---|---|---|---|---|---|---|---|---|---|---|---|
| 180 | Longva | 23528 | 23528_3 | 23.578 | -21.453680 | 5.208800 | 1.130580 | 10.41389 | 20.242150 | 8.90981 | 1983.2 | 62.70 | 3:15:40 | 10.533866 | False |
| 181 | Longva | 23528 | 23528_4 | 23.584 | -20.813970 | 5.649810 | 0.736780 | 14.53514 | 16.141490 | 7.40450 | 440.1 | 66.80 | 1:31:11 | 5.003877 | False |
| 182 | Longva | 23528 | 23528_5 | 23.599 | -25.532720 | 5.742800 | 0.707850 | 2.63444 | 20.491720 | 9.15287 | 73.6 | 63.20 | 0:20:43 | 3.417460 | False |
| 183 | Longva | 23528 | 23528_6 | 23.596 | -24.445400 | 4.978400 | 1.047750 | 2.68180 | 13.922630 | 6.09289 | 2034.4 | 56.00 | 5:53:58 | 7.315081 | True |
| 184 | Longva | 23528 | 23528_7 | 23.580 | -21.121350 | 5.219570 | 0.723230 | 8.94361 | 23.917530 | 8.04432 | 2.9 | 62.30 | 0:05:44 | 0.369444 | False |
| 185 | Longva | 23528 | 23528_8 | 23.585 | -16.634720 | 5.146130 | 1.024850 | 12.81111 | 26.768690 | 5.78107 | 2954.4 | 65.40 | 6:24:18 | 7.610650 | True |
| 186 | Longva | 23528 | 23528_9 | 29.603 | -16.418890 | 5.059970 | 0.911220 | 8.66000 | 17.717170 | 7.60150 | 3066.7 | 55.00 | 7:02:30 | 5.782987 | True |
| 187 | Longva | 23528 | 23528_10 | 23.597 | -18.956720 | 4.906620 | 1.024490 | 16.86556 | 16.670110 | 7.51869 | 154.2 | 47.40 | 0:49:52 | 3.222395 | False |
| 188 | Longva | 23528 | 23528_11 | 23.581 | -21.612160 | 4.766150 | 0.895940 | 10.96222 | 15.996020 | 6.17374 | 155.4 | 48.80 | 0:58:01 | 2.541989 | False |
| 189 | Longva | 23528 | 23528_12 | 23.578 | -17.631640 | 4.579900 | 0.836820 | 5.58069 | 18.132150 | 9.01495 | 587.6 | 40.90 | 1:35:26 | 6.312977 | False |
| 190 | Longva | 23528 | 23528_13 | 23.604 | -21.651070 | 4.839480 | 1.058290 | 7.62889 | 12.941940 | 8.55054 | 200.8 | 44.60 | 1:00:20 | 3.118277 | False |
| 191 | Longva | 23528 | 23528_14 | 29.602 | -18.688570 | 4.828960 | 1.072070 | 11.78097 | 15.250300 | 7.27487 | 183.8 | 46.80 | 1:43:57 | 3.059956 | False |
| 192 | Longva | 23528 | 23528_15 | 23.579 | -20.841740 | 5.097840 | 0.976430 | 7.10833 | 17.994600 | 6.15589 | 577.1 | 57.80 | 2:50:52 | 3.806113 | True |
| 193 | Longva | 23528 | 23528_16 | 23.595 | -23.974020 | 5.398930 | 0.858850 | 3.13250 | 18.915980 | 6.74338 | 801.0 | 60.10 | 4:02:18 | 4.561211 | False |
| 194 | Longva | 23528 | 23528_17 | 23.583 | -30.524230 | 5.046650 | 1.204510 | 2.44389 | 19.747650 | 7.95772 | 886.3 | 49.90 | 1:39:28 | 9.341551 | True |
| 195 | Longva | 23528 | 23528_18 | 23.600 | -28.067540 | 5.532370 | 1.568540 | 11.60444 | 19.035950 | 8.06793 | 3184.7 | 57.50 | 3:55:15 | 14.978483 | False |
| 196 | Longva | 23528 | 23528_19 | 23.596 | -21.536410 | 6.024630 | 1.162590 | 5.44278 | 23.073030 | 6.08074 | 4041.6 | 69.20 | 5:03:40 | 11.161489 | True |
| 197 | Longva | 23528 | 23528_20 | 29.605 | -18.091920 | 5.215880 | 1.236590 | 20.82125 | 20.524220 | 6.33467 | 3106.4 | 63.40 | 8:08:39 | 7.644103 | False |
| 198 | Longva | 23528 | 23528_21 | 23.579 | -20.162630 | 6.704590 | 1.401960 | 68.34208 | 50.528760 | 15.06599 | 1025.7 | 67.20 | 2:51:24 | 4.921902 | False |
| 199 | Longva | 23528 | 23528_22 | 29.578 | -13.994950 | 5.164250 | 1.618250 | 32.18972 | 43.560200 | 18.97783 | 1.9 | 67.20 | 0:04:41 | 0.390000 | False |
| 200 | Longva | 23577 | 23577_1 | 23.701 | -18.598865 | 4.234984 | 2.023945 | 49.83403 | 23.618480 | 40.87172 | 1246.7 | 78.70 | 4:58:04 | 3.875660 | False |
| 201 | Longva | 23577 | 23577_2 | 23.687 | -17.220235 | 4.597757 | 1.008998 | 54.49611 | 22.429310 | 5.96726 | 135.7 | 46.93 | 0:26:11 | 5.196835 | False |
| 202 | Longva | 23577 | 23577_3 | 23.678 | -16.749976 | 5.157668 | 1.274978 | 62.51389 | 32.761620 | 6.90900 | 2.5 | 59.03 | 0:04:38 | 0.262069 | False |
| 203 | Longva | 23577 | 23577_4 | 23.693 | -16.791657 | 4.886485 | 1.430363 | 48.05583 | 24.062760 | 7.69016 | 2528.9 | 63.70 | 3:35:58 | 6.681766 | False |
| 204 | Longva | 23577 | 23577_5 | 23.685 | -14.351723 | 6.173974 | 1.275234 | 38.56695 | 23.898460 | 16.40434 | 1675.3 | 63.03 | 5:11:34 | 4.302034 | False |
| 205 | Longva | 23577 | 23577_6 | 23.382 | -19.305649 | 7.170860 | 1.356799 | 66.76667 | 31.964460 | 11.59858 | 2484.7 | 85.53 | 5:36:19 | 7.481066 | True |
| 206 | Longva | 23577 | 23577_7 | 14.807 | -2.855181 | 7.985738 | 2.129549 | 72.14334 | 35.351160 | 24.03564 | 2349.6 | 35.63 | 4:08:18 | 9.804116 | False |
| 207 | Longva | 23577 | 23577_8 | 23.700 | -18.222106 | 6.851452 | 1.052838 | 95.48070 | 34.968420 | 11.67425 | 777.9 | 65.43 | 2:40:23 | 7.711277 | False |
| 208 | Longva | 23577 | 23577_9 | 23.676 | -18.171493 | 9.090194 | 1.452091 | 96.55347 | 51.344670 | 13.44182 | 144.7 | 62.87 | 0:39:11 | 3.514407 | False |
| 209 | Longva | 23577 | 23577_10 | 24.767 | -6.640865 | 11.403110 | 1.366550 | 43.64625 | 44.299480 | 8.88298 | 5.6 | 63.73 | 0:09:24 | 0.432759 | False |
| 210 | Longva | 23577 | 23577_11 | 23.694 | -12.776453 | 10.314752 | 1.211348 | 69.32805 | 36.253130 | 8.98936 | 659.3 | 46.87 | 1:00:03 | 7.909883 | True |
| 211 | Longva | 23577 | 23577_12 | 23.676 | -7.293715 | 10.777862 | 1.305850 | 39.57084 | 35.242580 | 10.65086 | 1856.2 | 59.80 | 4:06:35 | 7.004298 | False |
| 212 | Longva | 23577 | 23577_13 | 23.693 | -15.695071 | 7.034747 | 2.175067 | 40.09861 | 21.016720 | 17.60058 | 11.2 | 1.60 | 0:41:42 | 5.321429 | False |
| 213 | Longva | 23577 | 23577_14 | 29.703 | -3.016862 | 10.506119 | 1.245392 | 63.90208 | 31.913250 | 9.31802 | 2014.0 | 41.10 | 6:20:12 | 5.771973 | False |
| 214 | Longva | 23577 | 23577_15 | 23.685 | 2.124140 | 8.137018 | 1.993168 | 68.38611 | 43.483270 | 11.47615 | 262.9 | 32.50 | 2:07:01 | 4.213092 | False |
| 215 | Longva | 23577 | 23577_16 | 23.694 | 2.584414 | 11.023107 | 3.716570 | 84.16333 | 46.987360 | 33.09741 | 1541.1 | 35.53 | 3:40:52 | 9.139046 | False |
| 216 | Longva | 23577 | 23577_17 | 23.697 | 8.535046 | 11.446650 | 2.201470 | 83.21069 | 43.401660 | 14.27032 | 1727.0 | 76.10 | 3:50:02 | 8.696784 | True |
| 217 | Longva | 23577 | 23577_18 | 23.702 | 7.472612 | 11.820684 | 1.769986 | 85.73000 | 48.874590 | 17.88178 | 324.3 | 66.03 | 1:09:09 | 4.504327 | False |
| 218 | Longva | 23577 | 23577_19 | 23.688 | 8.319242 | 6.697714 | 2.006440 | 62.42903 | 29.939310 | 17.68299 | 166.3 | 69.40 | 0:37:23 | 4.120889 | False |
| 219 | Longva | 23577 | 23577_20 | 23.685 | -14.223055 | 7.862007 | 2.846925 | 63.05042 | 43.675390 | 16.42023 | 174.2 | 72.00 | 0:33:10 | 4.724500 | False |
| 220 | Longva | 23577 | 23577_21 | 23.678 | -15.223432 | 7.078260 | 2.032137 | 74.03056 | 77.091090 | 28.45028 | 557.3 | 60.20 | 0:55:47 | 9.600298 | False |
| 221 | Longva | 23577 | 23577_22 | 23.685 | -14.781218 | 5.803354 | 2.194861 | 51.09028 | 29.179210 | 12.97740 | 261.7 | 68.93 | 1:07:41 | 3.735381 | False |
| 222 | Longva | 23577 | 23577_23 | 23.706 | -18.911619 | 5.154168 | 1.429841 | 36.47806 | 18.781900 | 9.19395 | 330.0 | 66.97 | 0:44:52 | 7.192593 | False |
| 223 | Longva | 23577 | 23577_24 | 29.699 | -18.094701 | 5.391468 | 1.670123 | 31.35514 | 41.612530 | 22.95634 | 228.7 | 61.40 | 0:27:14 | 8.605625 | False |
| 224 | Longva | 23577 | 23577_25 | 23.703 | -20.160506 | 7.404583 | 1.802270 | 50.89889 | 50.233080 | 14.61450 | 1551.1 | 73.97 | 2:49:12 | 10.203905 | True |

Continued on next page

| | worksite | chainage | hole_id | hole_depth | hi_mean | fi_mean | wi_mean | hi_max | fi_max | wi_max | Gr_vol | Gr_endpres | Gr_time | Gr_meanflow | HJ_detected |
|---|---|---|---|---|---|---|---|---|---|---|---|---|---|---|---|
| 225 | Longva | 23577 | 23577_26 | 23.701 | -24.429502 | 4.924856 | 1.360447 | 35.73653 | 20.943800 | 14.58837 | 705.8 | 66.20 | 1:03:50 | 10.979427 | False |
| 226 | Longva | 23577 | 23577_27 | 23.690 | -20.980824 | 4.748416 | 1.116570 | 28.19069 | 20.544320 | 7.77307 | 269.1 | 63.37 | 2:07:36 | 2.978269 | False |
| 227 | Longva | 23577 | 23577_28 | 29.680 | -17.521741 | 4.639645 | 1.334847 | 54.06236 | 25.326540 | 8.29999 | 325.7 | 37.10 | 1:52:54 | 1.877343 | False |
| 228 | Longva | 23577 | 23577_29 | 23.680 | -20.811252 | 5.592520 | 1.155208 | 50.15333 | 27.328210 | 6.23151 | 11.7 | 60.00 | 0:11:24 | 0.835391 | False |
| 229 | Longva | 23577 | 23577_30 | 23.701 | -25.562257 | 7.035185 | 2.122200 | 62.82459 | 93.696420 | 21.94902 | 3125.3 | 64.73 | 4:27:03 | 10.942311 | True |
| 230 | Longva | 23577 | 23577_31 | 23.699 | -3.509429 | 15.384576 | 1.292914 | 47.00264 | 41.926010 | 7.53159 | 1051.1 | 63.83 | 1:46:24 | 9.171140 | False |
| 231 | Longva | 23654 | 23654_1 | 23.598 | -5.377500 | 9.764210 | 1.341670 | 36.73820 | 25.809690 | 7.60980 | 150.2 | 66.10 | 0:32:00 | 4.435751 | False |
| 232 | Longva | 23654 | 23654_2 | 23.583 | -11.559550 | 3.720070 | 1.277680 | 15.62667 | 17.620240 | 6.52654 | 39.7 | 59.50 | 0:15:11 | 3.193548 | False |
| 233 | Longva | 23654 | 23654_3 | 23.605 | -20.320440 | 4.303400 | 1.132570 | 5.08028 | 14.509210 | 6.19017 | 0.0 | 73.50 | 0:41:51 | 3.301852 | False |
| 234 | Longva | 23654 | 23654_4 | 23.584 | -22.823770 | 4.026610 | 1.097640 | 28.23195 | 24.253880 | 6.80613 | 499.2 | 63.50 | 0:59:50 | 8.388889 | False |
| 235 | Longva | 23654 | 23654_5 | 23.576 | -15.154530 | 4.239390 | 1.243560 | 26.59514 | 18.218070 | 10.54444 | 851.6 | 63.80 | 0:58:05 | 14.526149 | True |
| 236 | Longva | 23654 | 23654_6 | 23.606 | -22.709640 | 3.976670 | 1.089960 | 11.66292 | 12.221560 | 6.67741 | 262.2 | 61.90 | 0:42:44 | 6.109728 | False |
| 237 | Longva | 23654 | 23654_7 | 23.603 | -13.614510 | 3.695400 | 1.370030 | 20.61056 | 13.776640 | 7.21412 | 216.9 | 60.90 | 0:18:32 | 11.960714 | False |
| 238 | Longva | 23654 | 23654_9 | 23.582 | -7.780320 | 4.328770 | 1.142450 | 41.18041 | 17.043620 | 7.99914 | 231.0 | 61.60 | 0:30:45 | 7.555376 | False |
| 239 | Longva | 23654 | 23654_10 | 23.797 | -21.738940 | 5.311550 | 1.278320 | 19.12639 | 29.319170 | 10.12199 | 2430.4 | 64.30 | 2:51:37 | 16.824500 | True |
| 240 | Longva | 23654 | 23654_11 | 23.604 | -18.056880 | 5.436390 | 1.144190 | 37.71486 | 55.713450 | 7.76805 | 1612.9 | 64.60 | 2:42:45 | 12.675547 | False |
| 241 | Longva | 23654 | 23654_12 | 23.592 | -10.239640 | 5.450030 | 1.272670 | 56.66764 | 33.260710 | 17.79872 | 118.7 | 60.60 | 1:31:42 | 7.592967 | True |
| 242 | Longva | 23654 | 23654_13 | 23.608 | -11.861140 | 5.607960 | 1.300510 | 25.75292 | 22.968810 | 8.49886 | 901.9 | 65.60 | 1:42:53 | 9.249317 | False |
| 243 | Longva | 23654 | 23654_14 | 23.594 | -7.353640 | 6.206120 | 1.625020 | 51.42111 | 58.483110 | 36.13855 | 189.3 | 63.00 | 0:14:39 | 12.815730 | False |
| 244 | Longva | 23654 | 23654_15 | 23.599 | -8.327960 | 5.666560 | 1.413880 | 21.29917 | 26.104680 | 6.62185 | 672.0 | 60.50 | 1:04:50 | 10.984741 | False |
| 245 | Longva | 23654 | 23654_16 | 23.598 | 7.094400 | 12.578150 | 1.313500 | 58.75653 | 35.237550 | 11.01000 | 1211.2 | 61.70 | 1:47:03 | 11.213841 | False |
| 246 | Longva | 23654 | 23654_17 | 23.600 | -12.081440 | 6.560780 | 2.598520 | 100.34722 | 48.852390 | 25.66486 | 2686.0 | 62.80 | 2:24:56 | 17.303648 | False |
| 247 | Longva | 23654 | 23654_19 | 23.584 | -6.781780 | 7.031070 | 1.771630 | 85.95958 | 66.838540 | 23.45008 | 593.2 | 61.20 | 1:16:57 | 7.633117 | False |
| 248 | Longva | 23654 | 23654_21 | 12.504 | -3.130890 | 7.280790 | 3.668570 | 48.86944 | 26.645930 | 23.13129 | 2353.9 | 63.40 | 5:35:11 | 8.293866 | True |
| 249 | Longva | 23654 | 23654_22 | 23.592 | -0.249780 | 9.678410 | 2.473250 | 64.96528 | 39.519740 | 27.17802 | 117.1 | 61.40 | 0:47:14 | 2.395931 | False |
| 250 | Longva | 23654 | 23654_23 | 23.599 | 6.789130 | 14.143500 | 2.086600 | 71.23000 | 61.087920 | 21.50053 | 31.7 | 61.10 | 0:21:31 | 1.386923 | False |
| 251 | Longva | 23654 | 23654_24 | 23.579 | 3.520680 | 12.875460 | 1.546980 | 58.64180 | 58.145140 | 7.09880 | 0.9 | 62.30 | 0:07:04 | 0.000000 | False |
| 252 | Longva | 23654 | 23654_25 | 23.580 | -0.891640 | 11.686980 | 1.453220 | 50.10014 | 38.215180 | 11.60200 | 1.4 | 61.50 | 0:14:17 | 0.172414 | False |
| 253 | Longva | 23654 | 23654_26 | 23.575 | -4.356840 | 6.494160 | 1.682860 | 49.58750 | 22.291630 | 13.87884 | 1.4 | 68.70 | 0:09:23 | 0.000000 | False |
| 254 | Longva | 23654 | 23654_27 | 23.601 | -10.955160 | 7.674030 | 1.488400 | 50.94375 | 38.845470 | 12.49230 | 3746.1 | 61.90 | 5:43:09 | 15.858969 | True |
| 255 | Longva | 23654 | 23654_28 | 23.613 | -9.375130 | 8.001370 | 2.245670 | 138.01402 | 60.893880 | 16.77848 | 1130.6 | 63.00 | 1:11:45 | 15.746172 | False |
| 256 | Longva | 23654 | 23654_30 | 23.591 | -5.285930 | 10.585380 | 1.510940 | 35.58458 | 34.377650 | 11.00769 | 1228.8 | 65.10 | 2:31:14 | 6.144329 | False |
| 257 | Longva | 23654 | 23654_31 | 23.581 | -15.308260 | 10.136410 | 1.787220 | 42.26292 | 37.483950 | 15.84329 | 56.0 | 60.00 | 0:28:51 | 1.524138 | False |
| 258 | Longva | 23654 | 23654_32 | 23.585 | -29.836980 | 6.245420 | 1.199510 | 42.70556 | 27.866280 | 6.86274 | 895.0 | 63.50 | 1:32:19 | 9.626173 | False |
| 259 | Longva | 23654 | 23654_33 | 23.602 | -35.857260 | 5.165030 | 1.147730 | 14.62278 | 23.411870 | 6.94573 | 1555.6 | 63.60 | 2:53:43 | 6.575294 | True |
| 260 | Longva | 23654 | 23654_34 | 23.595 | -42.161630 | 4.473770 | 1.146660 | 3.49195 | 14.837760 | 8.80753 | 481.6 | 59.90 | 1:08:31 | 6.876214 | True |
| 261 | Longva | 23654 | 23654_36 | 23.581 | -13.721400 | 4.201580 | 1.110880 | 24.18597 | 14.841840 | 6.03554 | 114.8 | 59.80 | 0:19:22 | 3.826344 | False |
| 262 | Longva | 23654 | 23654_37 | 15.429 | -23.869610 | 4.615860 | 2.951660 | 34.30361 | 19.421010 | 23.25114 | 41.0 | 64.50 | 0:10:12 | 3.957143 | False |
| 263 | Longva | 23654 | 23654_39 | 23.574 | -43.103010 | 7.082310 | 1.288060 | 18.70236 | 28.184050 | 6.77657 | 431.9 | 58.20 | 0:43:22 | 9.979310 | False |
| 264 | Longva | 23654 | 23654_40 | 23.590 | -13.316930 | 6.701300 | 1.323090 | 43.31639 | 33.057740 | 5.93233 | 2417.5 | 59.90 | 3:17:01 | 12.383026 | False |
| 265 | Longva | 23654 | 23654_41 | 21.044 | -11.613540 | 6.728040 | 3.023740 | 58.75639 | 21.074660 | 34.30903 | 3189.8 | 61.70 | 2:58:32 | 17.467245 | False |
| 266 | Longva | 23654 | 23654_42 | 23.591 | -6.553400 | 4.914360 | 1.530270 | 28.38458 | 14.515680 | 7.32549 | 1522.3 | 62.10 | 3:10:48 | 5.387081 | False |
| 267 | Longva | 23654 | 23654_43 | 23.592 | -17.152530 | 4.713990 | 1.274480 | 12.72014 | 17.782160 | 6.27640 | 283.4 | 60.10 | 0:36:36 | 7.645249 | False |
| 268 | Longva | 23654 | 23654_44 | 23.588 | -22.688660 | 4.737970 | 1.300900 | -2.36709 | 13.842690 | 6.13571 | 133.9 | 59.60 | 0:14:51 | 8.806667 | False |
| 269 | Longva | 23498 | 23498_1 | 23.696 | -13.495660 | 5.246390 | 1.453790 | 48.75195 | 31.064730 | 30.49937 | 1833.1 | 61.60 | 2:57:20 | 9.159182 | True |

Continued on next page

| | worksite | chainage | hole_id | hole_depth | hi_mean | fi_mean | wi_mean | hi_max | fi_max | wi_max | Gr_vol | Gr_endpres | Gr_time | Gr_meanflow | HJ_detected |
|---|---|---|---|---|---|---|---|---|---|---|---|---|---|---|---|
| 270 | Longva | 23498 | 23498_2 | 23.684 | -21.175860 | 4.755440 | 2.543230 | 64.51069 | 30.562220 | 26.51306 | 593.1 | 61.00 | 0:52:49 | 10.631068 | False |
| 271 | Longva | 23498 | 23498_3 | 23.677 | -18.801330 | 5.097590 | 1.651240 | 42.57764 | 28.221710 | 17.47945 | 654.7 | 61.50 | 16:10:06 | 8.453137 | True |
| 272 | Longva | 23498 | 23498_5 | 23.673 | -11.893470 | 4.670360 | 1.479660 | 23.52570 | 18.950770 | 28.77197 | 594.3 | 60.20 | 1:53:16 | 7.463789 | True |
| 273 | Longva | 23498 | 23498_6 | 23.674 | -7.802690 | 5.924820 | 1.692230 | 49.22320 | 65.061170 | 17.20081 | 544.0 | 61.50 | 1:57:58 | 10.569090 | False |
| 274 | Longva | 23498 | 23498_7 | 23.680 | -8.960220 | 5.259100 | 0.934400 | 30.02639 | 23.509830 | 8.06864 | 2162.1 | 99.60 | 5:50:30 | 6.325698 | False |
| 275 | Longva | 23498 | 23498_8 | 23.703 | -13.425190 | 6.872560 | 1.013330 | 31.77056 | 16.704630 | 6.61998 | 9.8 | 60.80 | 0:08:48 | 0.924074 | False |
| 276 | Longva | 23498 | 23498_9 | 23.720 | -5.398770 | 7.194110 | 1.103410 | 65.44180 | 31.023400 | 8.91488 | 1758.9 | 65.00 | 3:48:00 | 7.549598 | False |
| 277 | Longva | 23498 | 23498_10 | 24.028 | -6.553320 | 7.683570 | 1.486200 | 40.99222 | 22.501320 | 18.79848 | 1634.7 | 94.40 | 5:42:49 | 4.996336 | False |
| 278 | Longva | 23498 | 23498_11 | 23.702 | -17.841480 | 6.944130 | 1.127900 | 42.11389 | 22.052300 | 9.75493 | 536.3 | 99.60 | 2:21:53 | 6.457195 | False |
| 279 | Longva | 23498 | 23498_12 | 17.498 | -13.851300 | 6.820270 | 3.474480 | 35.03680 | 19.333400 | 19.93071 | 10857.9 | 67.00 | 19:58:38 | 10.566391 | False |
| 280 | Longva | 23498 | 23498_13 | 29.393 | -12.421130 | 8.820340 | 1.743440 | 49.68055 | 31.034800 | 14.04293 | 9869.0 | 65.50 | 19:43:34 | 7.096947 | False |
| 281 | Longva | 23498 | 23498_14 | 23.684 | -19.166220 | 7.697330 | 2.733630 | 112.00409 | 63.328000 | 26.56109 | 2039.1 | 71.60 | 2:37:21 | 12.887394 | True |
| 282 | Longva | 23498 | 23498_15 | 23.694 | -22.584230 | 6.953450 | 1.900400 | 57.95042 | 29.828960 | 29.62827 | 1971.6 | 72.90 | 3:20:37 | 9.879634 | True |
| 283 | Longva | 23498 | 23498_16 | 23.683 | -21.531550 | 7.999980 | 1.477240 | 73.42097 | 42.425110 | 25.94655 | 495.1 | 63.10 | 2:22:54 | 3.701709 | False |
| 284 | Longva | 23498 | 23498_17 | 23.698 | -14.852530 | 7.628460 | 1.545090 | 155.86778 | 90.194100 | 14.69505 | 109.2 | 58.00 | 0:36:29 | 2.758182 | False |
| 285 | Longva | 23498 | 23498_18 | 23.678 | -28.607470 | 7.272020 | 1.474820 | 23.36000 | 32.528620 | 14.02043 | 1648.3 | 57.20 | 3:50:48 | 9.563233 | False |
| 286 | Longva | 23498 | 23498_19 | 23.676 | -20.959730 | 6.215390 | 1.000970 | 17.19528 | 18.476050 | 6.10068 | 2145.2 | 89.30 | 6:27:55 | 4.729886 | False |
| 287 | Longva | 23498 | 23498_20 | 23.692 | -24.075860 | 6.121430 | 1.009740 | 10.49653 | 18.080150 | 6.36269 | 152.6 | 61.20 | 1:25:20 | 1.838791 | False |
| 288 | Longva | 23498 | 23498_21 | 23.702 | -28.205810 | 6.244990 | 1.094390 | -1.61694 | 24.212070 | 6.22083 | 171.3 | 63.70 | 0:27:25 | 6.136145 | True |
| 289 | Longva | 23498 | 23498_22 | 23.675 | -22.340970 | 5.014330 | 1.184540 | 41.70820 | 31.884500 | 6.93000 | 106.7 | 80.90 | 0:25:42 | 4.296154 | False |
| 290 | Longva | 23498 | 23498_23 | 23.699 | -11.203930 | 4.475290 | 1.677560 | 30.65305 | 17.915720 | 19.61083 | 483.0 | 61.30 | 1:38:04 | 6.579908 | False |
| 291 | Longva | 23498 | 23498_24 | 23.699 | -11.174420 | 5.001940 | 1.530460 | 50.02097 | 19.551620 | 26.03443 | 0.7 | 63.30 | 0:03:50 | 0.454167 | False |
| 292 | Longva | 23498 | 23498_25 | 23.678 | -11.332420 | 4.941430 | 1.907320 | 61.05250 | 25.731560 | 24.87651 | 1.5 | 60.20 | 0:04:18 | 0.618519 | False |
| 293 | Longva | 23498 | 23498_26 | 15.155 | -3.992010 | 6.848450 | 2.258380 | 46.03875 | 26.003360 | 26.65509 | 13016.9 | 64.50 | 14:45:19 | NaN | False |
| 294 | Longva | 23498 | 23498_27 | 23.684 | -14.599790 | 7.187010 | 1.886890 | 30.30403 | 33.112180 | 21.49131 | 6829.3 | 61.80 | 8:56:22 | NaN | False |
| 295 | Longva | 23498 | 23498_28 | 19.986 | -3.038390 | 7.051650 | 1.746660 | 53.06681 | 22.186590 | 38.18222 | 3682.1 | 62.70 | 3:14:20 | NaN | False |
| 296 | Longva | 23498 | 23498_29 | 23.701 | -13.609280 | 5.670630 | 1.694710 | 55.70792 | 20.688230 | 9.67894 | 17.7 | 66.10 | 0:07:40 | NaN | False |
| 297 | Longva | 23498 | 23498_30 | 23.701 | -14.994310 | 5.027940 | 1.116690 | 50.96875 | 22.646380 | 22.80903 | 428.0 | 56.00 | 0:42:24 | NaN | False |
| 298 | Longva | 23498 | 23498_31 | 23.413 | -15.401870 | 6.444240 | 1.343680 | 38.13167 | 44.346790 | 12.08567 | 2824.0 | 60.00 | 3:40:46 | NaN | False |
| 299 | Longva | 23498 | 23498_32 | 19.995 | -10.771750 | 8.770430 | 1.495250 | 105.31236 | 41.417360 | 8.58317 | 364.6 | 31.70 | 0:28:26 | NaN | False |
| 300 | Longva | 23615 | 23615_1 | 23.593 | 1.199060 | 5.265360 | 1.180730 | 54.47653 | 58.376600 | 8.62893 | 1576.2 | 68.70 | 3:11:08 | 5.916370 | False |
| 301 | Longva | 23615 | 23615_2 | 23.602 | 17.576730 | 2.821840 | 1.128190 | 54.71070 | 25.486120 | 10.47774 | 1235.4 | 63.00 | 1:36:09 | 13.260127 | True |
| 302 | Longva | 23615 | 23615_3 | 23.602 | 1.733100 | 4.990990 | 1.064920 | 33.19667 | 25.274210 | 6.63499 | 1224.6 | 64.40 | 1:42:22 | 12.575627 | True |
| 303 | Longva | 23615 | 23615_4 | 23.592 | 3.282970 | 5.940120 | 1.471320 | 63.18222 | 37.961650 | 13.96838 | 706.8 | 60.60 | 1:57:58 | 5.921469 | False |
| 304 | Longva | 23615 | 23615_5 | 23.591 | -5.684540 | 5.180710 | 1.133540 | 35.11319 | 13.964860 | 7.11666 | 1458.3 | 63.90 | 3:32:08 | 8.309658 | False |
| 305 | Longva | 23615 | 23615_6 | 23.579 | -4.118410 | 4.776980 | 1.175090 | 26.57139 | 17.100840 | 6.19806 | 232.5 | 68.50 | 1:04:12 | 5.909535 | False |
| 306 | Longva | 23615 | 23615_7 | 23.589 | -12.910890 | 6.066500 | 0.688000 | 38.75055 | 19.180280 | 6.19155 | 1521.7 | 67.80 | 4:06:55 | 13.248386 | False |
| 307 | Longva | 23615 | 23615_8 | 23.593 | -14.105590 | 6.180810 | 0.907390 | 48.53750 | 21.349730 | 5.85116 | 3508.1 | 64.10 | 4:33:02 | 11.533127 | False |
| 308 | Longva | 23615 | 23615_9 | 23.603 | -4.499690 | 6.206390 | 2.086510 | 80.44833 | 20.790160 | 26.15937 | 1138.6 | 62.90 | 1:40:31 | 11.569559 | True |
| 309 | Longva | 23615 | 23615_10 | 23.592 | -18.635460 | 6.641230 | 1.176300 | 49.23944 | 21.853040 | 13.34505 | 202.7 | 67.50 | 0:40:03 | 4.939419 | False |
| 310 | Longva | 23615 | 23615_11 | 23.584 | -17.216700 | 6.301390 | 1.264530 | 56.50069 | 29.987510 | 12.69702 | 4.1 | 66.50 | 0:03:41 | 2.620000 | False |
| 311 | Longva | 23615 | 23615_12 | 23.609 | -18.527200 | 6.494050 | 1.012170 | 42.54945 | 21.331150 | 7.61757 | 2097.7 | 99.60 | 4:11:30 | 8.259531 | True |
| 312 | Longva | 23615 | 23615_13 | 23.572 | -18.175490 | 6.893120 | 0.983010 | 60.08333 | 23.448240 | 6.43540 | 108.7 | 64.80 | 0:38:20 | 5.741295 | False |
| 313 | Longva | 23615 | 23615_14 | 23.581 | -9.892430 | 6.572910 | 1.057630 | 65.18833 | 32.527940 | 6.10089 | 12.7 | 59.70 | 0:10:10 | 1.069643 | False |
| 314 | Longva | 23615 | 23615_15 | 23.598 | -9.706390 | 7.272300 | 1.906220 | 73.49097 | 46.580930 | 19.33557 | 2215.0 | 60.70 | 3:38:52 | 14.754928 | True |

Continued on next page

| | worksite | chainage | hole_id | hole_depth | hi_mean | fi_mean | wi_mean | hi_max | fi_max | wi_max | Gr_vol | Gr_endpres | Gr_time | Gr_meanflow | HJ_detected |
|---|---|---|---|---|---|---|---|---|---|---|---|---|---|---|---|
| 315 | Longva | 23615 | 23615_16 | 23.594 | -3.764440 | 7.060580 | 1.053630 | 63.97653 | 32.965990 | 10.53508 | 886.5 | 64.90 | 2:44:50 | 7.509826 | False |
| 316 | Longva | 23615 | 23615_17 | 21.317 | -9.705820 | 9.393570 | 2.291530 | 80.43111 | 76.118590 | 30.44518 | 2.4 | 66.00 | 0:12:21 | 0.166667 | False |
| 317 | Longva | 23615 | 23615_18 | 23.587 | -1.287010 | 10.308890 | 1.320090 | 55.64250 | 39.460800 | 31.80842 | 718.8 | 60.60 | 1:18:00 | 9.137740 | False |
| 318 | Longva | 23615 | 23615_19 | 23.591 | 1.620110 | 11.072370 | 1.679590 | 81.98000 | 48.936680 | 41.43594 | 3.5 | 65.00 | 0:10:19 | 0.209524 | False |
| 319 | Longva | 23615 | 23615_20 | 23.585 | 1.545600 | 11.099600 | 1.535400 | 57.91097 | 32.333870 | 31.85756 | 389.1 | 70.90 | 0:42:14 | 9.053543 | False |
| 320 | Longva | 23615 | 23615_21 | 23.586 | -1.117280 | 11.831400 | 2.184460 | 43.18625 | 44.347040 | 36.30793 | 502.2 | 59.90 | 2:20:11 | 4.468913 | False |
| 321 | Longva | 23615 | 23615_22 | 23.581 | 6.274920 | 12.217420 | 1.355320 | 125.16889 | 82.191410 | 8.07866 | 903.9 | 59.80 | 3:16:10 | 6.865390 | False |
| 322 | Longva | 23615 | 23615_23 | 23.588 | 5.739180 | 11.915090 | 1.618690 | 61.95764 | 53.438810 | 12.29576 | 24.1 | 60.00 | 0:20:34 | 0.708000 | False |
| 323 | Longva | 23615 | 23615_24 | 23.583 | 4.810090 | 12.591570 | 1.871680 | 109.40056 | 60.498730 | 39.09293 | 558.7 | 59.90 | 0:15:28 | 0.095745 | False |
| 324 | Longva | 23615 | 23615_25 | 23.592 | 2.181680 | 11.270770 | 1.247690 | 59.81972 | 35.975190 | 11.04279 | 831.7 | 64.70 | 1:14:06 | 10.202986 | False |
| 325 | Longva | 23615 | 23615_27 | 23.586 | -1.339780 | 8.335930 | 4.021940 | 45.66361 | 27.490800 | 38.65588 | 393.9 | 62.40 | 2:59:24 | 7.425150 | False |
| 326 | Longva | 23615 | 23615_28 | 23.590 | 1.217870 | 8.342960 | 2.336730 | 39.91167 | 40.383800 | 22.22141 | 1309.7 | 62.10 | 3:44:55 | 8.480162 | True |
| 327 | Longva | 23615 | 23615_29 | 23.603 | -0.882610 | 8.181270 | 2.509870 | 66.39403 | 77.066600 | 39.35574 | 1876.1 | 67.00 | 3:19:50 | 10.352430 | False |
| 328 | Longva | 23615 | 23615_30 | 23.579 | 1.934000 | 10.930360 | 2.038350 | 61.16237 | 39.340000 | 34.11737 | 157.6 | 61.10 | 0:44:52 | 3.247037 | False |
| 329 | Longva | 23615 | 23615_31 | 23.584 | -1.826790 | 7.784850 | 2.077100 | 68.33084 | 38.869440 | 30.76461 | 334.3 | 60.80 | 2:10:20 | 2.474544 | False |
| 330 | Longva | 23615 | 23615_32 | 23.594 | 4.070960 | 10.678760 | 1.180960 | 76.23930 | 52.291310 | 18.20951 | 1.3 | 63.10 | 0:09:33 | 0.494915 | False |
| 331 | Longva | 23615 | 23615_33 | 23.585 | 0.140290 | 10.894080 | 1.101460 | 56.66861 | 40.173820 | 14.75931 | 1825.8 | 57.80 | 4:50:29 | 10.030990 | True |
| 332 | Longva | 23615 | 23615_34 | 23.586 | -3.255250 | 10.602560 | 1.781000 | 67.12556 | 36.367450 | 19.19452 | 788.0 | 62.20 | 2:07:38 | 10.443014 | True |
| 333 | Longva | 23615 | 23615_35 | 23.598 | -3.105370 | 10.150750 | 2.536950 | 85.34472 | 32.902810 | 17.94224 | 635.0 | 61.20 | 0:53:00 | 11.992163 | False |
| 334 | Longva | 23615 | 23615_36 | 23.584 | -6.145560 | 6.423960 | 2.174240 | 37.98972 | 27.623230 | 28.51236 | 1563.1 | 63.50 | 1:09:52 | 22.812975 | False |
| 335 | Longva | 23615 | 23615_37 | 23.581 | -1.297430 | 6.704140 | 1.104720 | 42.08486 | 38.954070 | 6.32936 | 1076.5 | 63.90 | 1:15:01 | 15.335841 | False |
| 336 | Longva | 23615 | 23615_38 | 23.587 | 2.173050 | 7.371930 | 1.686100 | 72.94389 | 47.147330 | 20.75430 | 1808.2 | 63.60 | 2:15:16 | 13.637586 | True |
| 337 | Longva | 23615 | 23615_39 | 23.594 | -9.574980 | 7.105020 | 1.372110 | 59.91334 | 74.249880 | 8.28789 | 590.1 | 73.50 | 1:58:00 | 5.449902 | False |
| 338 | Longva | 23615 | 23615_40 | 23.602 | -2.053740 | 10.902160 | 2.625300 | 71.29236 | 82.532980 | 34.26441 | 945.9 | 64.10 | 1:29:15 | 10.588806 | True |
| 339 | Longva | 23707 | 23707_1 | 23.678 | -21.763010 | 3.612230 | 1.003080 | 4.21778 | 24.800570 | 6.01660 | 826.1 | 63.60 | 0:51:39 | 13.917222 | True |
| 340 | Longva | 23707 | 23707_2 | 23.696 | -31.443060 | 3.415610 | 1.060570 | 3.69861 | 17.329070 | 5.99834 | 218.9 | 63.90 | 0:22:32 | 9.397794 | False |
| 341 | Longva | 23707 | 23707_4 | 23.683 | -34.224940 | 3.841850 | 1.491300 | 6.95958 | 12.560470 | 6.29324 | 196.8 | 64.10 | 0:19:32 | 9.688983 | False |
| 342 | Longva | 23707 | 23707_6 | 23.694 | -35.126300 | 5.213330 | 1.138450 | -1.16236 | 19.128220 | 7.58905 | 158.3 | 63.80 | 0:17:42 | 8.583333 | False |
| 343 | Longva | 23707 | 23707_7 | 21.026 | -32.638360 | 5.961120 | 1.572720 | 63.14056 | 35.134530 | 24.71750 | 413.5 | 64.60 | 2:16:44 | 9.929461 | False |
| 344 | Longva | 23707 | 23707_8 | 23.679 | -37.590720 | 6.241610 | 0.774500 | 9.59209 | 20.469140 | 9.22576 | 117.5 | 59.50 | 2:17:53 | 7.143299 | False |
| 345 | Longva | 23707 | 23707_9 | 23.686 | -31.028020 | 6.734970 | 0.803060 | 12.68833 | 19.936930 | 8.13041 | 203.4 | 59.20 | 0:26:20 | 7.652830 | False |
| 346 | Longva | 23707 | 23707_10 | 23.705 | -26.212230 | 6.534460 | 0.987540 | 60.33625 | 30.727940 | 10.67328 | 141.3 | 63.30 | 0:18:08 | 8.495960 | False |
| 347 | Longva | 23707 | 23707_12 | 23.703 | -23.370950 | 6.935620 | 1.095640 | 37.53903 | 32.397570 | 7.79186 | 472.7 | 68.20 | 0:37:58 | 12.356332 | False |
| 348 | Longva | 23707 | 23707_14 | 23.686 | -16.067640 | 7.184670 | 1.169020 | 50.58264 | 39.359960 | 9.75005 | 974.0 | 63.50 | 1:24:50 | 12.910573 | False |
| 349 | Longva | 23707 | 23707_16 | 23.702 | -21.354840 | 7.645330 | 2.221530 | 59.17292 | 37.877470 | 23.15191 | 4242.2 | 72.50 | 5:42:17 | 15.676090 | True |
| 350 | Longva | 23707 | 23707_17 | 23.689 | -22.716430 | 7.179260 | 2.047200 | 12.57667 | 22.595640 | 22.59682 | 10.2 | 63.30 | 0:05:03 | 1.946875 | False |
| 351 | Longva | 23707 | 23707_18 | 23.692 | -14.677980 | 6.653210 | 1.289500 | 18.15556 | 21.962600 | 9.57363 | 2111.9 | 63.50 | 1:46:21 | 21.353235 | False |
| 352 | Longva | 23707 | 23707_19 | 23.675 | -19.498580 | 6.992070 | 2.325930 | 45.03153 | 53.099730 | 22.17895 | 1540.2 | 69.70 | 1:48:10 | 13.700021 | False |
| 353 | Longva | 23707 | 23707_20 | 23.688 | -19.743400 | 6.807440 | 1.887370 | 65.53042 | 52.849900 | 18.60124 | 505.6 | 62.10 | 8:28:18 | 15.598090 | True |
| 354 | Longva | 23707 | 23707_21 | 23.698 | -16.964400 | 6.364160 | 1.598670 | 10.05944 | 25.974230 | 10.96714 | 147.7 | 59.80 | 0:22:29 | 6.495588 | False |
| 355 | Longva | 23707 | 23707_22 | 23.679 | -16.776260 | 6.959710 | 1.003080 | 143.15556 | 84.562110 | 6.91224 | 559.2 | 61.80 | 1:13:52 | 7.578829 | False |
| 356 | Longva | 23707 | 23707_23 | 23.673 | -23.105300 | 6.505230 | 1.203720 | 70.29958 | 44.946420 | 8.10586 | 22.1 | 60.50 | 0:20:45 | 0.967460 | False |
| 357 | Longva | 23707 | 23707_24 | 23.678 | -31.782730 | 6.446680 | 1.060050 | 10.02806 | 29.043620 | 6.26052 | 176.6 | 60.20 | 0:24:01 | 7.236552 | False |
| 358 | Longva | 23707 | 23707_25 | 23.707 | -31.054150 | 6.145660 | 1.495420 | 7.46083 | 23.080440 | 10.38883 | 7.6 | 60.40 | 0:05:05 | 1.331250 | False |
| 359 | Longva | 23707 | 23707_26 | 23.698 | -25.963820 | 5.603740 | 1.090780 | 5.90139 | 35.896820 | 6.62362 | 685.4 | 59.80 | 1:33:22 | 7.246429 | False |

Continued on next page

| | worksite | chainage | hole_id | hole_depth | hi_mean | fi_mean | wi_mean | hi_max | fi_max | wi_max | Gr_vol | Gr_endpres | Gr_time | Gr_meanflow | HJ_detected |
|---|---|---|---|---|---|---|---|---|---|---|---|---|---|---|---|
| 360 | Longva | 23707 | 23707_27 | 23.695 | -21.134450 | 5.837410 | 1.152230 | 24.85042 | 16.472390 | 8.43381 | 941.2 | 65.40 | 1:23:15 | 12.029955 | False |
| 361 | Longva | 23707 | 23707_28 | 23.704 | -26.132750 | 4.984650 | 1.515460 | 37.78375 | 59.476090 | 15.91396 | 336.3 | 67.30 | 8:36:46 | 7.796386 | True |
| 362 | Longva | 23707 | 23707_29 | 22.525 | -38.090270 | 5.165260 | 1.316550 | -6.12389 | 17.901990 | 7.07957 | 5.5 | 67.60 | 0:16:25 | 1.087719 | False |
| 363 | Longva | 23707 | 23707_30 | 23.684 | -24.887790 | 5.201100 | 1.330250 | 98.31014 | 84.249030 | 31.38502 | 5.0 | 63.30 | 0:04:07 | 1.519231 | False |
| 364 | Longva | 23707 | 23707_31 | 23.706 | -21.561010 | 3.906540 | 1.007000 | 8.06847 | 16.403040 | 5.65921 | 10647.4 | 74.90 | 11:32:25 | 17.288527 | True |
| 365 | Longva | 23707 | 23707_32 | 23.692 | -26.429100 | 4.261400 | 1.096470 | 65.71125 | 75.079530 | 6.03636 | 35.8 | 64.10 | 0:16:47 | 2.027451 | False |
| 366 | Longva | 23707 | 23707_33 | 23.690 | -32.172010 | 4.320690 | 1.120770 | 0.53958 | 22.178090 | 6.17728 | 1458.3 | 63.20 | 2:44:42 | 13.068596 | False |
| 367 | Longva | 23707 | 23707_34 | 23.676 | -33.844330 | 5.203970 | 0.779900 | 11.10306 | 17.763110 | 6.72929 | 1248.9 | 61.40 | 1:38:31 | 10.984451 | True |
| 368 | Longva | 23707 | 23707_35 | 23.693 | -24.320260 | 5.488020 | 1.049510 | 8.77792 | 17.685340 | 8.97941 | 116.9 | 59.80 | 0:22:41 | 5.016788 | False |

# B Python source codes

```
import pandas as pd
pd.set_option('display.float_format', lambda x: '%.5f' % x)

#Define directory to excel file with MWD data
xls = pd.ExcelFile(r'HoleReport_5856.xlsx')
xl_dict = pd.read_excel(xls, sheet_name=None, header=16, usecols='V:Y')

#Empty list to append to
bh_lst = []

# Iterate through sheets (borehole) in excel file
for hole, sheet in xl_dict.items():

    # Convert each sheet to dataframe structure
    xl_df = pd.DataFrame(xl_dict[hole])

    # Produce descriptive stats of all nonzero samplings from each hole
    using describe() function
    xl_stats = pd.DataFrame(xl_df.mask(xl_df == 0).describe())

    # Append stats and holenr. to empty list
    bh_lst.append([xl_stats, hole])

df_fin = pd.DataFrame(bh_lst)
result = df_fin
# read to existing blank .txt-file
result.to_csv(r'C:\Users\kris_\OneDrive\Documents\Master\
    Master_datagrunnlag\PEL_5506\MWD\MWD_5506.txt',
                header=True, index=False, sep='\t', mode='a')
```

**Code Listing 1:** Source code for .xls to .csv algorithm for MWD DPI data gathering.

```
import pandas as pd
import glob

#Define directory to LOG-files in .txt format
path = r"C:\Users\kris_\PycharmProjects\Fv_659\LOG_5856\*.txt"
files = glob.glob(path)

# define empty lists to append to and column names of final dataframe
lst = []
cols = ['Hole_nr', 'Recipe', 'Mean_flow', 'End_pressure', 'Volume', 'Time']
#Itterate through LOG files
for file in files:

    #Convert to csv to able Pandas dataframe data-structure
    rawfile = pd.read_csv(file)
    df = pd.DataFrame(rawfile)

    #Extract hole nr. and recipe
    recipe = df.iloc[4, 0]
    holeloc = df.iloc[1,0]
    holeno = [int(i) for i in holeloc.split(';') if i.isdigit()]
    holeno = int("".join(map(str, holeno)))

    # Define placement of each variable column
    df['Time'],df['Pressure'],df['Flow'],df['Volume']=df['Worksite;AUSTNES'
    ].str.split(';',3).str
    flow_df = pd.DataFrame(data = df.loc[9:, 'Flow'])
    volume_df = pd.DataFrame(data=df.loc[9:, 'Volume'])
    volume_df.drop(volume_df.tail(1).index, inplace=True)
    pressure_df = pd.DataFrame(data=df.loc[9:, 'Pressure'])
    pressure_df.drop(pressure_df.tail(1).index, inplace=True)

    # Take timestamps from LOG files and convert to appropriate format
    time_df = pd.DataFrame(data = df.loc[9:, 'Time'])
    time_df.drop(time_df.tail(1).index,inplace=True)
    time_df = time_df[~time_df['Time'].str.contains("PAUSE")]
    time_df['Time'] = pd.to_timedelta(time_df['Time'])

    # Convert remaining columns to appr. format
    flow_df['Flow'] = pd.to_numeric(flow_df['Flow'])
    pressure_df['Pressure'] = pd.to_numeric(pressure_df['Pressure'])
    volume_df['Volume'] = pd.to_numeric(volume_df['Volume'])

    # Taking sum, max and mean of grouting variables
    mean_flow = flow_df.loc[:,'Flow'].mean(axis = 0, skipna = True)
    max_pressure = pressure_df.loc[:, 'Pressure'].max(axis = 0, skipna =
    True)
    sum_volume = volume_df.loc[volume_df.index[-1], 'Volume']

    # using timedelta to find grouting duration
    deltat = time_df['Time'].iat[-1] - time_df['Time'].iat[0]
    deltat = deltat - pd.to_timedelta(deltat.days, unit='d')

    # append all variable incl. hole-number to empty list structure
    lst.append([holeno, recipe, mean_flow, max_pressure, sum_volume, deltat
    ])
    df_fin = pd.DataFrame(lst, columns=cols)

```

```
# Using groupby() to group equal hole numbers together, and derive max, sum
    , mean values of all
groupedmax_pressure = df_fin.groupby(['Hole_nr'])['End_pressure'].max()
groupedsum_volume = df_fin.groupby(['Hole_nr'])['Volume'].sum()
groupedmean_flow = df_fin.groupby(['Hole_nr'])['Mean_flow'].mean()
groupedsum_time = df_fin.groupby(['Hole_nr'])['Time'].agg('sum')

# Concate variables (coloumns) to final dataframe: result_df, and print
    result
frames = [groupedsum_volume, groupedmax_pressure, groupedmean_flow,
    groupedsum_time]
result_df = pd.concat(frames, axis=1, join='outer')
print(result_df)
```

**Code Listing 2:** Source code for gathering grouting data from LOG-files.

```
import pandas as pd
import glob
import matplotlib.pyplot as plt
import matplotlib.dates as dates
import seaborn as sns
sns.set(rc={'figure.figsize':(11, 4)})

# Declare PF-index as function, taking two input parameters
def pf_index(flow, pressure):
    q = flow
    p = pressure
    return (0.9*q) - (0.9*p/1) + 81

# Define directory with LOG-files
path = r"C:\Users\kris_\PycharmProjects\Fv_659\LOG_5506\*.txt"
files = glob.glob(path)

# define empty lists to append to and column names of final dataframe
lst = []
cols = ['Hole_nr', 'Recipe', 'Mean_flow', 'End pressure', 'Volume', 'Time']
#Itterate through LOG files
for file in files:
    # read each file as .csv file and convert new dataframe
    rawfile = pd.read_csv(file)
    df = pd.DataFrame(rawfile)

    # Extract descriptions on each hole (hole number, stage, worksite, etc
    ..)
    recipe = df.iloc[4, 0]
    holeloc = df.iloc[1, 0]
    holeno = [int(i) for i in holeloc.split(';') if i.isdigit()]
    holeno = int("".join(map(str, holeno)))
    stage = str(rawfile.iloc[3][0])
    injection = str(rawfile.iloc[5][0])
    section = str(rawfile.iloc[0][0])
    worksite = str(rawfile.columns[0])

    df['Time'], df['Pressure'], df['Flow'], df['Volume'] = df['Worksite;
    AUSTNES'].str.split(';', 3).str
    # Delete first unwanted rows from the LOG files
    df = df.drop('Worksite;AUSTNES', axis=1)
    df = df.dropna(axis=0, how='any')

    # extract the data for each variables with correct formating
    flow_df = pd.DataFrame(data = df.loc[9:, 'Flow'])
    flow_df['Flow'] = pd.to_numeric(flow_df['Flow'])
    flow_df.drop(flow_df.tail(1).index, inplace=True)
    flow_df = flow_df.reset_index(drop=True)

    volume_df = pd.DataFrame(data=df.loc[9:, 'Volume'])
    volume_df.drop(volume_df.tail(1).index, inplace=True)
    volume_df = volume_df.reset_index(drop=True)

    pressure_df = pd.DataFrame(data=df.loc[9:, 'Pressure'])
    pressure_df['Pressure'] = pd.to_numeric(pressure_df['Pressure'])
    pressure_df.drop(pressure_df.tail(1).index, inplace=True)
    pressure_df = pressure_df.reset_index(drop=True)

```

```
    time_df = pd.DataFrame(data=df.loc[9:, 'Time'])
    time_df.drop(time_df.tail(1).index, inplace=True)
    time_df = time_df[~time_df['Time'].str.contains("PAUSE")]
    time_df['Time'] = pd.to_datetime(time_df['Time'])

    #time_df['Time'] = pd.to_timedelta(time_df['Time'])
    time_df = time_df.reset_index(drop= True)

    # - - Filtrate the pressure series with moving avg (SMA) moving median
    with span of 3
    filt_pressure = pressure_df.rolling(window=3, min_periods=1).median()
    filt_pressure.fillna(value=0, axis=0, inplace=True)

    pf_df = flow_df.join(filt_pressure)
    # Calling the PF index function in a lambda expression
    pf_df['PF_index'] = pf_df.apply(lambda x: pf_index(x['Flow'], x['
    Pressure']), axis=1)
    pf_df = pf_df.join(time_df)

    # Filtrate the PF index series with double moving avg (DMA) with span
    of 5
    pf_df['PF_index'] = pf_df.PF_index.rolling(window=5,min_periods=1).mean
    ()
    pf_df['PF_index'] = pf_df.PF_index.rolling(window=5,min_periods=1).mean
    ()#,min_periods=1
    pf_df.PF_index.fillna(value=0, axis=0, inplace=True)

    # Plot the resulting graphs for each hole
    plt.plot_date(pf_df.Time, pf_df.PF_index, linestyle='solid',
                  marker='None', label='PF Index', c='black')
    plt.plot_date(pf_df.Time, pf_df.Pressure, linestyle='dashed',
                  marker='None', label='Pressure', c='blue', alpha=1)
    plt.plot_date(pf_df.Time, pf_df.Flow, linestyle='dotted',
                  marker='None', label='Flow', c='green', alpha=1)
    plt.xlim(pf_df.Time.loc[0], pf_df.Time.iloc[-1])
    plt.legend()
    plt.xlabel('Elapsed time [HH:MM:SS]')
    plt.ylabel('PF Index, Pressure [Bar], Flow [l/min]')
    plt.title('Holenr;' + str(holeno)+'   '+stage+'   '+injection+'   '+str
    (section)+'   '+str(worksite))
    xax = plt.gca().get_xaxis()
    xax.set_major_formatter(dates.DateFormatter('%H:%M:%S'))
    plt.show()
```

**Code Listing 3:** Source code for calculating and graphing PF index, flow and pressure for each grouted hole.

```
import pandas as pd
import seaborn as sns
from sklearn import model_selection
from sklearn.linear_model import LinearRegression
from sklearn.neural_network import MLPRegressor
from sklearn.ensemble import RandomForestRegressor
from sklearn.neighbors import KNeighborsRegressor
from sklearn.svm import SVR
from sklearn.model_selection import train_test_split
from sklearn.preprocessing import StandardScaler
import numpy as np
import matplotlib.pyplot as plt

#defines master dataframe
df = pd.read_csv(r"GroutingMWDdb_fin.csv")

# Cleaning DF by dropping empty rows and columns and adding 'worksite'
    column
df.drop(df.columns[range(17,26)], axis=1, inplace=True)
df.drop(df.index[range(369, 472)], axis=0, inplace=True)
df.insert(0, 'worksite', 'Austnes')
df.worksite.replace(df.worksite.loc[150:], 'Longva', inplace=True, regex=
    True)

# converting values to correct format
df.chainage = df.chainage.astype(int)
df.chainage = df.chainage.astype(str)
df.HJ_detected.fillna(value=0, inplace=True)
df.HJ_detected = df.HJ_detected.astype(bool)
df['HJ_str'] = np.where(df['HJ_detected'], 'Pot. HJ event detected', 'No HJ
     event detected')
df['Gr_meanflow'] = np.abs(df['Gr_meanflow'])

#declear df with no NaNs (df_dropna)
df_dropna = df.dropna(axis=0)
df_dropna.reset_index(drop=True, inplace=True)
# convert time from HH:MM:SS to minutes
df_dropna['Gr_Pumptime'].astype(str)
df_minutes = df_dropna['Gr_Pumptime'].str.split(':').apply(lambda x: int(x
    [0]) * 60 + int(x[1]))
df_dropna['Gr_Pumptime'] = df_minutes.values

#feature variables
features = ['hi_mean', 'fi_mean', 'wi_mean']

scaler = StandardScaler()
x = df_dropna.loc[:, features].to_numpy()
x = scaler.fit_transform(x)
# select target variables ('Gr_Pumptime, Gr_endpres, Gr_vol_tot)
y = df_dropna['Gr_meanflow'].values.reshape(-1, 1)
y = scaler.fit_transform(y).ravel()
x_train, x_test, y_train, y_test = train_test_split(x, y, test_size=0.40,
    random_state=0)
# - - - - sklearn - - - - #
# prepare models in iterable list for cross validation
seed = 7
models = []
models.append(('LR', LinearRegression()))
```

```
models.append(('RFR', RandomForestRegressor()))
models.append(('KNR', KNeighborsRegressor()))
models.append(('SVR', SVR()))
models.append(('MLP', MLPRegressor()))

# Empty lists to append
results = []
result_print = []
names = []
# itterate evaluate each model in turn, 10 split CV
for name, model in models:
    kfold = model_selection.KFold(n_splits=10, random_state=seed)
    cv_results = model_selection.cross_val_score(model, x, y, cv=kfold,
   scoring='r2')
    results.append(cv_results)
    names.append(name)
    msg = "%s: %f (%f)" % (name, cv_results.mean(), cv_results.std())
    result_print.append(msg)
print(result_print)
# plot boxplots of model comparison
fig = plt.figure()
ax = sns.boxplot(x=names, y=results, palette="Set3").set_title('Algorithm
   Comparison - Target: mean flow')
plt.ylim([-1.5, 0.25])
plt.hlines(y=0, xmin=-0.5, xmax=4.5, linestyles= 'dashed')
plt.show()
```

**Code Listing 4:** Source code for cross validation of various ML models on the dataset.

# C Figures and misc.

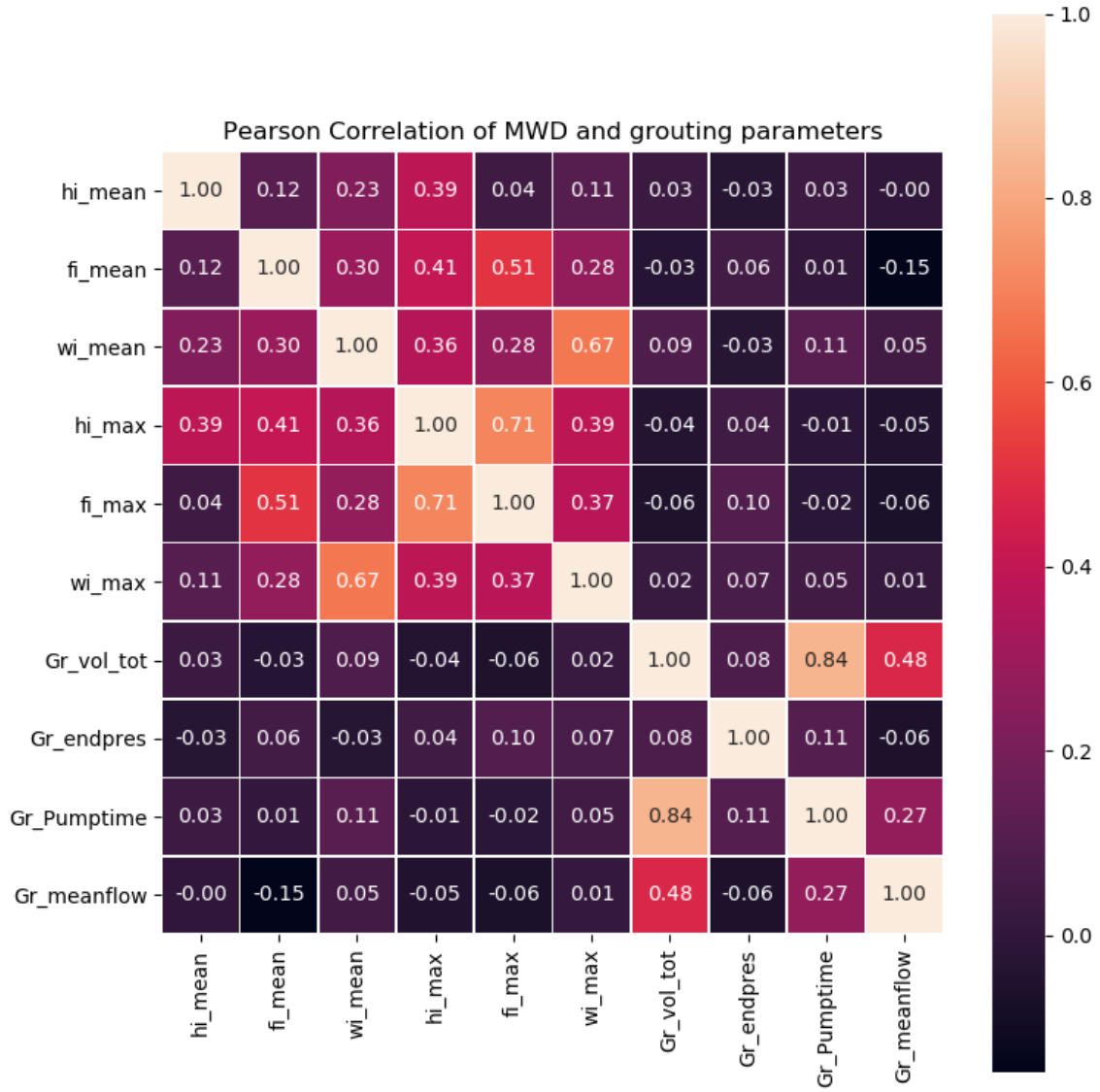


Heatmap depicting Pearson correlation coefficients between all involved variables (see table 7.7), color gradient ranges from light (positive linear correlation) to dark (0 to negative linear correlation).

## Grouting procedure for project Fv.659 Nordøyvegen, rock cover > 20m

(*Procedure can be changed according to the rock mass*)
Number of holes (incl. 4 hole at tunnel face): 30
Hole spread from contour: 5-10 m
d Length of holes: 24 m
Placement of grout gasket: 2 m inside hole.
Max end pressure: 80 bar for both tunnel crown and invert holes.

**Recipe 1** Portland cement
w/c = 0.9
Superplasitziser = 2%
Silicaslurry = 10%
Up to 500L grout take per hole before lowering w/c number. Where grout take is < 500L, end pressure needs to be held for 5 minutes before end of grouting.

**Recipe 2** Portland cement
w/c = 0.7
Superplasitziser = 2%
Silicaslurry = 10%
Up to 500L grout take per hole before lowering w/c number. Where grout take is < 500L, end pressure needs to be held for 5 minutes before end of grouting.

**Recipe 3** Portland cement
w/c = 0.5
Superplasitziser = 2%
Silicaslurry = 8%
After 1800L grout take per hole with insufficient end pressure, rest hole for 1-2 hours before resuming grouting.

**Recipe 4** Micro cement
w/c = 1.0
Superplasitziser = 1%
After 300L grout take per hole with insufficient end pressure, reduce w/c to 0.8 before resuming grouting.

**Recipe 5** Micro cement
w/c = 0.8
Superplasitziser = 1%
After 300L grout take per hole with insufficient end pressure, reduce w/c to 0.6 before resuming grouting.

**Recipe 6** Micro cement
w/c = 0.6
Superplasitziser = 1%
After 700L grout take per hole with insufficient end pressure, proceed with use of accelerator additive.

| | | | | | |
|---|---|---|---|---|---|
| Prosjekt navn | Nordøyvegen | | | | |
| Proskets nummer | 245583 | | | | |
| Rapport Dato (dato og uke) | 2019-12-05 uke 49 | | | | |
| Opprettet av | Jimmie Holmberg | | | | |

SKANSKA

## Injeksjonsrapport

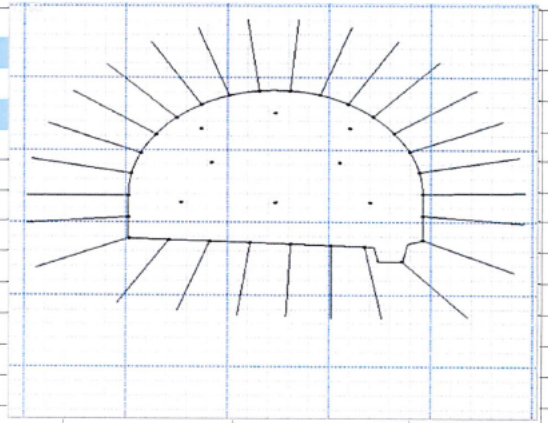

| | | | | | |
|---|---|---|---|---|---|
| **Stuff:** | Longva | **Antall Hull:** | 28 | | |
| | | ***(inkl 2 sonderhull)*** | | | |
| **Pel:** | 23 545,0 | **Hulldybde:** | 24 | | |
| | | (sonderhull 60 bm) | | | |
| **Ansvarlig formann:** | Jimmie Holmberg | **Borrmeter:** | 684 | | |
| **Tid/Dato:** | **Dato:** | **Klokkeslett:** | | | |
| Start | 2019-12-05 | 14:37 | | | |
| Stopp | 2019-12-07 | 01:57 | | | |
| Total Injekjsonstid | 35,33 | Timer | | | |
| Stopptid | 0,00 | Timer | | | |
| Injeksontid | 35,00 | Timer | | | |
| ***Materialforbruk*** | | | | | |
| **Prosseskode:** | **Beskrivelse:** | **Type:** | **Mengde:** | **Betegnelse:** | |
| 31.61 | Opp- og nedrigging for injeksjon | | 1 | stk | |
| 31.6291 | Enklepakker | Codan | 44 | stk | |
| 31.631 | Industrisement | Norcem | 36189 | kg | |
| 31.634 | Mauring | | 0 | kg | |
| 31.6391 | Mikrosilika | Meyco MS660 | 3619 | kg | (10%) |
| 31.6392 | Superplastisiser | Glenium C151 | 543 | kg | (1,5%) |
| 31.6393 | Styrt herding | Meyco SA162 | | l | |
| 31.69 | Økt eller redusert antall inj.linjer | Ekstra inj.linjer | | Timer | |
| | | Redusert inj.linjer | | Timer | |
| 31.691 | Ekstra herdetid | | 1 | Timer | (Tot 5 t herdetid) |
| | (Mellan kl 06-07) | | | | |

Dato/Sign: 7/12-19 Jimmie Holmberg

.General Information \ Generale \ Ogólna \ Sisäinen \ Generell \ Generell \ Důvěrné

Example of grouting report first page summary, from the Longva worksite, ch. 23545. Figure taken from *Skanska*